 Bull. Chem. Soc. Jpn. Vol. 81, No. 11, 1337–1376 (2008)

Accounts

Nano/Micro Patterning of Inorganic Thin Films

Kunihito Koumoto,*[1] Noriko Saito,[2] Yanfeng Gao,[3] Yoshitake Masuda,[4] and Peixin Zhu[5]

[1]Graduate School of Engineering, Nagoya University, Nagoya 464-8603

[2]National Institute for Materials Science, Tsukuba 305-0044

[3]Shanghai Institute of Ceramics, Chinese Academy of Sciences, Shanghai 200050, P. R. China

[4]National Institute of Advanced Industrial Science and Technology, Nagoya 463-8560

[5]Kawamura Institute of Chemical Research, Chiba 285-0078

Received February 20, 2008; E-mail: g44233a@cc.nagoya-u.ac.jp, saito.noriko@nims.go.jp

The present review is focused on the site-selective deposition of inorganic thin films on self-assembled monolayer (SAM) templates. SAMs were used to modify the substrate surface with chemical functional groups. The patterned SAM substrate was prepared by exposing the SAM substrate to UV light through photomasks for photocleavage. The patterned SAM was used as the templates for deposition of ceramic thin films in aqueous solutions. The preparation and characterization methods of SAMs, and the preparation of the patterned SAM templates are explained. Solution chemistry for the deposition of ceramic oxides and the physics and chemistry of interfaces are described. Experimental examples are given to explain how these aspects influence the formation of films and their properties. Various examples of site-selective deposition of ceramic oxides on SAM templates are explained with classification into three categories: patterning by site-selective attachment of homogeneously nucleated particles, patterning by surface-selective heterogeneous nucleation and growth, and patterning by catalyst-induced heterogeneous nucleation. We also describe pattern-deposition on flexible substrates and future views to improve the pattern resolution.

1. Introduction

Microfabrication is essential to much of modern science and technology; it supports information technology and permeates society by the integration of microelectronic and optoelectronic functionalities within a very small area, where "smaller" has meant better; less expensive, more components per chip, fast operation, high performance, and lower consumption of energy and materials.[1] Further, integration of a range of these small parts has resulted in portability; reduction in time, cost, reagents, sample size, and power consumption; and improvements in detection limits and types of functions.[1a] The dominant contributor to the cost of manufacturing chips is patterning technology, often known as photolithography, which is the most successful technology for high-volume manufacturing in microfabrication.[1,2] The technique is based on a projection-printing system (usually called a stepper) in which the image of a reticle pattern is focused and projected onto a thin film of a photoresist or light-sensitive polymer that is spin-coated on a wafer through a high numerical aperture lens system.[2] Selectively dissolving away either the exposed or the unexposed regions of the resist leaves a relief image on the silicon, which can then be transferred, by etching, to the underlying material to make the components that comprise the chip. A sequence of between 4 and 30 overlaid photolithographic levels is needed to make a complete chip.[2a] The resolution of this traditional top-down technique is approximately the wavelength of the light used (according to the Rayleigh equation), that is, 110 nm for ultraviolet light with a wavelength of about 193 nm.[1a] Hence, illuminating sources with shorter wavelengths are progressively introduced.[1,2]

Ceramic technology has been developed for thousands of years, resulting in numerous strategies for producing ceramics in the form of bulk materials, films, fibers, and powders. With the increasing development in nanoscience and nanotechnology, ceramic nanotechnology has been one of the most active areas of research. Besides a general trend toward miniaturization, nanosized ceramic oxide materials, such as semiconductor nanoparticles,[3–10] nanowires,[11–13] nanotubes,[14] and various types of artificial supramolecular entities.[15] along with integration materials including inorganic/organic hybrid materials[16,17] and thin films[18] are interesting because of the size-/thickness-dependent properties of materials and because of their potential for a broad range of applications. Functional ceramic thin films exhibit unique properties in electronics, coatings, displays, sensors, optical equipment, and numerous

Published on the web November 12, 2008; doi:10.1246/bcsj.81.1337

other technologies, and suit the need for scaling devices to small sizes, and are therefore attractive both in theory and practice. Various growth techniques have been applied to synthesize ceramic thin films. These techniques fall into at least two categories: vacuum-based methods such as chemical vapor deposition (CVD),[19] sputtering,[20] metal organic chemical vapor deposition (MOCVD),[21] atomic layer deposition (ALD),[22] and chemical solution methods including sol–gel, electrochemical deposition, and hydrothermal synthesis.[23,24] Vacuum-based techniques are an expensive investment, are limited to line-of-sight production, and usually require high-vapor-pressure chemicals or high-purity targets as starting materials. For conventional CVD methods, precursors exhibiting volatility are needed, which requires that the precursor is liquid or solid with a low melting point. For wet MOCVD, precursors are usually transferred to reactors by liquid delivery techniques, which makes it possible to use relatively nonvolatile metal–organic precursors but leads to difficulties in controlling the stoichiometric composition of the films. Wet chemical methods mentioned above can overcome some of the defects of vacuum-based methods by use of a homogeneous solution, but there are still processing issues, such as the control of the film thickness at the nanometer length scale, professional equipment, and complex processing.

There is considerable interest in alternative approaches that may be simple, cheap, and environmentally friendly or that are capable of producing films with novel or improved properties. The processes with low consumption of raw materials and energy, low generation of waste, and producer/user friendliness[25] are the basis of a series of concepts,[26] the so-called "green chemistry" (formal nomenclature in USA, U.K., Italy; common name in Japan), "green and sustainable chemistry" (GSC; formal nomenclature in Japan), and "sustainable chemistry" (in Germany), and their derivatives such as "environmentally benign chemistry," "environmentally friendly chemistry," or "clean chemistry." Techniques for the synthesis of ceramic thin films from aqueous solutions at low temperatures meet with some of the requirements mentioned above and are emerging as possible alternatives to vapor-phase and chemical-precursor techniques. The main techniques, including chemical bath deposition (CBD), successive ion layer adsorption and reaction (SILAR), liquid-phase deposition (LPD) methods, and electroless deposition (ED) with a catalyst, along with their variations, have been summarized in a review article.[27] CBD[28,29] can produce a solid film in a single immersion through control of the formation kinetics of the solid, typically without changing the metal oxidation states. This technique is used mainly to deposit sulfide and selenide thin films, while some relatively new reports involve preparation of oxides.[30] Unlike the CBD method, SILAR can deposit a solid by alternating the adsorption of metal ions and cationic ions from the corresponding solutions.[31] The LPD method refers to the formation of an oxide thin film by the hydrolysis of a metal–fluoro complex in an aqueous solution. Boric acid or aluminum metal can react with F^- to generate stable species and is added to accelerate the hydrolysis rate. The LPD method was first developed for depositing SiO_2 thin films and was later used to prepare other oxides, such as TiO_2, V_2O_5, VO_2, FeOOH (Fe_2O_3), and multicomponent metal oxide films.[32] Variations of the main techniques, such as photochemical deposition,[33] ferrite plating,[34] and deposition using a functional surface[35–45] are being investigated by various groups. The approaches using a functional surface to induce the film formation is inspired from the biomineralization process. It represents a typical low-temperature approach for ceramic films and has attracted much attention in the last decade.

As alternatives to conventional photolithography, soft lithography techniques have been recently developed to create patterns with submicrometer to nanometer features.[1,46,47] The self-assembly of molecular and colloidal building blocks to create larger, functional devices has attracted much interest. These materials are formed from interatomic and intermolecular interactions other than the traditional covalent, ionic, and metallic bonding forces. By using these techniques, ceramic thin films have been fabricated in solutions without high-temperature sintering in order to reduce energy consumption and allow application for various substrates having low heat resistance. In contrast to the technological world, organisms develop abundant micropatterned inorganic materials by biomineralization, which usually takes place under the assistance of a macromolecular template.[47c,47d] This macromolecule controls the nucleation, structure, morphology, crystal orientation, and spatial confinement of the inorganic phase. The understanding of biomineralization will catalyze new enthusiasm for bioinspired materials processing, which is important for the design, control, and optimization of materials synthesis at both the molecular and the macroscopic levels. For nanoscience and technology, it is necessary to develop new bottom-up approaches to self-assemble the chemically synthesized nanoblocks, nanoparticles, nanowires, nanodots, and nanotubes into large, functional ensembles. A number of nonconventional soft lithography methods have been developed to pattern a series of materials. Some of them are microtransfer molding (μTM),[48] micromolding in capillaries (MIMIC),[49] embossing[50] and casting,[51] which can pattern materials using liquid precursors such as sol–gels or colloidal suspensions on a submicrometer scale. Patterns of ceramics were also achieved by focused ion beam patterning,[52] electron beam direct writing,[53] nanoimprint lithography,[54] next generation lithography,[55] and self-patterning via either physical[56] or chemical routes.[57] These methods have been reviewed recently.[58,59]

The present review is focused on the site-selective deposition of ceramic thin films on substrates modified by self-assembled monolayer (SAM) with various functional groups. Patterned SAMs were used as templates for deposition of ceramics in aqueous solutions. On functionalized surfaces, nucleation and growth of ceramic oxides are controlled. As the method is analogus with biomineralization processes, it can be called bio-inspired processing. The methods for preparing pattened SAM templates, chemistry of solutions and interfaces for deposition of ceramic thin films, and examples of pattened ceramic thin films are described.

2. Growth of Inorganic Thin Films in Aqueous Solutions

2.1 Biomineralization. Nature has ingeniously succeeded in producing an impressive variety of inorganic functional structures with designed shapes and sizes on specific sites through a biologically controlled biomineralization process,

usually near room temperature and in aqueous solutions.[60] These structures are formed through template-assisted self-assembly, in which a self-assembled organic material serves as the structure scaffolding for the deposition of inorganic materials. This approach is an attractive alternative for the preparation of inorganic thin films, especially in applications in which the substrate cannot be exposed to high temperatures or for energy-efficient processes.

There are three constructional processes of biomineralization: supramolecular preorganization (delineated reaction sites), interfacial molecular recognition (site-specific inorganic nucleation), and assembly (crystal growth and termination).[60b] Prior to mineralization, an organized reaction environment is created by the construction of discrete, self-assembled, organic supramolecular systems from nanoscale to micrometers in size. In the second step, these preorganized architectures consist of functionalized surfaces that serve as templates for site-directed nucleation of inorganic clusters from aqueous solution.[60b] In some cases, these structurally organized organic surfaces catalytically or epitaxially induce growth of specifically oriented inorganic thin films.

2.2 SAM-Assisted Site-Selective Deposition of Inorganic Solids. By mimicking the chemistry found in biological nucleation proteins, control of the nucleation and growth of ceramic oxides has been attempted. Due to their favorable film properties, self-assembled monolayers (SAMs) have long been popular as templating agents for functionalizing surfaces.[61–66] SAMs are highly ordered and oriented molecular assemblies, formed by the chemisorption of an active surfactant of general formula $RSiX_3$ (where "R" is an organic functional group and "X" is an alkoxide or halide) on a solid surface, typically by a hydrolysis–condensation reaction or the formation of metal–sulfur bonds. The final structure on the solid support is determined by three interactions: the strong bond between the headgroup and the substrate surface, the van der Waals interaction between the hydrocarbon chains, and the interaction between the tail groups which is often repulsive due to the same orientation of their dipole moments. A schematic description of SAM formation processes for thiol on Au and organosilane on Si is shown in Figure 1.

Ceramic thin films have been deposited through solutions (especially aqueous solutions) directly onto SAMs.[35–45,47f] Solutions can be supersaturated under different conditions, resulting in precipitates of various microstructures in terms of size and morphology at the interface with either amorphous or crystalline states. SAMs can improve heterogeneous nucleation,[67] increase interaction forces such as electrostatic attractions between the SAM and the particles generated in the solution,[42] and form oriented crystals.[68] The as-deposited thin films on SAMs exhibit nanostructured characteristics in terms of particle size and roughness, and amorphous or crystal phases.[35–45] As a low-temperature and environmentally benign process, it enables the flexible selection of substrate materials from oxides, metals, plastics, and glass.

2.3 Chemistry at Solution/SAM Interfaces. The characteristics of ceramic particles in solution, dispersion/agglomeration, morphology, size, and size distribution, are dominated by surface chemistry. The surface forces, exhibiting attraction or repulsion between particles have effects on the dispersion/

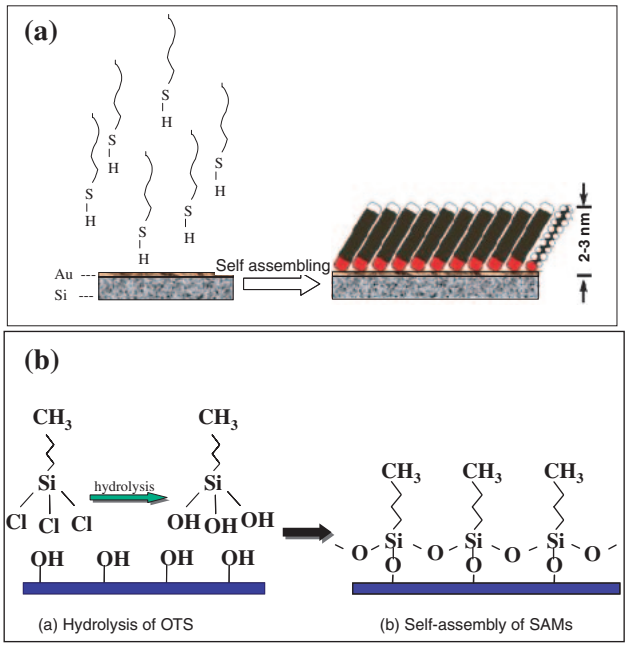

Figure 1. Schematic description of structure and formation process of (a) thiol-type and (b) organosilane-type on Au and Si surfaces, respectively.

agglomeration. The surface tension and volume force govern the size and size distribution. Adsorption of ions or molecules from the dispersion solution depends on the characteristics of the surface, most particularly on the electrostatic charge density and on the structure of coordination sites. Because of the presence of hydroxy groups, the surface of ceramic oxide formed in solution is usually electrically charged. The charge on the surface may be positive, negative, or zero depending on the nature of oxides and the solution environment, and gives the surface an acid, basic, or neutral characteristic, respectively. The surface acidity, represented by point of zero charge (PZC), is basically dominated by the nature of oxides, electronegativity of the cation, crystal structure and morphology, and chemical composition of particles, but still changes with the solution conditions of pH or adsorbed species.[69a] The charge of the cation affects the polarization of oxygen in the surface groups (ex. M–OH, $M–OH_2^+$, and $M–O^-$), resulting in electron transfer between cation and oxygen. Most of the SAM surfaces are also positively or negatively charged depending on the surface functional groups and the solution conditions. Such surface charge characteristics of SAMs are related to acid–base properties of SAM terminals for ionic groups and the adsorption capability for nonionic groups.[70a] Functional terminal groups such as carboxylate ($–COOH \rightarrow –COO^- + H^+$), sulfate ($–OSO_3Na \rightarrow –OSO_3^- + Na^+$), and sulfonates ($–SO_3H \rightarrow –SO_3^- + H^+$) may dissociate protons or cations in solution, which leaves behind a negatively charged surface, whereas amines ($–NH_2 + H^+ \rightarrow –NH_3^+$), and ammonium ($–NR_3Br \rightarrow –NR_3^+ + Br^-$) may carry positive charges.[70a] Nonionic groups such as methyl in octadecyltrichlorosilane (OTS) and thioacetate may carry weak positive charges by preferential adsorption of anions from solution.[70a]

The acid–base properties and zeta potentials of a variety of SAM surfaces have been investigated by Shyue et al.

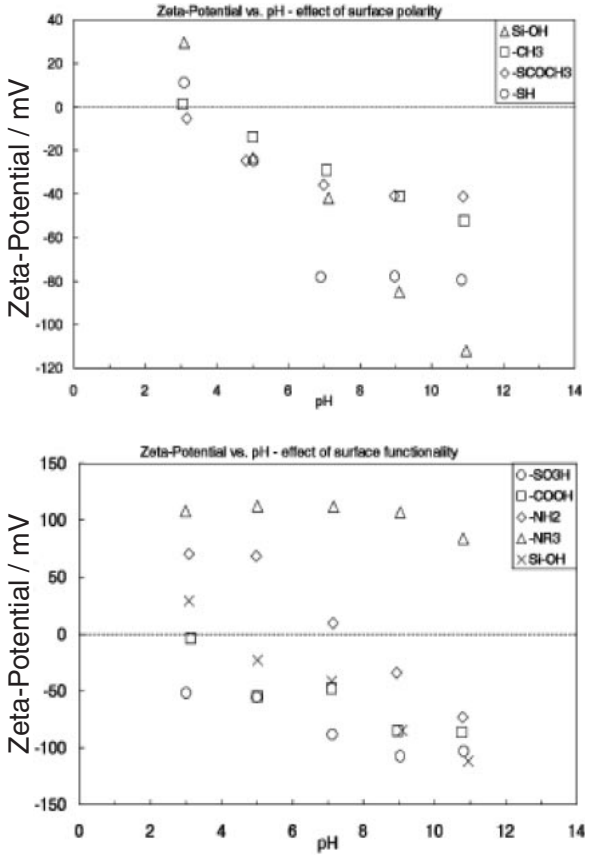

Figure 2. Zeta potential of SAMs of (a) nonionic surfaces and (b) ionic surfaces.[71a]

(Figure 2).[71a] The acid–base characteristics of amine- and sulfonate-SAMs, as revealed by XPS studies, differs significantly from that of these groups in diluted solution, with the observed pK_a differing by about 7 units from that of the diluted system. Moreover, the degree of protonation or deprotonation changed more gradually with pH than those in solution. The zeta potentials of ionic SAMs (±50–100 mV) were much higher than nonionic SAMs (±0–40 mV). Nonionic OTS and thioacetate showed a moderate negative zeta potential, suggesting preferential adsorption of negatively charged species. Alkylammonium SAMs showed a strong positive zeta potential at all pH values; comparably, sulfonate groups showed a highly negative surface charge at high pH. The weakly acidic carboxylate SAMs only showed a negative surface charge in mildly acidic and basic environments. The zeta potential of amine switched from positive to negative with the pH shifting from acidic to basic despite its intrinsic positive property.[71a]

Surface force apparatus (SFA)[72] and atomic force microscopy (AFM)[73,74] are used for measuring forces between two macroscopic surfaces or between a fine tip and a surface, respectively. Tang and DeGuire reported experimental results on the measurement of the interaction between a ZrO_2 particle and the SAM surface.[71b] They attached 20 micron ZrO_2 particles to a cantilever of an atomic force microscope and measured the interaction between the particle and a sulfonate-SAM surface on Si. The jump-in distance and adhesive force were measured in KNO_3 solutions with the pH ranging from 2 to 9 and ionic strength ranging from 0.45 M to 4.5×10^{-5} M. The observed forces in all cases were larger for sulfonate SAM-covered silicon than that for bare silicon. With the sulfonate surface, the force was repulsive at high pH and attractive at low pH, and it increased with decreasing pH and ionic strength. Experimental results were in most cases consistent with predictions from DLVO theory, indicating that DLVO forces play a key role in the interactions between these surfaces under such conditions.

The Derjaguin–Landau–Verwey–Overbeek (DLVO) theory[70] has been frequently used for explaining the interaction between particles and substrate surfaces, which can also be used to explain the formation mechanism of the deposition of ceramic thin films from aqueous solutions.[41,43a,71b] The DLVO model is derived from an energy balance composed of attractive and repulsive interactions and has historically described the interaction and behavior of surfaces and colloids. In recent years, attention also has been paid to non-DLVO forces in colloid systems (hydration forces, hydrogen-bonding and hydrophobic interactions, non-charge-transfer Lewis acid base interactions, and steric interactions), which implicate the structure of water.

Some mechanisms have been proposed for understanding the formation mechanism of oxides on SAM surface in solution. It is generally considered that the interactions in film formation include van der Waals forces, electrostatic forces, hydrophobic–hydrophilic interactions, and the generation of chemical bonds (either covalent or hydrogen bonds) (see most of the papers on SAM-assisted oxide formation). In all these cases, surface properties play an important role in film formation, either by surface-promoted heterogeneous nucleation or by physical or chemical attraction of preformed solids in solution. The accurate understanding of the film formation mechanism may help to optimize film formation conditions for tailoring film deposition behavior and film performance (microstructure, density, crystallization, size, and size distribution). Bunker et al. proposed ion-by-ion growth for the heterogeneous nucleation on the SAM surface or old nuclei/particle.[47f] Shin et al. suggested that film was grown by attachment of homogeneous nuclei/clusters formed in solution.[43a] Even particle growth itself is also dominated by adherence of nuclei/clusters rather than by ion-by-ion growth.[43a] The existing two mechanisms are not independent but may operate at different stages of a deposition process, which was confirmed in our experiments and will be discussed later. Because heterogeneous nucleation is kinetically favorable, the surface-induced heterogeneous nucleation may govern deposition at low supersaturation (for example, the so-called induction period), while at high supersaturation, nucleation occurs on almost all surfaces regardless of their energy state. The morphology of the particles existing in the film is much different from that observed in the precipitate after deposition; the former is much smaller than the latter. This finding suggests the difference in growth behavior: only small-sized clusters or particles were attracted to the substrate surface, while serious coagulation occurred between clusters or particles in the solution. Although not clearly, the result reveals the complexity of the solution deposition process, indicating the interdependence of solution conditions and surface functionalities, and implying different mechanisms operate in different systems.

2.4 Nucleation and Crystal Growth in Aqueous Solutions. 2.4.1 Nucleation and Growth: The precipitation of a solid phase is related to the surface bearing specific functional groups and the solution conditions. Initial nucleation can occur either in solution (homogeneous) or on the surfaces of a substrate (heterogeneous), depending on the net interfacial energy of the system. If the interaction between the growing nucleus and a substrate surface represents a lower net interfacial energy, heterogeneous nucleation is favored over homogeneous nucleation.

The classical theory for nucleation and crystal growth[75] indicates that the free energy change associated with the precipitation of an inorganic cluster from solution onto a surface is given by

$$\Delta F = -nk_{\mathrm{B}}T\ln S + \gamma_{\mathrm{il}}A_{\mathrm{il}} + (\gamma_{\mathrm{is}} - \gamma_{\mathrm{sl}})A_{\mathrm{is}} \quad (1)$$

where S represents the degree of supersaturation in the solution; n is aggregation number; k_{B} is Boltzmann's constant; T is temperature; γ_{il}, γ_{is}, and γ_{sl} represent the inorganic/liquid, inorganic/substrate, and substrate/liquid interfacial tension, respectively; and A_{il} and A_{is} represent the corresponding interfacial areas. When the net interfacial energy for the nucleation on the substrate is lower than that for inorganic/solution interfacial energy, that is, $(\gamma_{\mathrm{is}} - \gamma_{\mathrm{sl}})A_{\mathrm{is}} < \gamma_{\mathrm{il}}A_{\mathrm{il}}$, heterogeneous nucleation is favored over homogeneous nucleation. This is the case for the thermodynamically controlled formation of a solid. At high levels of supersaturation, homogeneous nucleation dominates the formation of a solid phase. The generation of particles begins with the formation of tiny nuclei in a supersaturated medium followed by growth. The free energy of a spherical nucleus with radius r can be described as follows:[76]

$$\Delta G = \Delta G_{\mathrm{s}} + \Delta G_{\mathrm{v}} = 4\pi r^2\gamma + 4/3\pi r^3\Delta g_{\mathrm{v}} \quad (2)$$

where γ stands for the surface tension between the two phases and Δg_{v} is the difference in the free energy per volume unit between the two phases. ΔG as a function of r reaches the maximum, where the corresponding radius of r^* is defined as the critical nucleus radius. Nuclei with a radius smaller than r^* will redissolve, while nuclei with a radius exceeding r^* will grow further.

The classical nucleation theory is based on a fundamental assumption that prior to reaching supersaturation that initiates the nucleation the system can be treated as homogeneous; that is, the components are present in a molecularly dispersed state. The present knowledge of nucleation[77] however, suggests the existence of a subcritical nucleus, the so-called precursor. The nucleation and particle growth process is not only dependent on the incorporation and loss of individual basic blocks (atoms, ions, monomers, and molecules), but it also relies on the interaction among precursors, or between clusters each other, which also contributes to the nucleation. No nucleation occurs in a solution with low supersaturation, homogeneous nucleation occurs at high supersaturation, and film formation via heterogeneous nucleation is possible in the intermediate supersaturation region called a "window." The precipitation of a solid phase involves four kinetic steps:[69] (1) formation of a zero-charge precursor; (2) creation of nuclei; (3) growth of nuclei; and (4) aging of the particles in the suspension. For a monocation system, when the solution becomes supersaturated, the interaction between soluble precursor molecules generated by the hydrolysis reaction drastically changes to be slightly attractive. Molecules continue to move, but a certain probability of collision could give rise to the formation of clusters of molecules, a solid phase. Whether the cluster can further grow or not is dominated by the relative energy state, exhibiting random fluctuation. The free energy difference between the liquid and the solid is the driving force toward the formation of a solid, whereas the surface tension results in redissolution of the existing clusters. Both of them are correlated with the radius of the cluster. Once the radius of the cluster is over a critical value, the total free energy begins to decrease and the stable nucleus is formed. Creation of nuclei occurs through the condensation of the zero-charge precursor and is closely related to the precursor concentration. At lower supersaturation, the condensation rate is almost zero; once the precursor concentration exceeds a critical concentration C_{min}, the condensation rate increases abruptly and polynuclear entries: the nuclei are formed in an explosive manner throughout the solution.

Growth of nuclei is controlled by mass transport and by the kinetics of the addition and removal of individual species such as atoms, ions, or molecules to and from the particle surfaces. Ostwald ripening is generally the major mechanism of crystal growth. However, in certain nanophase materials under some conditions, aggregation-based growth was reported to occur in the formation of TiO_2, ZnO, and others.[78,79]

Crystallization and morphology control are two issues involved in the growth process. Growth through crystallization or the formation of an amorphous state is a complex issue. The Ostwald rule declares that the phase formed by nucleation is not necessarily the thermodynamically most stable structure but is the structure whose free energy is closest to the melt.[76] Although the amorphous phase is a thermodynamically metastable state, it is probably kinetically stabilized because the system is constrained to evolve without heating or other induction and may not transform to the lowest activation energy path. For a solution deposition process, it is important to understand how to suppress or control the transformation from one structure to another energetically more favorable structure because both of these two structures, amorphous or crystalline, are crucial for some specific applications. Investigations of the biomineralization process make it possible to answer this question, considering that living organisms have been able to regulate the structural transformation with the aid of proteins. Additives also influence nucleation and crystallization processes.[80–83] Additives can be ions and low molecular weight molecules such as surfactants, nanoparticles (seeds), and neutral or other soluble polymers and they may promote or suppress the nucleation and growth process, form the oriented crystals, or modify the morphology of the particle. An example is ZnO, which has been found to be present in different morphologies, typically from rods,[83–85] wires,[86] and tubes,[87] to more complex architectures.[88,89] These structures can be obtained by regulating the solution conditions, such as pH, concentration, temperature, precursor chemistry, or by addition of a trace of additives.[83–89]

2.4.2 Aqua Chemistry for Solid Deposition: The degree of supersaturation has obvious effects on the formation and

growth of nuclei, the nucleation mechanism, morphology, crystallinity, and the control of film properties (such as thickness, density, transparency, and refractive index). In solutions encapsulated within preformed supramolecular assemblies, the regulation of supersaturation conditions can generally be achieved by facilitated ion flux, complexation–decomplexation switches, local redox and pH modifications, and changes in local ion activities via ion strength and vectorial water fluxes.[90] Under these conditions, the kinetics of surface-mediated processes can influence phase transformation and aggregation in crystal growth. In most cases, chemical reactions and experimental conditions (concentration, temperature, acidity, nature of the anions, etc.) dominate this process.[69] Hence, by design of various chemical reactions, such as local redox, hydrolysis–condensation, and ligand-exchange, the supersaturation degree of the solution can be purposely adjusted. Among these, most usually involve aqua chemistry and hydrolysis–condensation reactions.

The formation of a solid phase from solutions is a result of a process of inorganic polycondensation involving the hydrolysis of metal ions and the condensation of hydroxylated complexes. In aqueous solution, all ions are hydrated to some extent by the formation of a hydration sphere of water molecules around the central atom even for the halide anions.[91] In very high oxidation states, the positive charge on the central atom increases to such an extent as to polarize the coordination water, resulting in spontaneous deprotonation by free water acting as a base and the formation of oxo and/or hydroxo species, which is related to another concept of hydrolysis of metal ions.[91] Jolivet and co-workers have developed a partial charge model, a guide for understanding the behavior of metal ions in solution, including hydrolysis, condensation, complexation, and formation of the solid phase along with control of its characteristics (such as morphology, orientation of crystals, polymorph, and size).[69a] They state that when two atoms combine partial electron transfer occurs so that each atom acquires a positive or negative partial charge, which results in the increase or decrease in the electronegativities of related atoms. Electron transfer continues until the electronegativities of all the constituent atoms become equal to the mean electronegativity.[69a] Two main mechanisms as schematically shown below are involved in the condensation of cations: olation reaction and oxolation reaction take place by the formation of hydroxo bridges (ol bridges) and oxo bridges, respectively.

$$\text{Olation:} \quad \text{M–OH} + \text{–M–OH}_2 \rightarrow \text{M–OH–M–} + \text{H}_2\text{O} \quad (3)$$

$$\text{Oxolation:} \quad \text{M–OH} + \text{HO–M} \rightarrow \text{M–O–M} + \text{H}_2\text{O} \quad (4)$$

The electronegativity of the elements influences the condensation through the mechanism of either olation or oxolation.[69a] Four critical values, $\chi_{B,z}$, χ_{Ol}, χ_{PA}, and χ_{A}, separate the charge-electronegativity diagram into five domains (B, z, Ol, PA, and A means base, formal charge, olation, polyacid, and acid, respectively). When χ/M (the electronegativity of hydrolyzed cation) $> \chi_{A}$ or $\chi/M < \chi_{B,z}$, condensation in the solution cannot occur and the element will exist as a monomeric cation or anion. $\chi_{B,z} < \chi/M < \chi_{Ol,z}$ limits a domain where cations may condense through olation only and form stable hydroxides (e.g., Al and Zn). If $\chi_{Ol,z} < \chi/M < \chi_{PA,z}$, condensation may occur through both olation and oxolation and lead to oxyhydroxides Fe^{III} or to oxides Ti^{IV} depending upon the relative rate of olation and oxolation. Elements for which $\chi_{PA,z} < \chi/M < \chi_{A,z}$ will condense through oxolation, leading to polyacid formation. According to this model, the calculated partial charge for the water molecules ($\delta(H_2O)$) is closely related to the tendency of the metal ions to form either an oxide precipitate or a mixed hydroxide/oxyhydroxide precipitate.[69a] Take the Zr^{IV} as an example. For the aqua ion of zirconium, $\delta(H_2O)$ is positive, such that the water molecule is repelled by the metal center and allows the oxo bridge formation. Hence, zirconium will hydrolyze and condense to generate zirconium oxide or oxyhydroxide depending on the solution conditions. The electronegativity–pH diagram[69a] for the aqua ion of $Zr_4(OH)_8(OH_2)_{16}{}^{8+}$ suggests that Cl^- is retained in the solid of zirconia when it is precipitated at higher pH. The sulfate ion is easier to complex with zirconium than is Cl^- and can form various complexes of zirconium over a wide range of pH values. Significant amounts of impurities such as Cl^- or $SO_4{}^{2-}$ should be easily embedded in the ZrO_2.[92,93] At higher pH, the sulfate group, weakly coordinated to the metal ion, is easily replaced by other anions.[12] In an aqueous solution containing zirconium sulfate and urea, a basic zirconium carbonate ($Zr_2(OH)_6CO_3 \cdot 2H_2O$) can precipitate.[94] F^- also has a strong ability to form complexes in solution with many metal ions such as Si^{IV}, Ti^{IV}, and Zr^{IV}; precipitation of F into the corresponding oxides via the LPD method has been well-known.[95]

2.4.3 Morphological Evolution in Solution: Control of crystalline phase, morphology, and microstructure has attracted a great amount of interest from the viewpoint of fundamental studies and practical applications because these characteristics are closely correlated with optical, electric, chemical, and catalytic properties. Treating in solution affords possibilities to achieve all or some of the above properties during the nucleation and growth process. As interesting and useful materials, ZnO and TiO_2 have been synthesized in solution with fine control over their crystalline and morphological features. Several solution systems have been reported to be effective in the growth of ZnO crystals either in solution or on substrates.[80,81k,81j,83–88,96–123] The most well-known work was conducted by Vayssieres, who successfully prepared ZnO rods, tubes and their arrays on glass substrates from a solution containing equimolar $Zn(NO_3)_2$ and hexamethylenetetramine (HMT, $C_6H_{12}N_4$) at 90–95 °C.[84,85,97,98] This method was further extended to produce other films with well-ordered structures.[99] Yan et al. conducted a series of research on morphology control of ZnO in solution by hydrothermal treatment of $Zn(NH_3)_4{}^{2+}$ or $Zn(OH)_4{}^{2-}$ precursors in various solvents including microemulsion; the process led to the production of ZnO with tubular, rod or complex microstructures.[88,100,101] Liu and Zeng synthesized ZnO nanorods by using zinc salts, NaOH and ethylenediamine at about 25 °C.[102] A ring-like ZnO was also produced by using a flake precursor zinc hydroxide chloride hydrate ($Zn_5(OH)_8Cl_2 \cdot H_2O$) and ammonia at 120 °C.[103] Masuda et al. achieved site-selective crystallization and patterning of ZnO with different morphologies and crystallographic characteristics on self-assembled monolayers from an aqueous solution of zinc acetate and ammonia.[104] Yin and Sato obtained an unique nanoscrew-shaped ZnO by

treating a low-concentration $Zn(NO_3)_2$–HMT solution for a long time.[105] Time-dependent study suggests that the formation of the nanoscrews was mainly controlled by an aging effect, which resulted in partial dissolution and recrystallization occurring simultaneously but on different sites of the particle.[105] We have also carried out the morphology-controlled growth of ZnO films on a seeded conductive glass from solutions using zinc chloride and HMT/ammonia as raw materials.[85] Arrayed ZnO nanorods were perpendicularly aligned with high number densities and tuned slenderness ratios. Organic additives such as citric acid or some surfactants have been also involved in the crystallization of ZnO in solution.[83,106] These additives can change the crystallization habits, resulting in the production of abundant hierarchical structures. A biomimetic process that uses organic additives (soluble polymers or amino acids) to modify the growth of ZnO can develop various ZnO crystals from solution.[80,81k,81j,107–115] The polymer has been considered to be adsorbed to different crystallographic planes of ZnO nanocrystals, which changes the nucleation and subsequent growth rate along specific orientations and should be responsible for the generation of hierarchical structures. The formation of ZnO crystals with various morphologies and crystallographic characteristics are closely linked to the reconstruction of inorganic-polymer intermediates, anchoring and desorbing of polymer molecules, and Ostwald-ripening effect.

Control of the morphology of ZnO particles can be achieved by both a thermodynamic and a kinetic process, but in most cases that is through a kinetic manner by controlling the formation of zero-charge precursors; this stage can be realized by controlling either the amount of base in a reaction medium or the amount of Zn^{II} species.[116] The latter was realized by controlling a starting concentration of Zn^{II} at the beginning of reaction or through slow release of chelated Zn^{II} species in a basic solution in the later period of the reaction.[117] Slow release of Zn^{II} was usually brought about by sagaciously selecting a chemical agent that favors stabilizing free Zn^{II} by forming Zn^{II} complexes. It can be also possible to modify the dissolution–recrystallization process such as the Ostwald-ripening effect and make it favorable for kinetic control. The Ostwald-ripening effect may result in partial dissolution of some crystallographic planes or some sites of the same crystallographic planes, so as to give ZnO with different morphologies and crystalline characteristics.[87,105,118,119] This process somewhat resembles that of a top-down reconstruction. In $Zn(NO_3)_2$–HMT solution, a rod-shaped ZnO formed at the early stage of the reaction has been observed to become nanoscrews,[105] nanotubes,[87] and even nanoplates[119] after a long time aging. The ions in solution can interact with the primarily formed nanocrystals at specific reaction sites, in most cases demonstrates preferable dissolution of the (002) crystallographic plane. These interactions lead to the formation of hierarchical structures, large particles or transforming to more stable polymorphs.[105] In a reported case, $[Zn(NH_3)_4]^{2+}$ and NH_4^+ may randomly diffuse to the surface of preformed ZnO crystals and was selectively adsorbed on specific crystallographic planes, eroding the corresponding crystallographic planes and preventing from anchoring new ions.[105]

The crystallization-growth behaviors can be also be modified by partially promoting or inhabiting the growth of some crystallographic planes, by the adsorption of ions,[83,85,106] a typical bottom-up process. A designed chemical environment is therefore important. As reported previously, the NH_3 in solution can decrease the encounter probability of the nucleus, prohibiting the growth of particles.[88]

Several works of ours have been conducted to pursue the morphology evolution and to clarify a complex problem derived from the metamorphic features in the morphology of ZnO during soaking in aqueous solutions.[85,109,121] The studies have shown that both specific solution chemistry and treatment parameters such as temperature, time, and pH have effects on the growth by selective promotion or prohibition of some characteristically crystalline planes.[85,109,121] With a solution containing hexamethylenetetramine and ammonia, the solution pH can be controlled by releasing OH^- from the decomposition of hexamethylenetetramine during incubation. The changes can afford abilities to regulate the degree of supersaturation, which can alter the progressing of both nucleation and crystal growth. Nanowire-aligned films with controlled ratios for length/diameter of wires have been synthesized by purposely changing the concentrations of starting materials (Figure 3).[85,120] The crystalline morphology can be also regulated by an aging process (Figure 4).[121] In this stage, a dissolution–recrystallization[84,87,88,97–103,105] and/or an aggregation-based mechanism[81k,81j,105–109,113,116] dominates the reconstruction of ZnO with unique crystalline morphologies. With a low concentration of ammonia, a film with particles of cone-shaped tips can be obtained (Figures 4A and 4B). After soaking for different times either isolated single crystalline cone-shaped ZnO or a dense transparent ZnO layer can be grown on a ZnO-seeded F-doped SnO_2 substrate (FTO) (Figures 4E and 4F).[121] The individual ZnO cones were found to be able to dissolve again with prolonged soaking time, accompanied by transformation from single crystalline to polycrystalline states, suggesting reversibility.[121] The dense ZnO layer about 4 μm in thickness, shows a transparency of above 70% in the visible range, and is promising for optoelectronic applications (Figures 4C and 4D).[121] The findings reveal that one can purposely optimize the morphology, crystallography, and organization to pursue special properties by kinetically controlling the nucleation and crystallization process.

A similar consideration can also be extended to the case of TiO_2, an interesting and useful inorganic.[122,123] A supersaturated aqueous solution containing peroxotitanium complex ions was prepared to synthesize TiO_2 and its precursors in solution under mild conditions. The conditions including pH, concentrations of titanium and incubation temperatures have important effects on the nucleation and growth along with the crystalline and morphological evolution. At room temperature, precipitates were amorphous,[122c] and can transform to anatase at 250 °C.[122b] Figure 5 shows the surface and cross section of the film after annealing. The morphology of the deposited film can be regulated by chemical kinetics, which was partially controlled by solution conditions.[122a] Porous films with various morphologies from particulate to curved-sheet were prepared on different substrates including Si, polymers, and glass (Figure 6).[122a] It shows the morphology of these films prepared

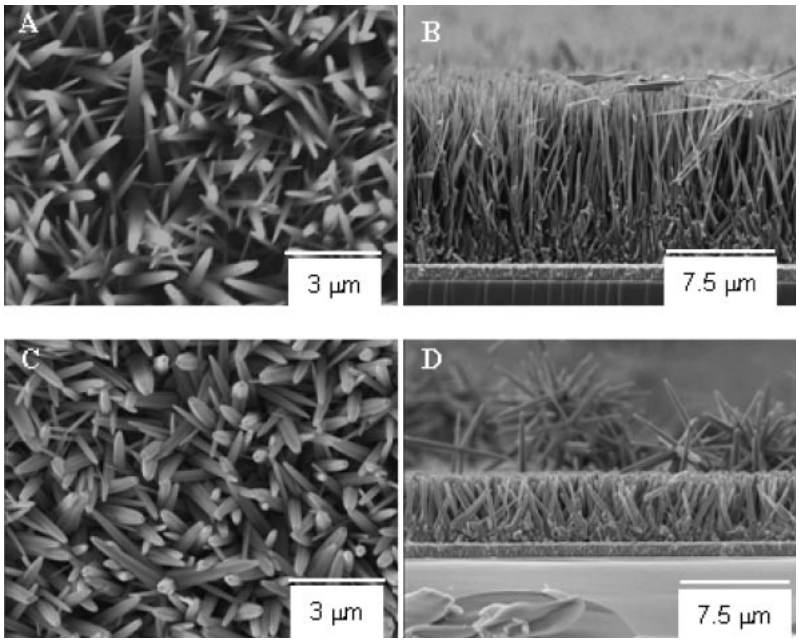

Figure 3. SEM micrographs of ZnO nanowire films prepared from a solution containing 20 mM $ZnCl_2$ and hexamethylenetetramine with different amounts of ammonia. (A), (B): 5 mL; (C), (D): 2 mL.[121]

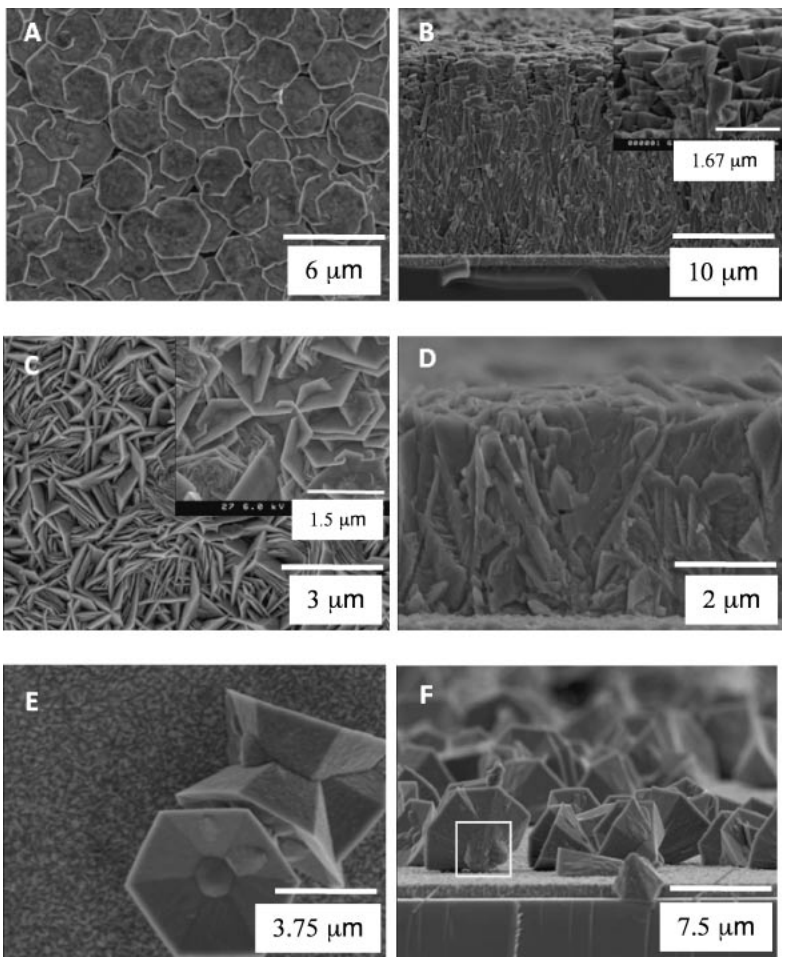

Figure 4. SEM graphs of ZnO films obtained from 0.02 M $ZnCl_2$/HMT solution at 95 °C: A, B: containing 5 mL of NH_3 for 97 h; C, D: containing 7 mL of NH_3 for 72 h; and E, F: containing 7 mL of NH_3 for 97 h. The scale bar for image inset of B and C is 1.67 and 1.50 μm, respectively.[120]

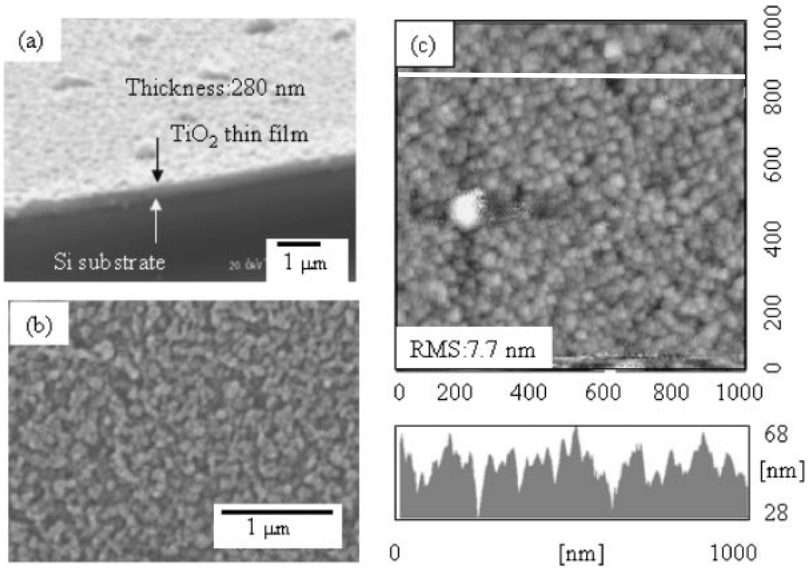

Figure 5. Cross-sectional SEM photograph (a), surface morphology (b) and topography (c) along with height profile along the corresponding line shown in the image for the TiO_2 thin film (corresponding thin film obtained after soaking for 24 h after annealing at 700 °C for 2 h in air.[122b]

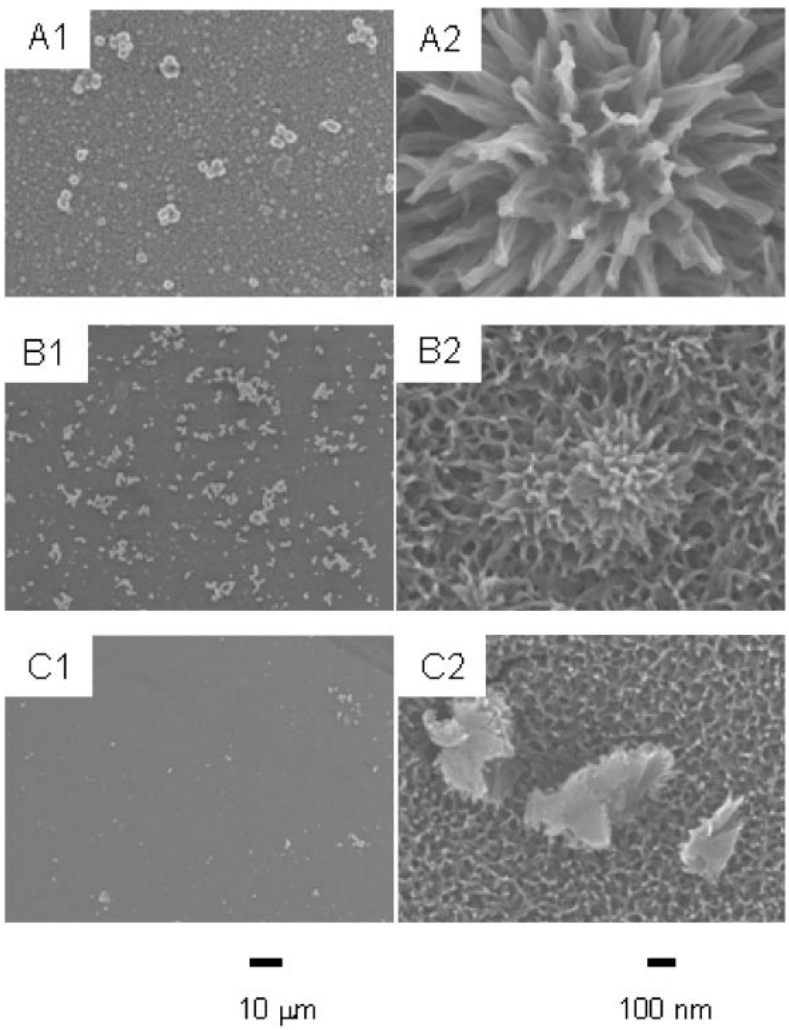

Figure 6. SEM photographs of TiO_2 precursor films deposited at 95 °C for 24 h in 5 mM peroxotitanium complex solutions with different pH (A1, A2: pH 1.0; B1, B2: pH 1.5; C1, C2: pH 2.0).[122a]

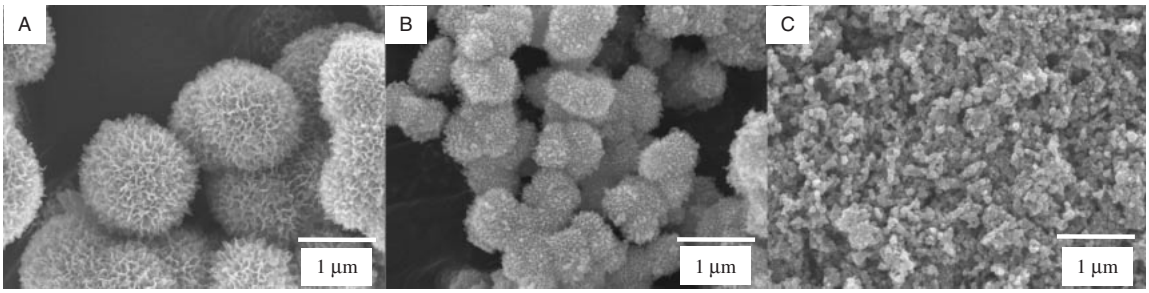

Figure 7. SEM graphs of TiO_2 powders after annealing of those obtained under different pH; A: pH 1.0, B: pH 1.5, C: pH 2.0; the scale bars are 1 μm.[122a]

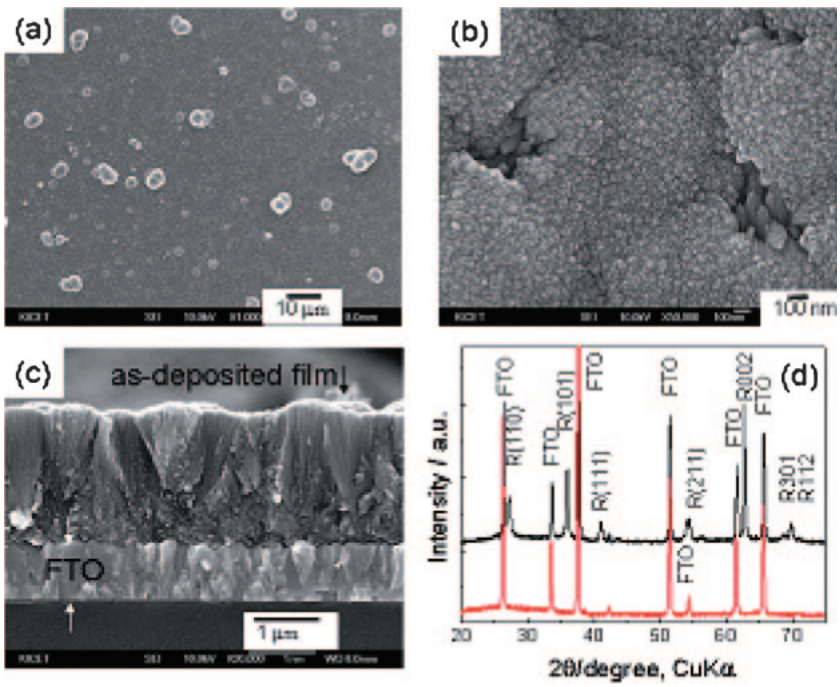

Figure 8. SEM micrographs (a–c) and XRD patterns (d) of TiO_2 thin film prepared on a glass substrate pre-coated with a transparent conducting oxide (FTO) layer. (a): low-magnification; (b) high-magnification; (c) cross-sectional. R refers to the rutile phase. The red XRD pattern is for the FTO substrate.[123]

under different pH. Porous microstructures of films permitted us to prepare a crack-free film 2–3 μm thick. These films were still amorphous under the treatment conditions. Figure 7 shows the corresponding postannealed powders obtained under different pH. Dye-sensitized solar cells using annealed (anatase) films of different morphologies as electrodes gave conversion efficiency ranging from 1.3–3.1%.[122a] Improvement of performance may be achieved by either increasing the film thickness or inducing crystallization in solution.[122a] Solar cells using TiO_2 nanoporous films demonstrated high performance, namely overall conversion efficiency of 3.1% (AM1.5) for a 3-μm thick film.[122a] For further optimizing the film properties, efforts are being made to address the following questions, including in situ crystallization, preparation of one-dimensional arrays, increasing the film thickness and optimizing the adherence of films to substrates. By increasing the temperature of solution to 90 °C, the rutile film can be crystallized at pH 1.[123] Figures 8 and 9 show the morphology and X-ray diffraction pattern of the rutile film.

3. Preparation of SAM Templates

3.1 SAM Preparation. In general, SAMs can be fabricated through chemisorption of organic molecules to solid surfaces through either the liquid phase[124,125a–125c,126] or the vapor phase.[125d–125n,127] The hydrolyzed organosilane bonds to the native silica layer of p-Si substrate by the formation of a covalent siloxane (Si–O–Si) bond, and they condense with each other, creating a SAM with a functional terminal group.[124,126a] The cross linking and van der Waals interactions between chains stabilize the highly ordered, two-dimensional arrangement of SAMs.[124,126a] In a silanization reaction, the hydrolysis of silanes determines the overall reaction speed and depends on the reactive groups bonding to Si atoms in silanes. It decreases in the order $Cl > OCH_3 > OCH_2CH_3$.[125e]

A schematic description of the SAM formation process is shown in Figure 10. P-type Si(100) wafers employed for the substrates were cleaned ultrasonically in acetone, ethanol, and deionized water, followed by immersion in boiling water

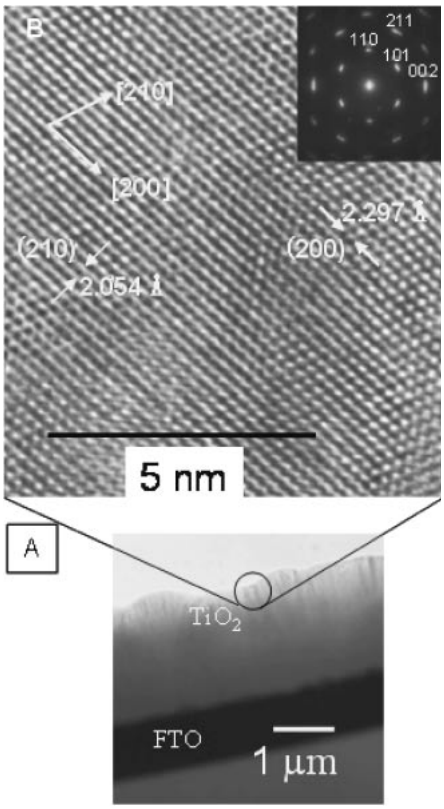

Figure 9. HRTEM graphs of a rutile TiO_2 film along [211] direction. A: low-magnification cross-sectional image; B: high-magnification image.[123]

for 5 min. After being dried at 50 °C in air, the substrate was exposed to UV light for 2 h. SAM materials were organosilanes such as heptadecafluoro-1,1,2,2-tetrahydrodecyltrichlorosilane, octadecyltrichlorosilane (OTS), and phenyltrichlorosilane (PTCS). SAMs were prepared by immersing the cleaned and dried substrates into an anhydrous toluene (99.8%, water <0.002%) solution containing 1 vol % SAM materials for 5 min under an N_2 atmosphere. The hydrolyzed organosilane bonded to the native silica layer of p-Si substrate by the formation of a covalent siloxane (Si–O–Si) bond, creating a SAM with a terminal CH_3 group.[126] After being dried under N_2 atmosphere, the substrates with SAMs were then baked at 120 °C for 5 min to remove residual solvent and to promote chemisorption of the SAMs. A detailed description of the SAM fabrication process appears in previous reports.[35,36,38,40] Selective modification of SAMs was conducted by exposing the sample to UV light through a photomask; photocleavage at the Si–C bond formed volatile (or removable) by-products, and an extremely reactive Si radical left on the surface immediately reacted with trace water to form polar functional silanol (Si–OH) groups.[126] The difference in physical and chemical properties of a patterned SAM suggests different nucleation/growth behaviors when the substrate was immersed in a deposition solution.

3.2 SAM Characterization. SAMs are extremely thin layers with a typical thickness of several nanometers depending on the molecular structure. Characterization of the SAM surface usually involves a series of surface analysis techniques, structural observations, and chemical/physical property measurements. Scanning electron microscopy (SEM) can be used for surface observations; patterned SAMs with different functional regions show image contrasts due to the difference in the lowest unoccupied molecular orbital (LUMO).[127] For

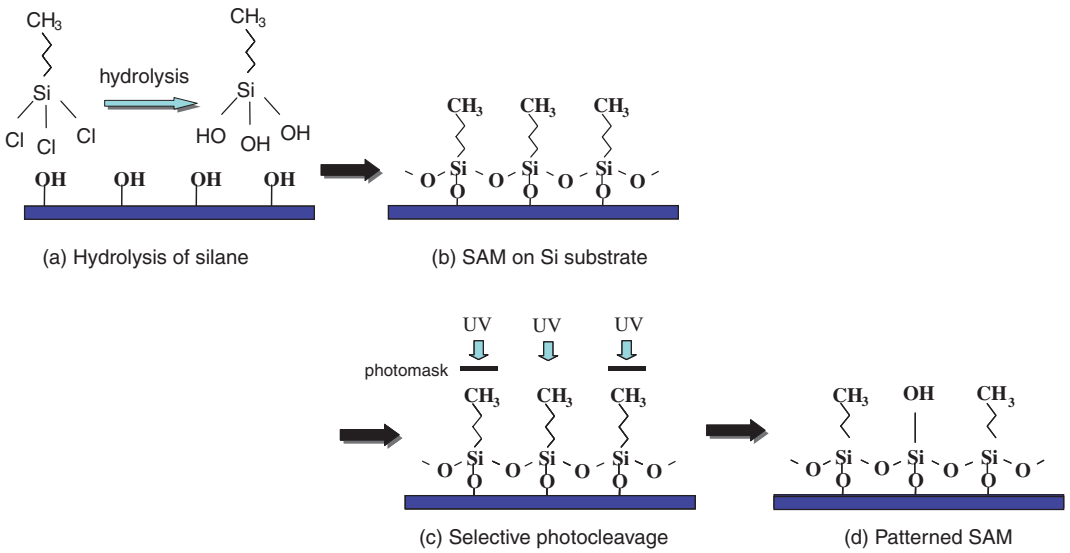

Figure 10. Illustration of SAM formation. (a) Octadecyltrichlorosilane hydrolyzed by the liberation of HCl. (b) SAM fabrication: the hydrolyzed organosilane bonded to the native silica layer of p-Si substrate by the formation of a covalent siloxane (Si–O–Si) bonds, creating a self-assembled monolayer (SAM) with a terminal of CH_3 group. (c) Selective modification of SAMs by exposing to UV light through a photomask; photocleavage at the Si–C bond formed volatile (or removable) products, and an extremely reactive Si radical left on the surface immediately reacted with trace water to form polar functional silanol (Si–OH) groups. This functionalized surface should be reactive to a variety of chemical coupling reactions, such as chemical adsorption of ceramic precursor from a solution. (d) Patterned SAM.

further detailed structure determination, AFM or scanning tunnel microscopy (STM) is needed.[124] TEM can also be used to confirm the success in preparation of SAMs and determination of the SAM thickness.[128] An ellipsometer can operate at ambient atmosphere for measuring the thickness along with the refractive index of SAMs.[129] Powerful synchrotron radiation techniques such as near edge X-ray adsorption fine structure (NEXAFS), X-ray adsorption near edge structure (XANES), and extended X-ray adsorption fine structure (EXAFS) also may be used for determining surface structures. Some common equipment in a chemical laboratory can be employed for the understanding of surface physics and chemistry of a SAM, including attenuated total reflection Fourier transform infrared spectroscopy (ATR-FT-IR) and grazing-angle spectroscopy,[130] secondary ion mass spectroscopy (SIMS),[131] ultraviolet (UV) spectroscopy,[132] X-ray photoelectron/Auger electron spectroscopy (XPS/AES),[133] fluorescence probes,[134] and scanning probe microscopy such as lateral force microscopy (LFM),[135] and Kelvin force microscopy (KFM).[136] A high-resolution mass sensing technique with nanogram sensitivity, quartz crystal microbalance (QCM),[137] is also involved in the characterization of the kinetics and dynamics of the formation of SAMs. In many of these applications, QCM is not a mass sensor but provides valuable information about reactions and conditions at the liquid–solid or gas–solid interfaces. Measurements of zeta potential[138] and (water) contact angles[139] are simple and widely used methods for the confirmation of the SAM formation and characterization of their surface properties. Other analysis techniques for characterization of SAMs are discussed in Ref. 124b.

3.3 Patterning of SAMs. There are several methods to pattern a SAM surface in the laboratory; they can be divided into two categories: site-selective modification[35,36,38,40,65,136,137] and direct patterning.[1,140] In site-selective modification processes, a SAM is prepared on the whole surface of a substrate first by chemisorption of molecules in either the gaseous phase or liquid solutions. The patterning of the SAM can be accomplished in situ without disrupting the monolayer by a number of techniques using additional energy sources. These techniques share almost the same mechanism; that is, organic molecules of SAM on the substrate surface undergo changes (energy conversion and/or chemical reactions, often irreversible) in a site-confined manner. In practice, these changes can be induced by mechanical, physical, optical, electrical, chemical, or magnetic means or a combination of them. Deep UV irradiation employs different lamps with wavelengths ranging from 354 to 157 nm. Mercury (Hg), excimer, krypton fluoride, argon fluoride, and F_2 lamps irradiate UV light of 354, 170, 193, 248, and 157 nm in center light wavelength, respectively. Selective photocleavage and/or photoinduced ozone can decompose the exposed areas, creating new functional terminals different from the original ones.[35,36,38,40,65,136,137] Recently, several techniques to pattern SAMs were reported. Photocatalyst-assisted photolithography,[65g] near-field scanning optical microscopy (NSOM),[136b] X-ray,[62] electron beam,[62a,63] ion bombardment,[64] and an STM or an atomic force microscope (AFM)[136c–136m] were shown to be effective for patterning of SAMs. Unlike the modification processes mentioned above, in which no ink is involved, microcontact printing (μCP), nanotransfer printering (nTP), and dip pen nanolithography (DPN) represent methods that combine high-resolution "stamps" or "pens" with SAM "inks" for patterning through direct writing of SAMs in the requisite areas.[1,140,141] In a μCP process, an elastomeric, patterned stamp is first inked by immersing the patterned face in an ink solution, and then it is dried and makes contact with the surface of a substrate. Ink, which may be SAMs, catalysts, colloid particles, proteins, and other chemical species, attaches to specific sites of a substrate, really replicating the pattern of the stamp.

These methods enable the patterning of a SAM surface with sizes ranging from micrometer to deep nanometer scale. Among the introduced methods for patterning of SAMs, almost all modification-related techniques and DPN methods show difficulties in patterning on unplanar surfaces. This problem has been partially resolved by using μCP or nTP. In addition, after SAM patterning the surface functionality of SAMs can be in situ transformed to other groups with various physical and/or chemical properties,[71a,138c,142] which may enable optimization of film deposition processes by the design of surface reactivity and allow an understanding of the interrelationships between film properties and surface functionality as well as structure configuration. Shyue et al. reported a wide variety of surfaces could be obtained by starting with a single surfactant, which was used to prepare alkyl bromide SAMs on Si.[71a] Various surfaces were created with terminal groups, including thioacetate, sulfonate, thiol, nitrile, dodecanoic acid, amines, which show different acid–base properties and zeta potentials of the surface. Li et al. reviewed methods for the transformation of functional groups of SAMs on flat gold surfaces.[138c] SAMs with various types of functional groups (headgroups) were bond to an Au surface and transformed to requisite groups by in situ chemical reactions. Transformation was started with functional groups such as amino, carboxylic acid, anhydride, and hydroxy. Some SAMs that were electroactive or photochemically active were easily modified through corresponding electrochemical or photochemical reactions.

4. Micropatterning of Inorganic Thin Films on SAM Templates

4.1 Introduction. Various kinds of thin films of metal oxides have been deposited on SAMs with different functional groups by bioinspired processess at temperatures lower than 100 °C. Representative are TiO_2,[35–37,39,42a,43a,45,122b,143–156] ZrO_2,[38,92,157–162] SnO_2,[42b,129,163–169] Y_2O_3,[170,171] ZnO,[172–179] La_2O_3,[180] Ta_2O_3,[181] iron oxides[182–187] including FeOOH,[47f,67,175–186] Fe_2O_3,[187] and Fe_3O_4,[182,183] along with complex oxides such as $SrTiO_3$,[40] $CaCO_3$,[68,188,189] apatite,[41,190a–190d] and others.[190e–190h]

In general, synthesis of monometallic oxides is usually a result of inorganic polycondensation involving the hydrolysis of metal ions in solution and condensation of hydroxylated complexes. The reaction behavior for different elements is significantly different because of the specificity in element chemistry. Preparation of polymetallic oxides, however, needs control of the formation of the polymetallic complex, which is crucial for the control of the stoichiometry. The growth of these films was mostly induced using a sulfonate-SAM with a terminal

SO_3H group, an amino- or phenyl-group-functioned surface, thiol-anchored SAMs on Au, or others, especially silanol groups derived from UV-modification of SAMs. Deposition of thin films from solutions requires control of the reactive process so that nucleation and growth occur preferably on surfaces rather than in solutions. The chemistry of precursors also influences the hydrolysis process. Solution conditions such as temperature, concentration, pH, and starting molar ratio influence the reactions that occur and the properties of the obtained films. For a proton-generated hydrolysis reaction, small differences in pH, temperature, or solution composition in terms of concentration and/or molar ratio can have a great effect on the solution's supersaturation and local chemical environment, significantly affecting growth rate, roughness, morphology, and sometimes crystallization and crystallographic orientation of the film.

In addition to solution conditions, film growth is also dominated by surface properties. Deposition is indeed restricted to some substrates, which makes it possible to fabricate a patterned film. Patterning of thin film on the SAM template directly in solution serves as an ideal system to understand solution and surface-interface chemistry for bioinspired processing of ceramic films.

Site-selective deposition (SSD) of thin films has been achieved and nano/micropatterns of them have been fabricated in our study. We proposed direct SSD of amorphous TiO_2 thin films using hydrolysis,[36a,36b,154,192–194] amorphous Ta_2O_5 thin films using hydrolysis,[181] amorphous SnO_2 thin films using hydrolysis,[163,168,195] amorphous TiO_2 thin films using a peroxotitanate complex deposition (PCD),[122b,122c] and amorphous $SrTiO_3$ thin films[40a,40b,196–198] (Figure 11a). A patterned SAM of octadecyltrichlorosilane (OTS) which has silanol groups and octadecyl groups was used as a template for the patterning of amorphous TiO_2 thin films. Amorphous TiO_2 was selectively deposited on silanol regions in the titanium dichloride diethoxide (TDD) solution using the hydrolysis reaction of TDD to produce micropatterns of thin films that had high feature edge acuity. TDD can form chemical bonds with silanol groups to form amorphous TiO_2 thin films, but cannot form chemical bonds with octadecyl groups. This difference was used for site-selective deposition. Additionally, the surface of hydrophilic silanol groups has many adsorbed water molecules, however the surface of hydrophobic octadecyl groups has fewer adsorbed water molecules. TDD needs water molecules to hydrolyze and thus amorphous TiO_2 thin films can be formed on silanol regions much faster than on octadecyl regions. Condensation between TDD and silanol groups and between TDD molecules releases water molecules, and this promotes further condensation. These two mechanisms, i.e., the difference in ability to form chemical bonds and the difference in adsorption of water molecules, are essential factors in the site-selectivity of this method.

A catalyst pattern was used for site-selective deposition to prepare micropatterns of ZnO[178,179,183] and Fe_3O_4.[182a,182b] (Figure 11b) This method uses a catalyst pattern as a template which induces the deposition of thin films. The feature edge acuity of micropatterns depends on that of the catalyst pattern, and thus high feature edge acuity of the catalyst pattern leads to high feature edge acuity of the pattern of thin films.

Homogeneous nucleated clusters or particles were attached to form films on SAMs by electrostatic interaction,[41,171,190a,199,200] hydrophobic interaction,[104,171] or interaction between thiol groups and metals[201] (Figure 11c). A patterned SAM having amino groups showing positive zeta potential and silanol groups showing negative zeta potential was used as a template. Homogeneously nucleated HAp particles or dispersed Ni particles which show negative zeta potential were adhered on amino groups by electrostatic interaction. This process is simple and effective for the deposition of nano/microparticles. HAp particle layers were further grown to form thin films in the solution. This technique can be used to prepare micropatterns of thin films or particle layers.

Additionally, site-selective elimination[202] was proposed as shown in Figure 11d. Site-selectivity resulted from the difference in adhesion strength of depositions. The patterned SAM having OTS regions and silanol regions was immersed in a solution containing a Ti precursor and subjected to ultrasonication during immersion. Heterogeneously nucleated TiO_2 and homogeneously nucleated TiO_2 particles adhering to the OTS-SAM could be easily eliminated from the substrate by ultrasonication, whereas those on silanol groups maintained their adhesion against mechanical vibration by ultrasonication. TiO_2 can form chemical bonds such as Ti–O–Si with silanol groups, but cannot form them with octadecyl groups, resulting in the difference in adhesion strength, which is the essence of the site-selectivity of this method. The site-selective elimination method can be used to fabricate nano/micro-scale patterns in the solution by immersing a substrate that has regions on which depositions adhere strongly and regions on which depositions adhere weakly, enabling elimination by treatment such as ultrasonication.

The concept of SSD using a seed layer[148] is shown in Figure 11e. We used a quartz crystal microbalance (QCM) to evaluate in detail the process by which anatase TiO_2 is deposited from an aqueous solution and found that its nucleation and initial growth were accelerated on amorphous TiO_2 thin films compared with on octadecyl, phenyl, amino, or hydroxy (silanol) groups. In this process, amorphous TiO_2 was shown to reduce the nucleation energy of anatase TiO_2 and provided nucleation sites for the formation of anatase TiO_2. Amorphous TiO_2 thin film was deposited on silanol regions of patterned OTS-SAM from TDD solution.[36a,36b,192,193] This substrate was immersed in an aqueous solution containing Ti precursor to be used as a template for SSD. Anatase TiO_2 was selectively deposited on amorphous TiO_2 regions to form thin films and thus a micropattern of anatase TiO_2 thin films was fabricated. The concept of SSD using a seed layer is to use a pattern of seed layers as a template which accelerates the deposition of thin films by the formation of nucleation sites, the reduction of nucleation energy, the promotion of film growth or other factors.

Moreover, site-selective immersion[35b] was proposed using a SAM with a pattern of hydrophilic and hydrophobic surfaces (Figure 11f). In the experiment, a solution containing Ti precursor contacted the hydrophilic surface, and briefly came in contact with the hydrophobic surface. The hydrophilic surface solution was replaced with fresh solution by continuous movement of bubbles, thus anatase TiO_2 was deposited and

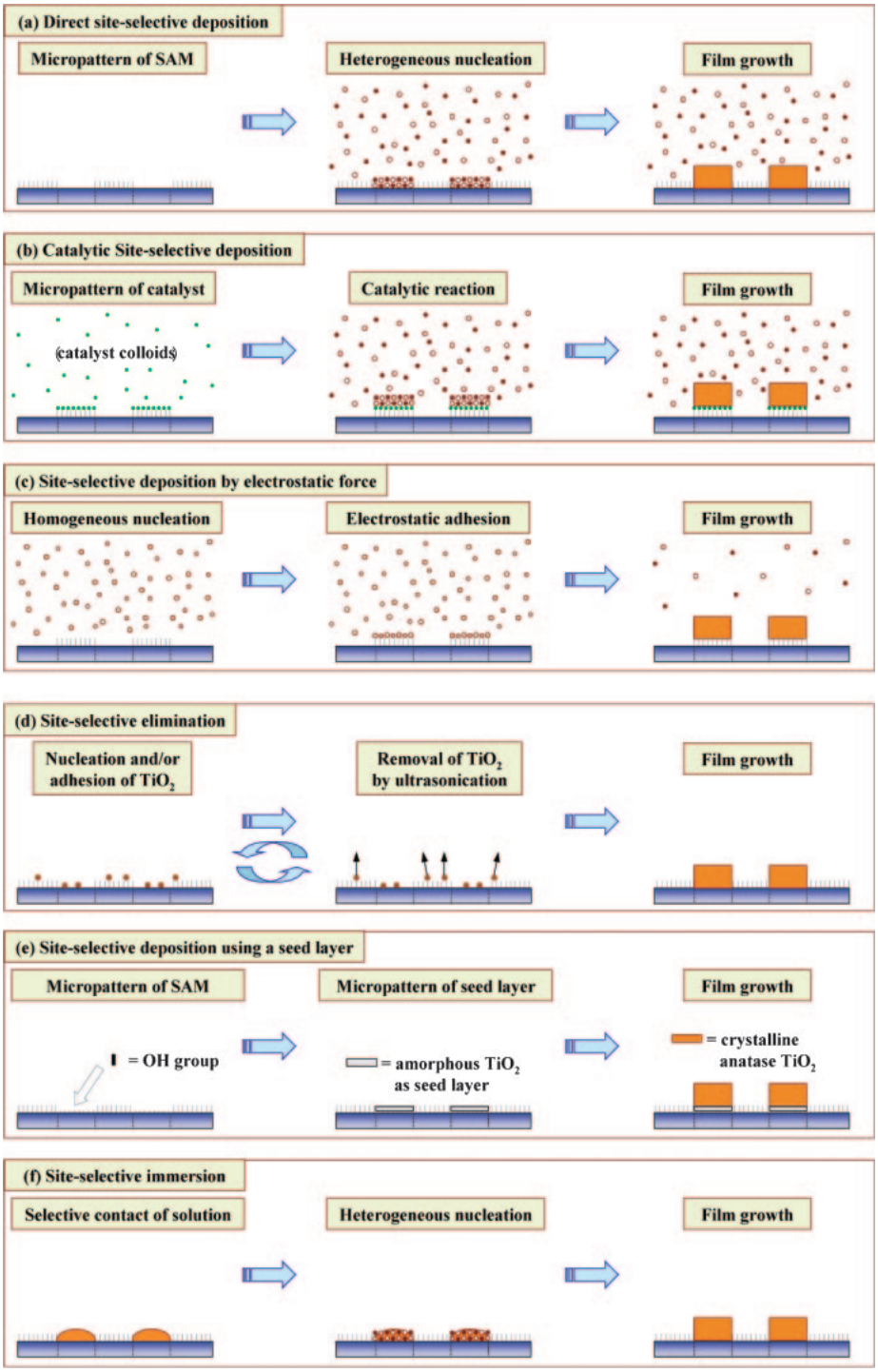

Figure 11. Conceptual processes for site-selective deposition of thin films by (a) direct site-selective deposition, (b) catalytic site-selective deposition, (c) site-selective deposition using electrostatic interaction, (d) site-selective elimination, (e) site-selective deposition using a seed layer, or (f) site-selective immersion.[191]

thin film was grown on the hydrophilic surface selectively. Site-selectivity in this process results from the difference in solution contact period. Other SSDs were achieved in solutions (Figures 11a–11e), however, site-selective immersion was conducted out of the solution. The immersion times of hydrophilic regions and hydrophobic regions were controlled to produce SSD. Though it is difficult to obtain a pattern with high feature edge acuity with this method, the technique can be used to fabricate any kind of micropattern provided film can be deposited from a solution.

4.2 Film Formation by Attachment of Homogeneously Nucleated Particles. 4.2.1 An Example of Apatite: Our research group investigated the different deposition behaviors of apatite onto planar substrates covered with amine (NH_2)/hydroxy (OH) terminated self-assembled monolayers (SAM) in a supersaturated simulated-body-fluid (SBF) by adjusting

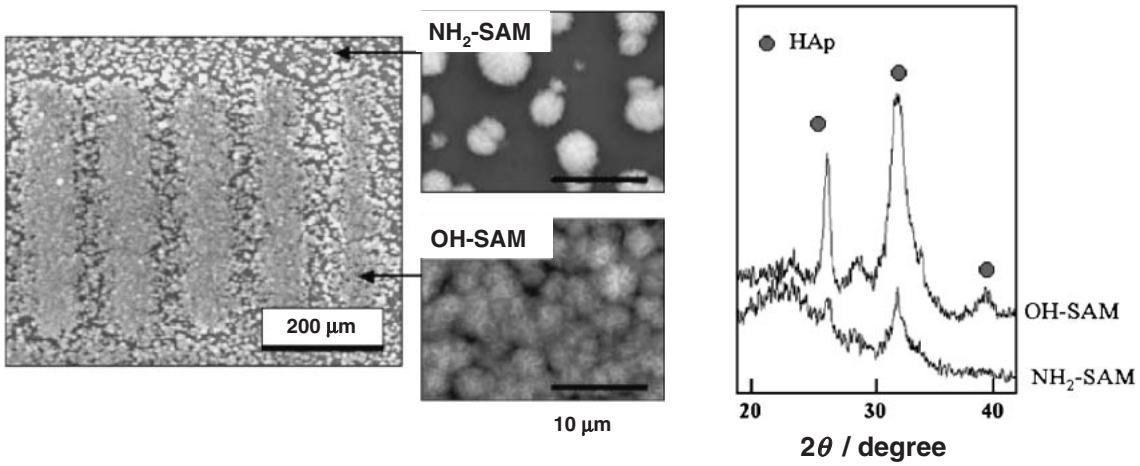

Figure 12. Formation of HAp micropattern and XRD patterns of depositions on the terminated SAMs after 10 day of soaking in 1.5 SBF with a lower supersaturation degree (pH 7.2) at 37 °C.[203]

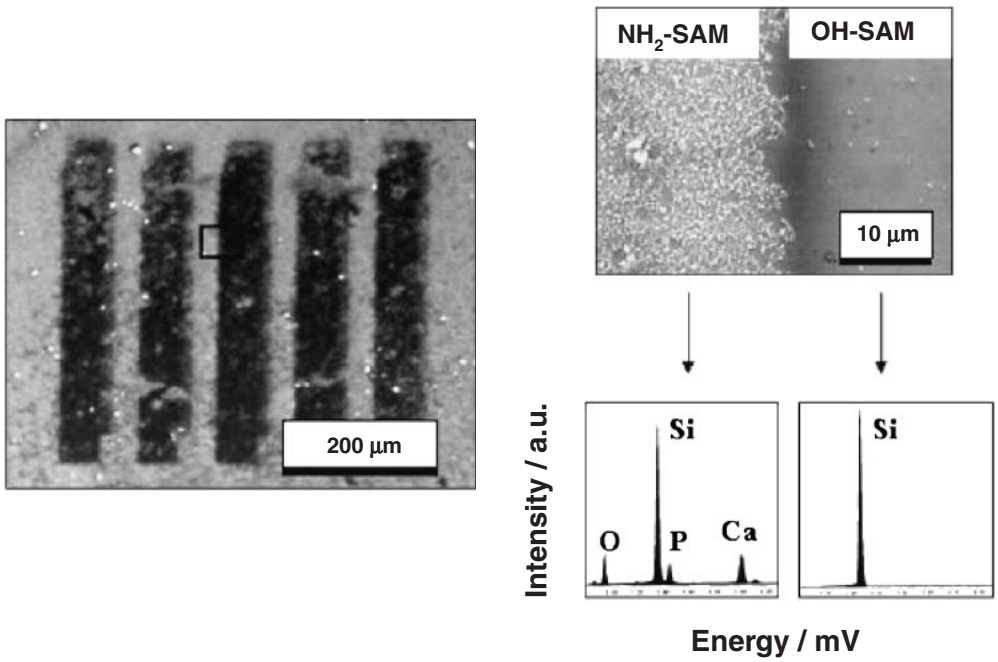

Figure 13. Formation of reversal HAp micropattern after 5 h of soaking in 1.5 SBF with a higher supersaturation degree (pH 7.6) at 50 °C.[203]

the super saturation degrees.[41,190a,203] According to classical nucleation theory, heterogeneous nucleation always preferentially takes place in a supersaturated solution due to the lower free energy of nuclei on the foreign bodies. However, if the induction period of homogeneous nucleation is reduced to a very short time, the influence from heterogeneous nucleation may be weakened. SBF is very similar to the body fluids of human beings in inorganic composition and has been usually employed to investigate the biocompatibility of materials.[204] The supersaturation degree of SBF can be easily controlled by changing pH, temperature of solution as well as ionic strength.[205] Normally, the accumulation of Ca^{2+} ions due to electrostatic attraction increases supersaturation near the negative surfaces, and as a result the initial nucleation is preferentially triggered. Therefore, the negatively charged surfaces are always favorable for the heterogeneous nucleation of apatite in a SBF solution without any homogeneous particles, whereas the nucleation is inhibited on positive surfaces.[206–209] This is consistent with our results obtained in a stable SBF solution (pH 7.2). The preferential nucleation of apatite was observed on negative surfaces (OH-SAM) rather than on positive ones (NH_2-SAM), resulting in the micropatterns of apatite on the silicon surfaces partially site-covered with OH and NH_2 headgroups (Figure 12).[203] The higher XRD peaks of deposits on OH-SAM than on NH_2-SAM revealed that a relatively larger quantity of apatite particles had formed on OH-SAM while very little on NH_2-SAM. However, on the other hand, we obtained an oppositely selective deposition of apatite onto NH_2/OH terminated SAMs when SBF solution was carefully adjusted to an unstable condition (pH 7.6, 50 °C) (Figure 13).

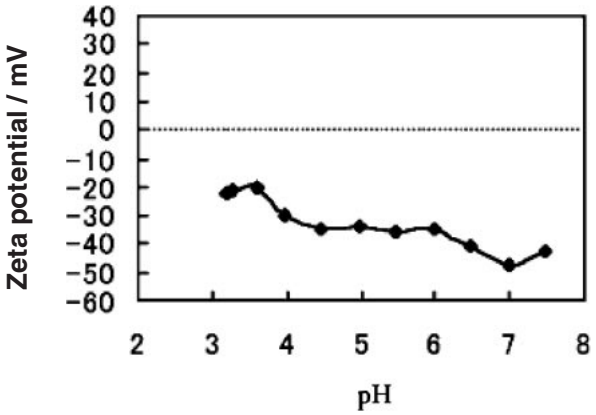

Figure 14. Zeta potential of copper particles formed in a pH 7.3 solution.[211]

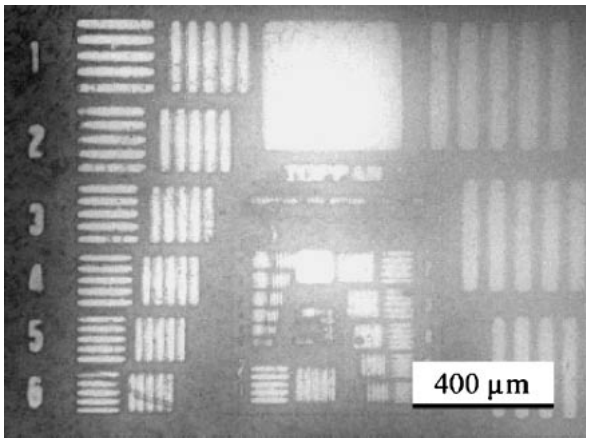

Figure 15. Optical micrograph of the copper micropattern formed on NH_2(black)/OH(white)-SAMs in an electroless bath buffered at pH 7.3.[211]

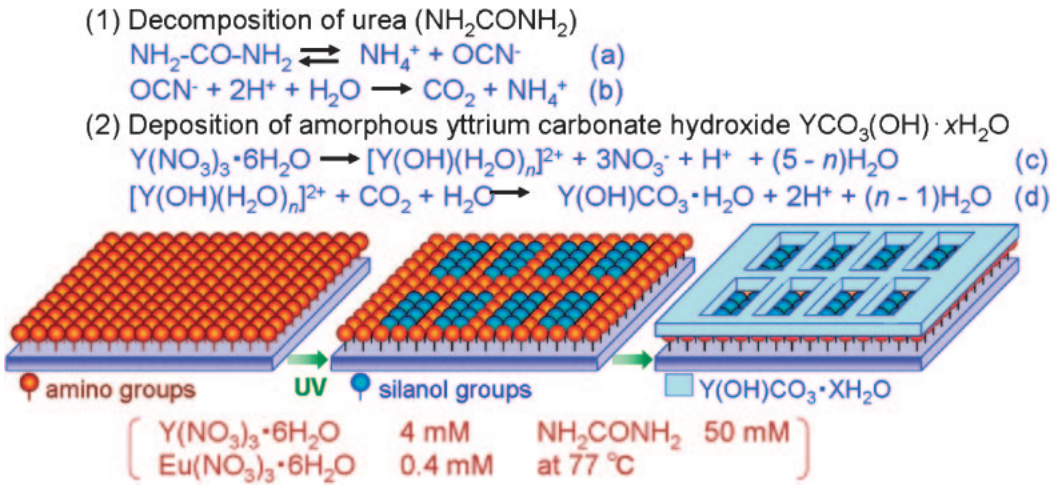

Figure 16. Conceptual process for site-selective deposition of visible-light emitting Y_2O_3:Eu thin films using a self-assembled monolayer.[171]

Homogeneous nucleation was observed in 1 h after the beginning of the soaking experiment. EDX spectra revealed the presence of Ca, P, and O elements on NH_2-SAM but nothing on OH-SAM. Obviously, the negatively charged apatite particles[190a,210] were electrostically forced to selectively deposit onto the positive NH_2-SAM and repulsive interaction inhibited it on OH-SAM. On the basis of the electrostatic adhesion of charged particles, we also succeeded in preparing a micropattern of metallic copper on silicon wafers modified with NH_2/OH terminated SAM in an electroless solution.[211] The special electroless (EL) bath solutions were prepared with dimethylamine borane (DMAB) as a reducing agent and sodium citrate ($Na_3C_6H_5O_7$) as a complexing agent coordinated with copper ions to trigger the formation of nano-sized copper particles in the EL solution. Zeta potential measurement for copper particles formed in the pH 7.3 solution revealed strongly negative surfaces of these particles and the isoelectric point was lower than pH 3.0 (Figure 14). Subsequently, the selective deposition of copper metal micro particles was attained on positive NH_2-SAM (Figure 15).

4.2.2 An Example of Y_2O_3: Fabrication of visible red light emitting europium-doped Y_2O_3 and its micropatterning was developed using an 3-aminopropyltriethoxysilane (APTS)-SAM.[171] The patterned APTS-SAM was immersed in an aqueous solution containing $Y(NO_3)_3\cdot 6H_2O$ (4 mM), $Eu(NO_3)_3\cdot 6H_2O$ (0.4 mM), and NH_2CONH_2 (50 mM) at 25 °C. The solution was heated to 77 °C gradually as shown in Figure 16 since urea (NH_2CONH_2) decomposes to form ammonium ions (NH_4^+) above 70 °C (eq a). The decomposition of urea at elevated temperature plays an essential role in the deposition of yttrium oxide. The aqueous solution of urea yields ammonium ions and cyanate ions (OCN^-) at temperatures above 70 °C (eq a). Cyanate ions react rapidly according to eq b. Yttrium ions are weakly hydrolyzed in water to $[Y(OH)(H_2O)_n]^{2+}$ (eq c). The resulting release of protons (H^+) and/or hydronium ions (H_3O^+) accelerates urea decomposition (eq b). The precipitation of the amorphous basic yttrium carbonate ($Y(OH)CO_3\cdot H_2O$) can take place through the reaction in eq d. The controlled release of cyanate ions by urea decomposition causes deposition of basic yttrium carbonate once the critical supersaturation in terms of reacting component is achieved. Since the decomposition of urea is quite slow, the amount needed to reach supersaturation within a given period of time must be considerably higher than the

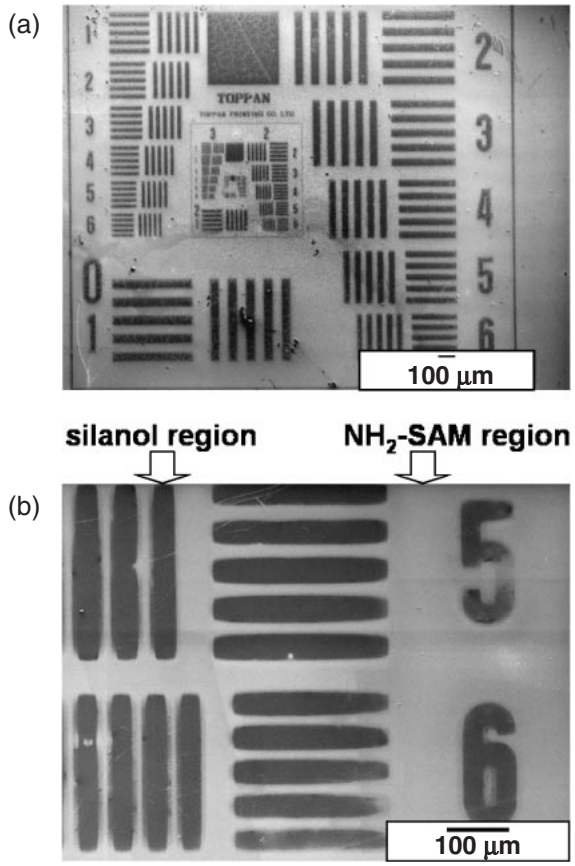

Figure 17. (a) SEM micrograph of patterned Y_2O_3:Eu thin films, (b) magnified area of (a).[171]

stoichiometric amount of yttrium ions, as revealed by previous studies of lanthanide compounds.

Yttrium carbonate films were observed to deposit on amino regions of a patterned SAM after the immersion in an aqueous solution (Figure 17). Deposits showed white contrast, while silanol regions without deposition showed black contrast in SEM observation. Narrow lines of depositions having 10–50 μm width were successfully fabricated in an aqueous solution. Patterned APTS-SAM showed high ability for site-selective deposition of yttrium carbonate in solution systems.

Yttrium, europium, oxygen, and carbon were observed from thin films on amino regions, while silicon and oxygen were detected from non-covered silanol regions by EDX (Figure 18). The molecular ratio of yttrium to europium was determined to be 100:8. It was close to that of $Y(NO_3)_3 \cdot 6H_2O$ to $Eu(NO_3)_3 \cdot 6H_2O$, i.e., 100:10, in the solution because the chemistry of $Eu(NO_3)_3$ is similar to that of $Y(NO_3)_3$ to incorporate europium in the precipitation. The content of europium was in the range we had expected. Y_2O_3:Eu with atomic ratio Y:Eu = 100:≈8 was reported to have strong photoluminescence. Carbon was detected from yttrium carbonate. Silicon and oxygen were detected from silicon wafer covered with a natural oxide layer (amorphous SiO_2).

Amino regions were covered with thin films composed of many large particles (about 100–300 nm in diameter) and very high roughness (RMS 25.6 nm) (Figure 19). Silanol regions, on the other hand, showed only nano-sized small particles (about 10–50 nm in diameter) and very low roughness (RMS 1.7 nm). The high site-selectivity of deposition and the big difference in surface morphology and roughness were clearly shown by AFM observation. The thickness of the films was estimated from AFM scans across deposited and undeposited regions of the substrate. It increased with immersion time after 45 min (0 nm at 45 min, 60 nm at 70 min, and 100 nm at 90 min (Figure 19)). The average growth rate (70 nm/h = 100/90 min) was higher than that previously reported (2 nm/h = 35 nm/15 h). An amorphous yttrium basic carbonate film was deposited at 80 °C from aqueous solutions of $YNO_3 \cdot 5H_2O$ and urea on Si wafers coated with sulfonate-functionalized organic self-assembled monolayers in previous studies. The thickness was then evaluated by TEM after treatment with ultrasonication for half an hour in distilled water. The difference of growth rate was caused mainly by the difference of the substrate treatment by ultrasonication. Additionally, the thickness of our film was smaller than the particle size in solution (227 nm at 100 min). Heterogeneous nucleation and attachment of initial particles of yttrium carbonate occurred without the attachment of aggregated large particles. The yttrium carbonate was then grown on the substrate to form a film of 100 nm thickness after immersion for 90 min. The particles of about 100 nm in height were removed by ultrasonication for 30 min and a film of several nm in height remained as reported.

The film was shown to be an amorphous phase (Figure 20a) by XRD measurement. The film showed no diffraction peak after annealing at 400 °C for 1 h, however, it showed 222, 400, and 440 diffraction peaks of crystalline cubic Y_2O_3 without any additional phase after annealing at 600 °C for 1 h and the intensities of diffraction peaks increased further by annealing at 800 °C for 1 h (Figure 20b). The film was shown to be a polycrystalline Y_2O_3 constructed from randomly deposited Y_2O_3 particles without crystal-axis orientation. The crystal structure model and diffraction pattern of Y_2O_3 were calculated from the crystal structure data of ICSD #23811 as shown in Figure 20. Crystallization by annealing confirmed from XRD measurement is consistent with XPS evaluation.

We attempted to remove Y_2O_3 films from the silicon substrate by debonding with scotch tape or by ultrasonication for 5 min in water. However, the films maintained their bonds with the substrate, indicating that strong adhesion had formed between films and substrate.

Thin film annealed at 800 °C for 1 h, i.e., crystalline Y_2O_3:Eu thin film, was shown to be excited by 230–250 nm (center: 243 nm) and emit red light photoluminescence centered at 611 nm in the fluorescence excitation spectrum (Figure 21a). Neither deposited film nor film annealed at 400 °C for 1 h showed photoluminescence, on the other hand, films annealed at 600 or 800 °C for 1 h emitted light centered at 617 nm by 250 nm in fluorescence emission spectra (Figure 21b). The fluorescence intensity of the film annealed at 800 °C was stronger than that of the film annealed at 600 °C. Fluorescence intensity increased by phase transformation from amorphous yttrium carbonate to yttrium oxide and crystal growth by the heat treatments, and is consistent with the crystallization observed by XRD. The spectra are described by the well-known $^5D_0$–^7F_J line emissions ($J = 0, 1, 2, \ldots$) of the Eu^{3+} ion with the strongest emission

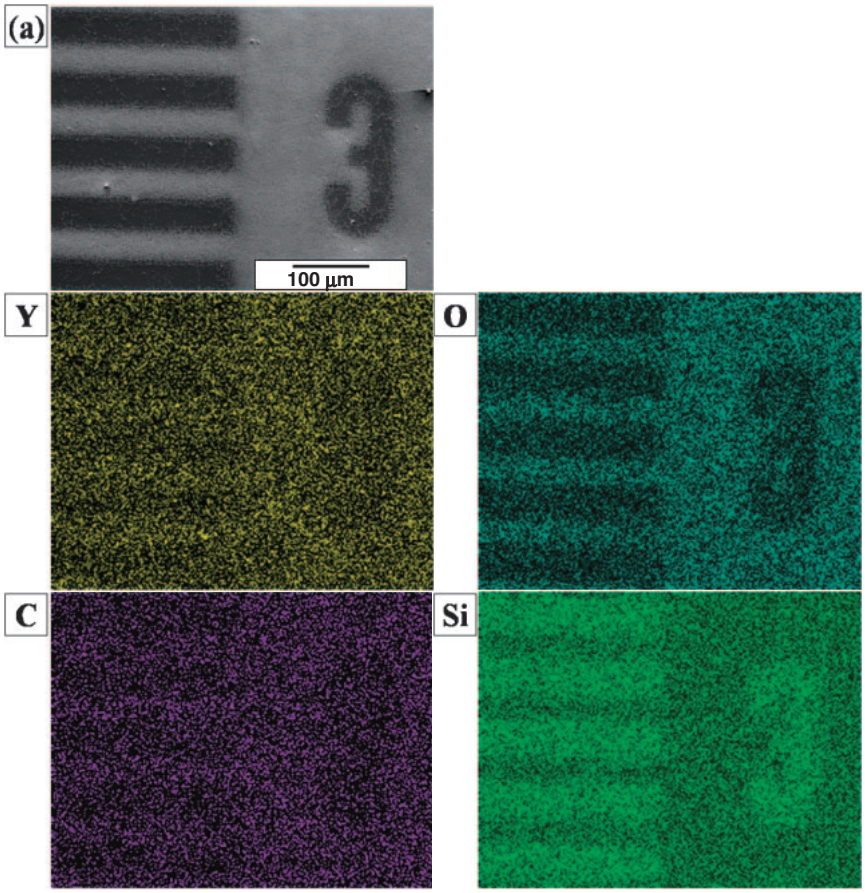

Figure 18. (a) SEM micrograph of patterned Y_2O_3:Eu thin films. Characteristic X-ray images of Y, O, C, and Si for (a) Y_2O_3:Eu thin films.[171]

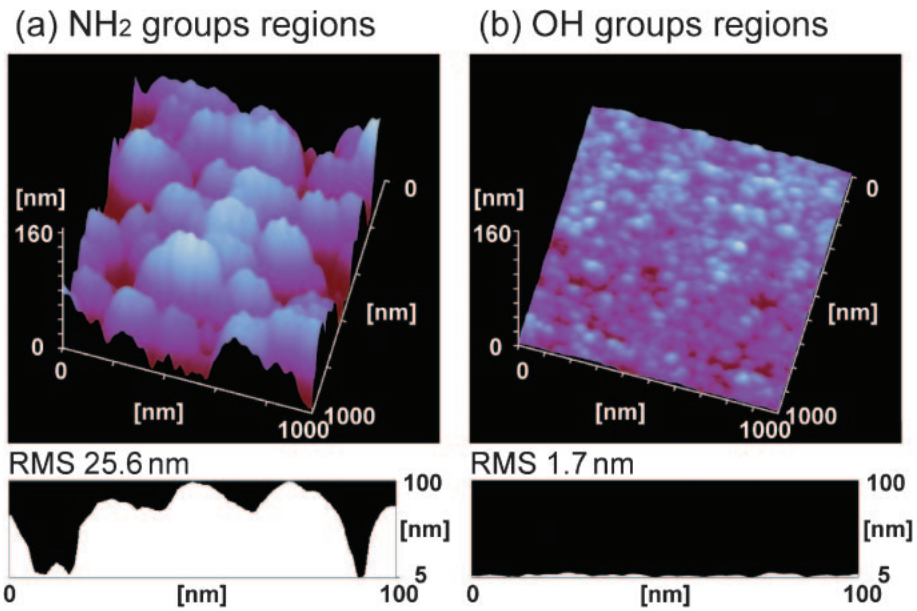

Figure 19. (a) AFM images cross-section profile of Y_2O_3:Eu thin films on NH_2 groups regions. (b) AFM images cross-section profile of Y_2O_3:Eu thin films on OH groups regions.[171]

for $J = 2$ at 612 nm. The thin film annealed at 800 °C produced visible red light photoluminescence by excitation from Nd:YAG laser (266 nm) (Figure 21, inset). The white square shows the edges of the Y_2O_3:Eu thin film and the red color shows visible red emission from the irradiated area on the substrate.

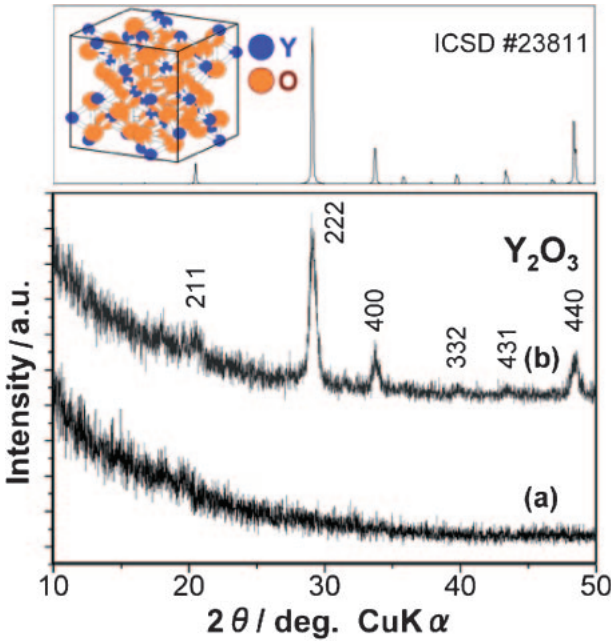

Figure 20. XRD patterns of Y_2O_3:Eu thin films (a) before (b) after annealing at 800 °C for 1 h. (The upper picture) Crystal structure model diffraction pattern of cubic Y_2O_3 calculated from crystal structure data of ICSD #23811.[171]

In summary, we have proposed a novel process for fabricating visible red light emitting Eu-doped Y_2O_3 and its micropattern using a self-assembled monolayer and an aqueous solution system. The patterned APTS-SAM with amino groups regions and silanol groups regions achieved site-selective deposition of yttrium oxide in an aqueous solution. The deposited films were crystallized by annealing at 600 or 800 °C for 1 h. Crystalline Y_2O_3:Eu produced visible red light photoluminescence centered at 611 nm by excitation from Nd:YAG laser (266 nm). This study showed the high potential of aqueous solution systems and self-assembled monolayers for the fabrication of functional metal oxide thin films and their micropatterns.

4.2.3 An Example of ZnO: Site-selective deposition of UV- and visible-light-emitting ZnO crystals was successfully achieved in an aqueous solution at low temperature.[104] Patterned OTS-SAMs were immersed into a solution containing zinc acetate (15 mM) and ammonia (30 mM) as complexing agent ($[NH_3]/[Zn] = 2.0$) at 50 °C for 3 h (Figure 22). ZnO crystals having long hexagonal cylinder shape (inset of Figure 23b) were homogeneously nucleated to make the solution turbid shortly after adding ammonia. Crystals showed sharp hexagonal facets of about 100 nm in diameter and larger than 500 nm in length. The morphology indicated high crystallinity of ZnO nanoparticles. The nanoparticles were deposited and further grown on hydrophobic octadecyl group regions of a patterned SAM selectively (Figure 24). Consequently, a micropattern of light-emitting ZnO crystals was successfully fabricated in an aqueous solution without Pd catalyst. ZnO crystals were also deposited on hydrophobic regions of patterned SAMs such as DTS (dodecyltrichlorosilane)-SAM, HTS (hexyltrichlorosilane)-SAM, PTS (propyltrichlorosilane)-SAM, MTS (methyltrichlorosilane)-SAM, PTCS (phenyltrichlorosilane)-SAM, or APTS (aminopropyltriethoxysilane)-SAM. This showed that the method is highly versatile and offers good potential for the fabrication of devices.

ZnO crystals were deposited on hydrophobic SAM regions such as OTS-, APTS-, or other SAMs rather than hydrophilic silanol regions. Zeta potential of ZnO crystals deposited on a silicon substrate was measured to be 10 mV at pH 8.1 and ZnO crystals should thus have positive zeta potential not less than 10 mV in the solution at pH 7.04. SAM of OTS, silanol and APTS showed zeta potential of −3, −38.2, or +22.0 mV, respectively. ZnO having positive zeta potential should be deposited on silanol regions having negative zeta potential rather than other SAMs, if the site-selective deposition was caused only by electrostatic interactions. The site-selective deposition of ZnO crystals would be caused by not only electrostatic interactions as shown by the relation of zeta potentials. ZnO crystals having long hexagonal cylinder shape were deposited on a hydrophilic silicon substrate to evaluate

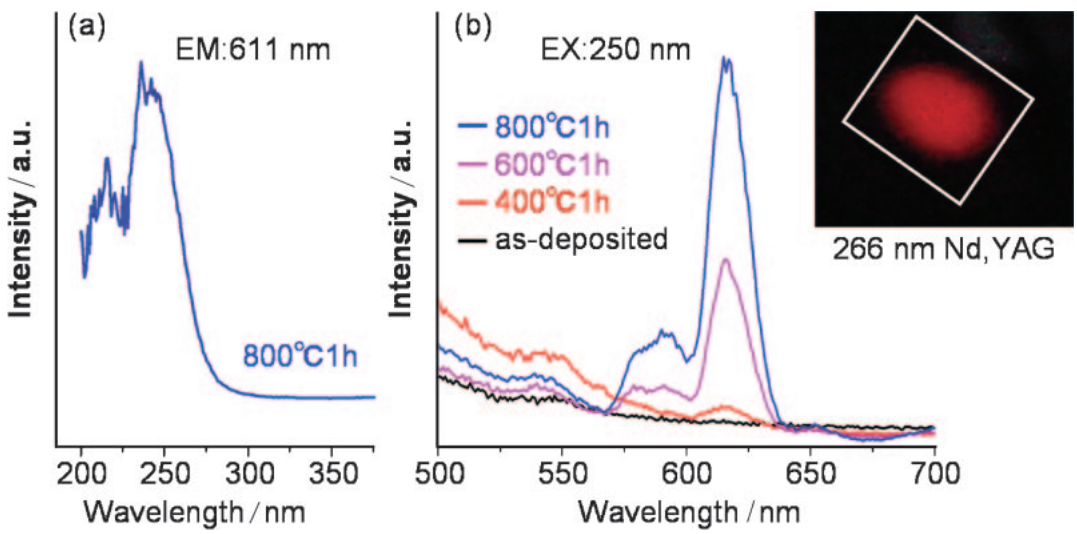

Figure 21. (a) Fluorescence excitation spectrum (emission: 611 nm) for Y_2O_3:Eu thin film after annealing at 800 °C for 1 h. (b) Fluorescence emission spectra (excitation: 250 nm) for Y_2O_3:Eu thin films before after annealing at 400, 600, or 800 °C for 1 h. Inset: Photoluminescence image for Y_2O_3:Eu thin film annealed at 800 °C for 1 h (excitation: 266 nm).[171]

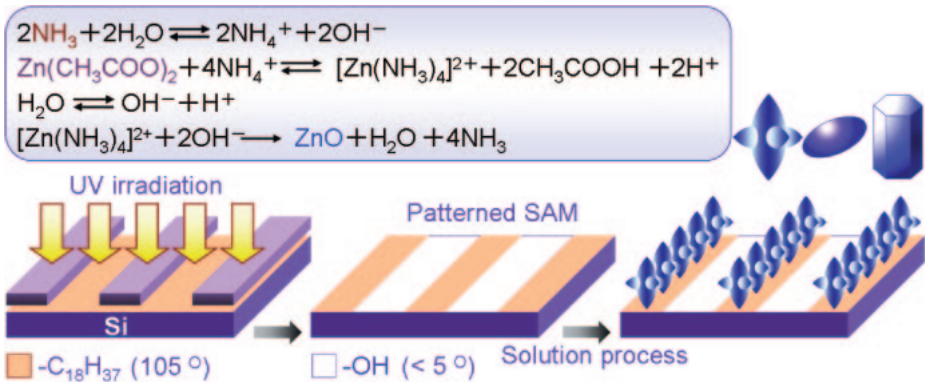

Figure 22. Conceptual process for self-assembly patterning of light-emitting crystalline ZnO nanoparticles in an aqueous solution.[104]

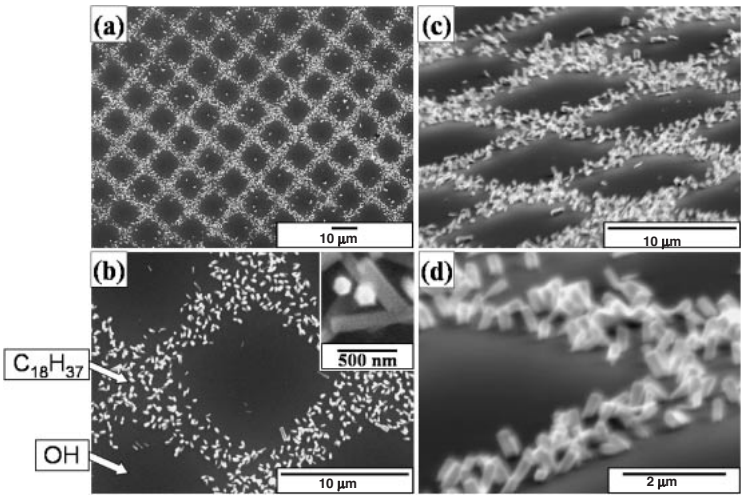

Figure 23. SEM micrographs of (a) patterned crystalline ZnO (long hexagonal cylinder, $[NH_3]/[Zn] = 2.0$), (b) magnified area of (a), (c) tilted image of (a), and (d) magnified area of (c).[104]

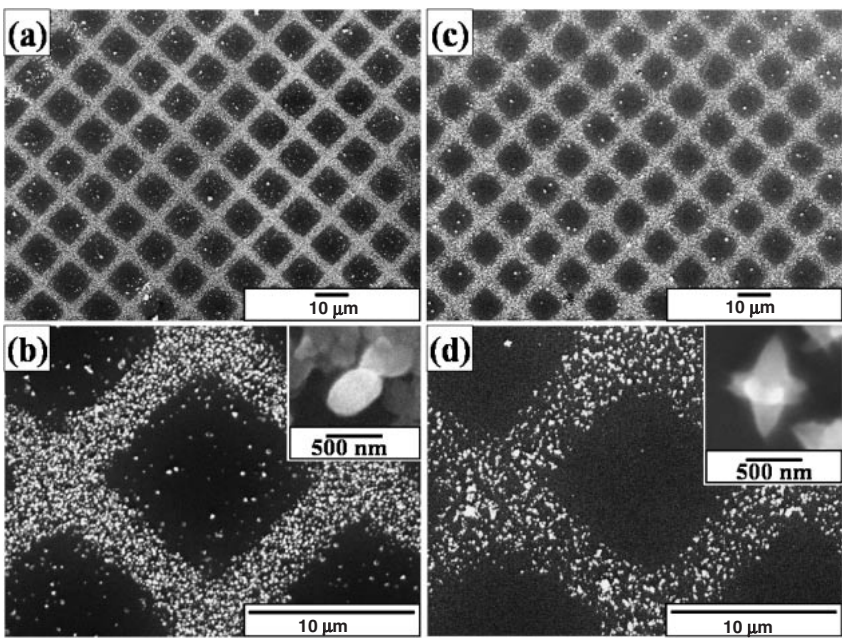

Figure 24. SEM micrographs of (a) patterned crystalline ZnO (ellipse, $[NH_3]/[Zn] = 4.0$), (b) magnified area of (a), (c) patterned crystalline ZnO (multi-needles, $[NH_3]/[Zn] = 6.0$), and (d) magnified area of (c).[104]

the surface of crystals. The substrate covered with many deposited ZnO crystals exhibited high water contact angle (WCA 140°). The deposited ZnO crystals were found from the experiment to have hydrophobic surfaces. Surfaces of naked ZnO crystals would be hydrophilic because of surface hydroxy groups and they would become hydrophobic by being covered with organic molecules having hydrophobic functional groups. CH_3COO^- ions coming from $Zn(CH_3COO)_2$ might be adsorbed to ZnO crystal surfaces by the interaction between Zn and $-COO^-$ to cover the surface with hydrophobic $-CH_3$ groups and some $Zn(CH_3COO)_2$ would exist in the surface layer of ZnO crystals. Additionally, deposited ZnO crystals of long hexagonal cylinder shape became hydrophilic (<10°) and their zeta potential shifted positively by UV irradiation in air. ZnO crystals deposited on a silicon substrate showed zeta potential of 10 mV at pH 8.1, 0 mV at pH 8.8, and −15 mV at pH 9.2, while they shifted to 20 mV at pH 8.1, 10 mV at pH 8.8, and 7 mV at pH 9.2 by UV irradiation. The decomposition of CH_3COO^- ions and the breakage of the bond between CH_3COO and Zn would be caused by light excitation, ozone and active oxygen by UV irradiation in air. This finding suggests that organic molecules, such as CH_3COO^- ions, which show negative zeta potential and can be removed by UV irradiation, would be absorbed onto the surfaces of ZnO crystals. Furthermore, ZnO crystals were confirmed to deposit on a hydrophobic poly(ethylene terephthalate) surface rather than on a hydrophilic poly(ethylene terephthalate) surface modified by UV irradiation in the same solution. Additionally, organic molecules were reported to adsorb to growing ZnO crystals, in which poly(ethylene oxide)-*block*-poly(methylacrylic acid) (PEO-*b*-PMAA) was adsorbed preferentially to the {0001} face of ZnO to retard crystal growth perpendicular to this face. Consequently, site-selective deposition was achieved by effective molecular recognition caused by combination of the forces composed mainly of hydrophobic interactions between functional groups of SAMs and ZnO crystal surfaces.

Patterned SAMs were also immersed into solution containing zinc acetate (15 mM) and ammonia (60 or 90 mM) as complexing agent ($[NH_3]/[Zn] = 4.0$ or 6.0) for 3 h. ZnO crystals having ellipse or multi-needle shape (two large needles and four small needles) (insets of Figures 24b and 24d) were homogeneously nucleated to make the solution turbid shortly after adding ammonia. Nucleation and deposition of ZnO crystals were accelerated by addition of ammonia. Each ZnO crystal was about 500 nm in size. The crystals were deposited and further grown on hydrophobic regions of patterned SAMs selectively (Figure 24). Micropatterns of light-emitting ZnO crystals having ellipse or multi-needle shape were fabricated on patterned SAMs such as OTS-SAM, DTS-SAM, HTS-SAM, PTS-SAM, MTS-SAM, PTCS-SAM, or APTS-SAM in aqueous solutions.

XRD spectra of ZnO crystals having ellipse or multi-needle shape showed dominant peaks corresponding to ZnO(0002) planes revealing that ZnO crystals were deposited with a high degree of orientation of their *c* axes perpendicular to the substrate (Figure 25). Enhanced (0002) and $(10\bar{1}0)$ peaks from ZnO crystals having long hexagonal cylinder shape showed that crystals were deposited to make (0002) or $(10\bar{1}0)$ planes

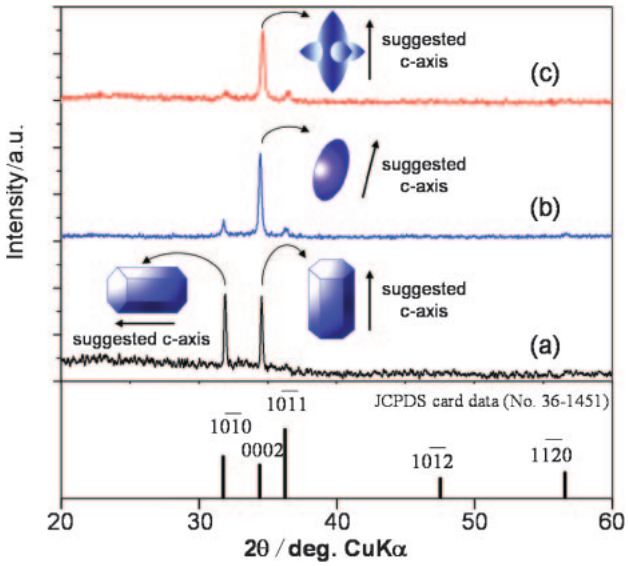

Figure 25. In-plane X-ray diffraction profiles of ZnO changing with the morphology: (a) long hexagonal cylinder, (b) ellipse, and (c) multi-needles.[104]

parallel to the substrate. Crystals having high crystallinity and high purity with no additional phase were shown to be prepared in an aqueous solution with precise control of their morphologies without the use of Pd catalyst. The aqueous solution system showed high ability for fabricating nano/micro devices composed of crystalline materials. ZnO crystals are well known to grow along the *c* axis. The *c* axes of ZnO crystals deduced from their shapes and the deposited directions revealed from XRD spectra are shown in Figure 25. The orientations evaluated from XRD patterns were consistent with SEM observations and were shown to be controlled precisely by the solution conditions.

Photoluminescence properties of ZnO crystal patterns were further evaluated. Micropatterns of ZnO crystals were observed by an optical microscope (Figure 26) and strong visible-luminescence from ZnO crystals excited by 330–385 nm light was observed by a photoluminescence microscope. ZnO crystals showed strong UV luminescence (around 390 nm) attributed to band-edge luminescence and visible-light luminescence caused from oxygen vacancy (450–600 nm). All of the crystals showed photoluminescence (Figure 27) due to high purity and high crystallinity with optimal oxygen vacancy, and this caused the bright visible-photoluminescence image. Luminescence properties can be controlled by changing the crystalline morphologies. ZnO crystals deposited from an aqueous solution were shown to have high visible-light-emitting properties.

In summary, micropatterns of ZnO crystals were successfully fabricated on patterned SAMs and ZnO crystals emitted strong UV- and visible-light photoluminescence. Additionally, the morphology and photoluminescence properties of ZnO crystals were shown to be controlled by changing the solution conditions. This result is a step toward fabricating nano/micro-devices for next-generation visible-light-emitting displays.

4.3 Patterning by Surface-Selective Heterogeneous Nucleation and Growth. 4.3.1 An Example of Amorphous TiO_2: Liquid-phase patterning of amorphous TiO_2 was

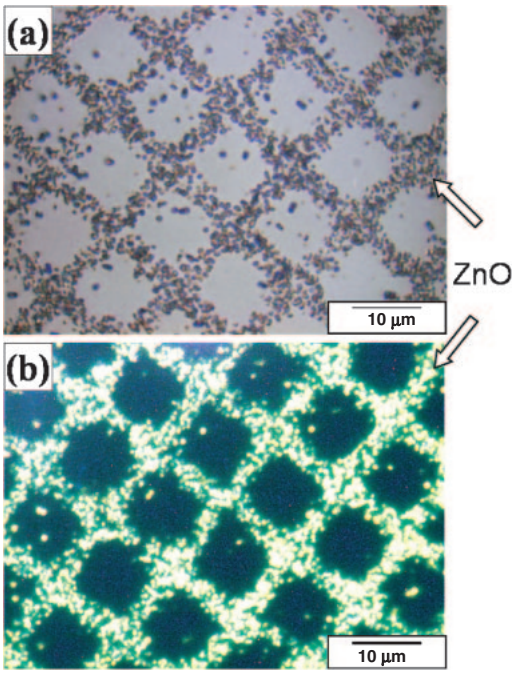

Figure 26. (a) Optical microscope image (b) photoluminescence image of patterned ZnO particles (ellipse) under white light or UV light (330–385 nm).[104]

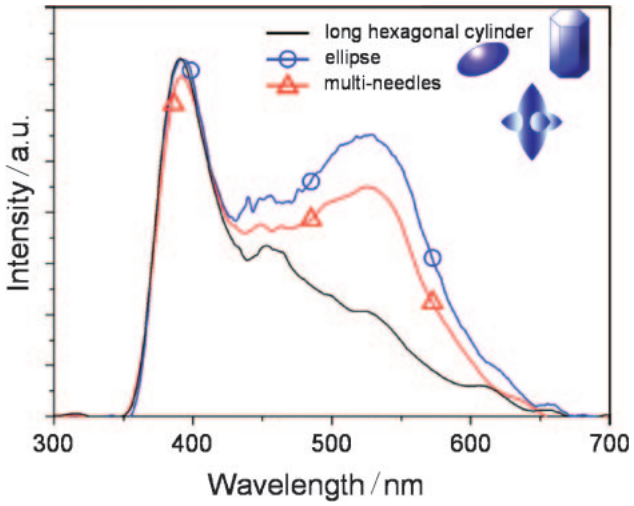

Figure 27. Photoluminescence properties for ZnO crystals, long hexagonal cylinder, ellipse, and multi-needles.[104]

realized using self-assembled monolayers. Patterned SAM substrates of OTS were immersed into an anhydrous toluene solution containing 0.1 M TDD (titanium dichloride diethoxide) for 5–30 min under a N_2 atmosphere using a glove box (Figure 28). In the case experiments were done in air, many particles were homogeneously nucleated in TDD solution and they adsorbed on deposited thin films. It shows that elimination of traces of water is important to fabricate high quality thin films. All glassware was dried in a dry box at 50 °C before use. Estimated partial pressure of H_2O in the N_2 atmosphere was below 0.1 hPa. Both titanium chloride and titanium alkoxide are known to form chemical bonds with silanol groups, however, the fact that the reactivity of silicon chloride is higher than that of silicon alkoxide, namely Si–Cl > Si–F > Si–OCH_3 > Si–OC_2H_5 > Si–OC_3H_7 > Si–OC_4H_9 would firmly suggest that Ti–Cl would have higher reactivity than Ti–OC_2H_5. Accordingly, chlorine atoms of TDD react with H_2O changing into OH which further react with silanol groups of SAM resulting in the formation of Ti–O–Si bonds. Ethoxy groups, OC_2H_5, of TDD are hydrolyzed into hydroxy groups which are further condensed to form Ti–O–Ti bonds. Thickness of films can be easily controlled by soaking time, because chlorine atoms react with silanol groups quickly to form a few molecular layers and ethoxy groups hydrolyze gradually. After SAM substrates were rinsed with toluene and preserved in air, blue thin films appeared on silanol surfaces of OTS-SAM but were not observed on methyl surfaces. Micropattern of a thin film was thus successfully fabricated on patterned OTS-SAM.

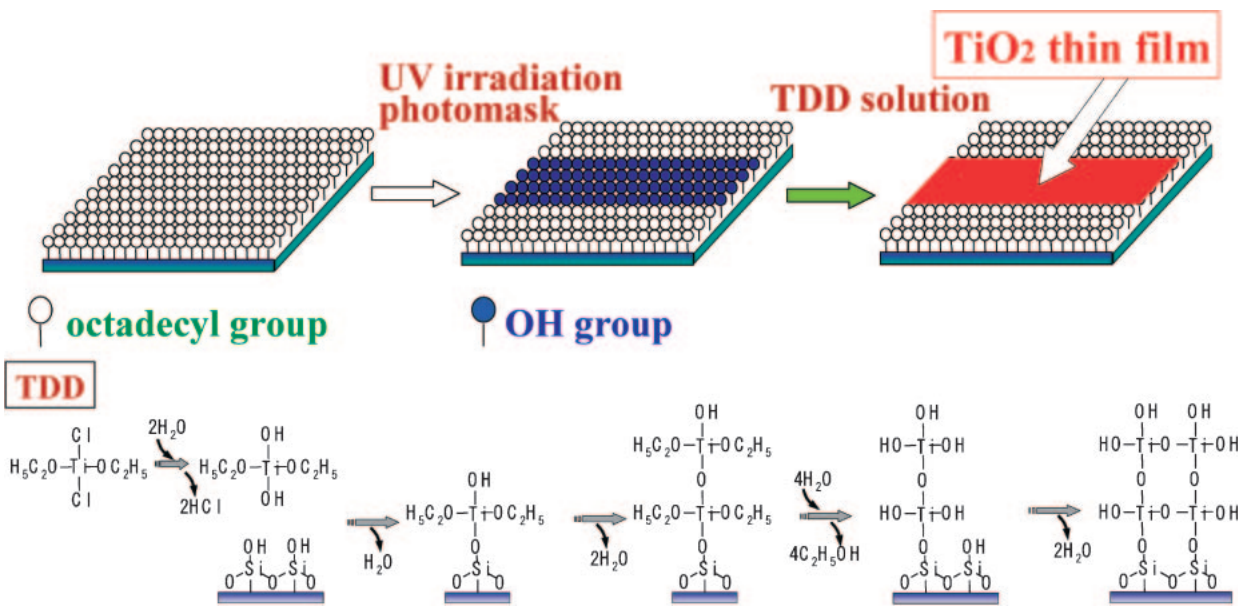

Figure 28. Conceptual process for selective deposition of titanium oxide thin film using a self-assembled monolayer.[36a]

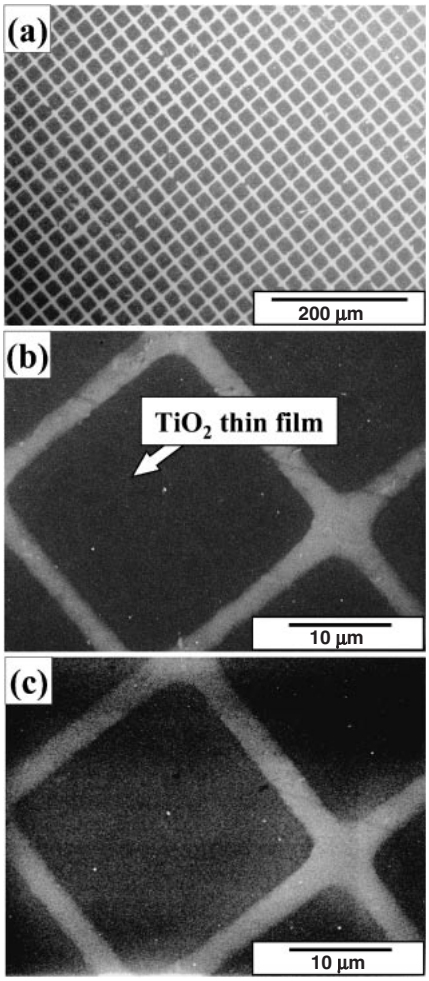

Figure 29. SEM photographs of (a) a micropattern of as-deposited thin films (30 min soaking), (b) magnified area of (a), and (c) after annealing of (b) at 600 °C for 3 h.[36a]

Selective deposition of thin films on OTS-SAM was confirmed by scanning electron microscope observation (Figures 29 and 30). These films did not peel off during sonication in acetone, and showed strong adhesion to the substrate. The line edge roughness was estimated in the same manner as used for titanium dioxide films fabricated with a liquid-phase deposition process. Line width measurements at 15 equally spaced points on each line in Figure 29b indicate an average printed line width of 23.3 μm. Line edge roughness, as measured by the standard deviation of the line width, is ≈0.5 μm. This represents ≈2.1% variation (i.e., 0.5/23.2) in the nominal line width. This variation is much better than that of the pattern fabricated with a liquid-phase deposition process and the usual 5% variation afforded by current electronics design rules. This variation is similar to that of a transmission electron microscopy (TEM) mesh (2.1%) we used for Figure 29. Therefore, variation of titanium dioxide pattern can be improved through the use of a high-resolution photomask. Titanium dioxide wire shown in Figure 30 was fabricated using a high-resolution photomask. The line width variation of this pattern is well below 2.1%. These observations firmly indicate that micropatterns of titanium dioxide were successfully fabricated using OTS-SAM. OTS-SAM is suitable for selective deposition of a film, because only silanol groups react with TDD and methyl groups inhibit deposition of a film.

Thickness of films was evaluated by an atomic force microscope. Films obtained after soaking for 5 and 30 min were 6.9 and 27.4 nm thick, respectively. Energy dispersive X-ray analysis indicated that thin films consisted of titanium, oxygen and a small amount of chlorine (Ti:Cl = 1:0.1) as shown in Figure 30. Thin films are considered to be of titanium dioxide from this observation.

Thin films were further evaluated by X-ray photoelectron spectroscopy (XPS). The spectral peaks corresponding to Ti 2p (458.5 eV) were observed from thin films deposited on the silanol region (Figure 31). This binding energy is higher than

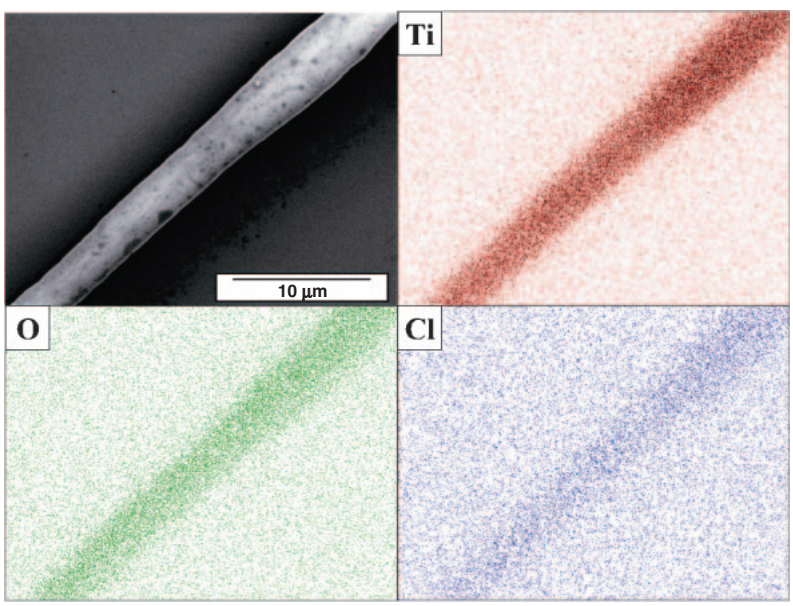

Figure 30. EDX analysis of titanium dioxide micro wire on OTS-SAM; (a) SEM image and characteristic X-ray images of (b) Ti, (c) O, and (d) Cl.[36a]

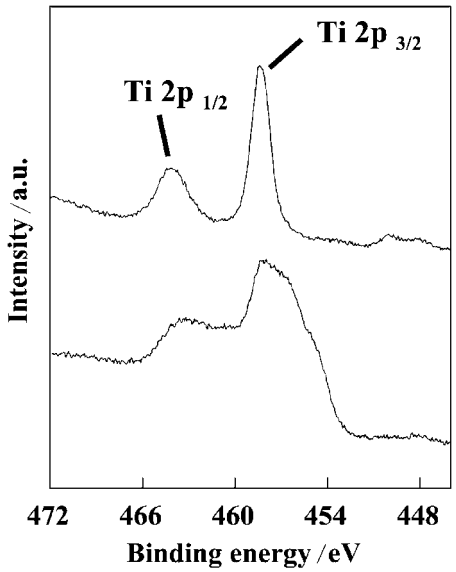

Figure 31. XPS spectra of Ti 2p for titanium oxide thin film formed on the silanol region of OTS-SAM (30 min soaking) (a) before and (b) after Ar^+ sputtering.[36a]

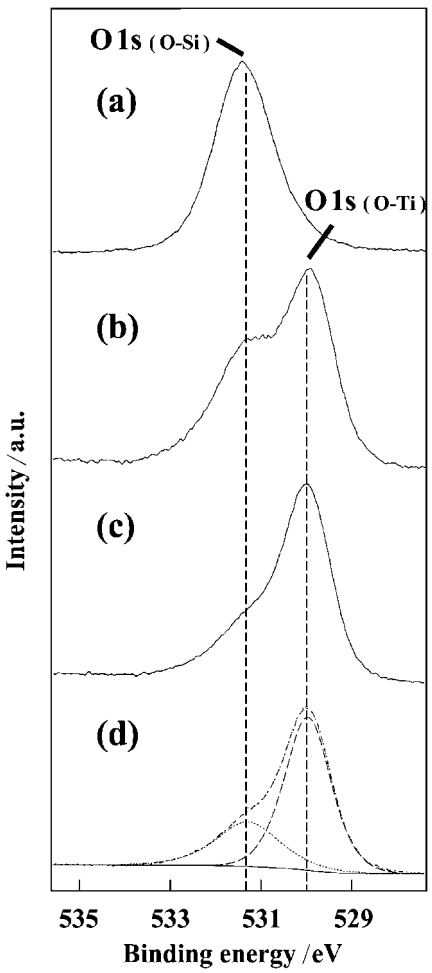

Figure 32. XPS spectra of O 1s; (a) methyl region of OTS-SAM, (b) thin film formed on silanol region (5 min soaking), (c) thin film formed on the silanol region (30 min soaking), and (d) after Ar^+ sputtering of (c).[36a]

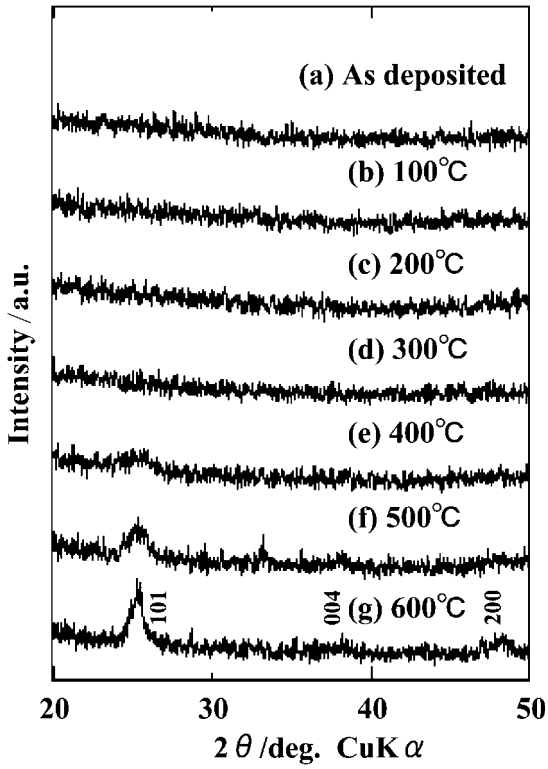

Figure 33. XRD patterns of thin films changing with the change in annealing temperature.[36a]

that of Ti metal (454.0 eV), TiC (454.6 eV), TiO (455.0 eV), TiN (455.7 eV), and Ti_2O_3 (456.7 eV), and similar to that of TiO_2 (458.4–458.7 eV). This suggests the titanium atoms in thin films are positively charged relative to that of titanium metal by formation of direct bonds with oxygen. On the other hand, this spectrum was not observed from methyl regions.

OTS-SAM surfaces showed O 1s (531.3 eV) which can be assigned to a silicon oxide layer on the surface of silicon wafer (532.0 eV) (Figure 32a). O 1s peak centered at 530.1 eV was observed from thin films deposited on silanol regions (Figure 32b), and not observed from methyl regions. The intensity of this peak increased with soaking time (Figure 32c) and was not observed from methyl regions even after soaking for 30 min. Hence, the peak (530.1 eV) was assigned to the deposited film. This binding energy is similar to that of TiO_2 (529.9 and 530.1 eV), and it showed oxygen is negatively charged compared to neutral oxygen molecules (531.0 eV) possibly through the formation of direct bonds with Ti.

The ratio of oxygen to titanium was evaluated after 20 min of Ar^+ ion sputtering to avoid the influence of a contaminated layer on the surface (Figures 31b and 32d). O 1s peak can be deconvoluted into two curves (ratio of 529.7 eV (films) and 531.3 eV (silicon oxide) is 1:0.22). The ratio of oxygen to titanium was estimated as 2.2:1. Additionally, small amounts of chlorine and carbon were also detected (Ti:O:C:C = 1:2.2:0.17:0.37), but the spectral peaks corresponding to C and Cl disappeared after annealing at 400 °C.

X-ray diffraction measurements for the thin films showed that they are composed of amorphous phases (Figure 33). Heat treatment of the films has demonstrated that amorphous phase converts into crystalline anatase phase above ≈400 °C and its

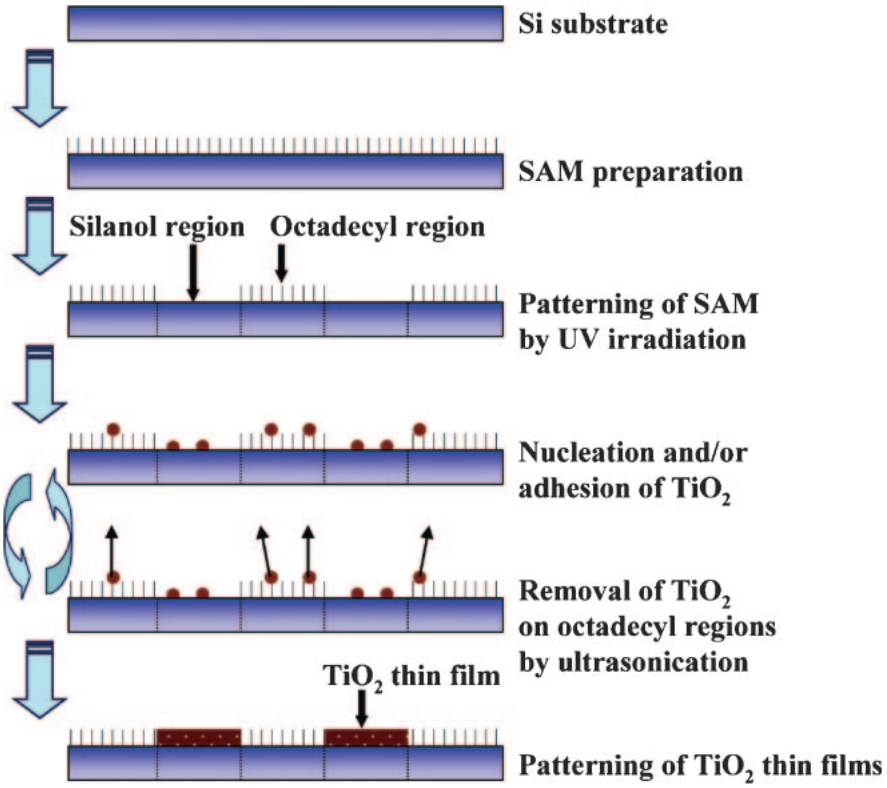

Figure 34. Conceptual process of site-selective elimination for the patterning of anatase TiO_2 thin films from an aqueous solution.[104]

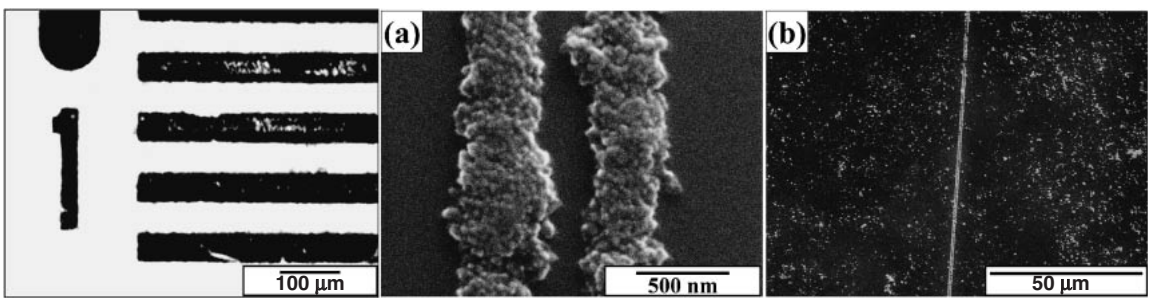

Figure 35. Optical micrograph and (a), (b) SEM micrographs of micropattern of anatase TiO_2 thin films deposited for 4 h from the solution without the addition of HCl.[104]

crystallinity becomes better with higher annealing temperature. The anatase phase further transforms into rutile and/or other phases by annealing above 1000 °C. Additional peaks of SiO_2 were also observed after annealing at 1000 °C possibly due to the oxidation of the Si substrate itself.

After annealing a micropattern of titanium dioxide shown in Figure 29 at 600 °C for 3 h, no cracks were observed by SEM or atomic force microscopy (AFM), and the resolution of this pattern remained almost unchanged (Figure 29c). These results suggest that high-resolution micropatterns of anatase-type TiO_2 can be fabricated by our newly developed patterning and heat treatment process.

In summary, site-selective deposition of amorphous TiO_2 was realized in solutions using self-assembled monolayers. Molecular recognition of SAMs was effectively utilized to control nucleation and film growth. This process can be applied to liquid-phase patterning of other kinds of amorphous metal oxides.

4.3.2 An Example of Anatase TiO_2: Nano/micro-scaled patterns of anatase TiO_2 were successfully fabricated in an aqueous solution at 50 °C.[104] Patterned octadecyltrichlorosilane (OTS)-SAM with octadecyl regions and silanol regions was immersed in an aqueous solution containing ammonium hexafluorotitanate ($[NH_4]_2TiF_6$), boric acid (H_3BO_3), and HCl at 50 °C for 4 h with ultrasonic treatment (Figure 34). An appropriate amount of HCl was added to the solution to control pH. Solutions (100 mL) with 0, 0.1, or 0.6 mL of HCl showed pH 3.8, 2.8, or 1.5, respectively.

Thin films were observed on the silanol group regions to form nano/micro-scaled patterns at pH 3.88, 2.8, or 1.5. The films deposited for 4 h from the solution without the addition of HCl are shown in Figures 35, 36 and 37. Thin films were

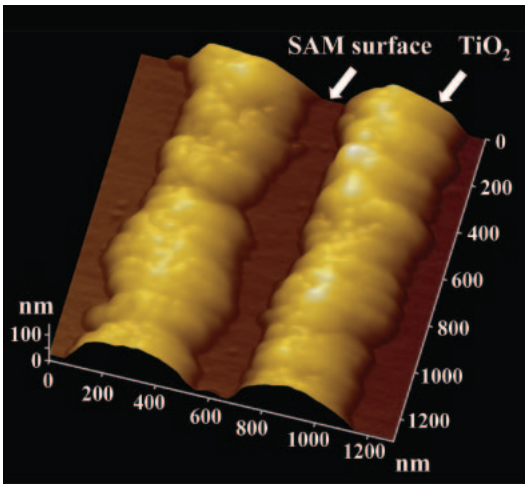

Figure 36. AFM image of micropattern of anatase TiO_2 thin films on OTS/OH-patterned SAM fabricated by LPD using ultrasonication (The films were deposited for 4 h from the solution without the addition of HCl.).[104]

observed as being dark in an optical micrograph (Figure 35). Separated parallel lines 200–400 nm in width at 100–200 nm intervals were successfully fabricated with this method (Figures 35a and 35b). The length of the separated parallel lines reached more than 100 μm (Figures 35a and 35b). A cross section of the lines was shown as a semicircle, and the thickness of the center of the lines was estimated to be about 100 nm by AFM observation (Figure 36). Feature edge acuity of the pattern was higher than that of the pattern fabricated by our lift-off process or by site-selective immersion. Site-selective deposition was realized at any pH such as pH 3.88, 2.8, or 1.5. Patterns which have higher feature edge acuity can be obtained at low pH conditions because films were formed slowly without the deposition of homogeneously nucleated particles.

For the adhesion of TiO_2 films to silanol groups, the pH of the deposition solution is critical. Pizem et al. reported that adherent TiO_2 films formed from solutions similar to those used here at pH 3.9 (i.e., the pH used in the films of Figures 35, 36 and 37), but that the films were less adherent at pH 2.9.[39c] They related this difference in adherence to an increased electrostatic attraction of TiO_2 to the oxidized surface of silicon at the higher pH. In our experiment, there also was less adherence of TiO_2 at pH 2.8 and 1.5 than that at pH 3.5 due to low supersaturation shown in eq a and low electrostatic attraction.

However, some depositions were observed on octadecyl group regions in Figure 35b. One probable cause is that pinholes and other defects in the films provide at least some degree of access of water to underlying unreacted OH groups in the OTS films. Once exposed to the solution, these sites can act as nucleation points for TiO_2 growth. Because the depositions are performed at elevated temperatures, it is likely that pinholes and defects will continually open and close on the OTS film surfaces due to thermal motions of alkyl chains in the films. The TiO_2 precursors formed in these defects would act as points for eventual growth of TiO_2 over the entire SAM-covered region. This would provide a weakly bound TiO_2 film on the OTS film regions due to the limited number of connections to the underlying silanol sites in the film regions. In fact, Sagiv and others have shown that macroscopic defects induced in alkylsiloxane films can readily be accessed by solution species.[126t] More recently, Dressick and co-workers demonstrated that solvent accessibility to underlying substrates in aromatic siloxane films is also important and may be an even greater factor in controlling the properties of those films, which may account for our previous selectivity observation using phenylsiloxane films, as shown in the lift-off process.[66c]

In the lift-off process, thin films were formed on the entire area of patterned SAM that has silanol group regions and phenyl (or octadecyl) group regions. After being dried, the substrate was sonicated in water to lift off thin films on phenyl (or octadecyl) group regions selectively. Thin films on phenyl (or octadecyl) group regions were peeled off along the cracks that formed during the drying process. Thin films on phenyl (or octadecyl) group regions without cracks were not peeled off because depositions strongly connected to each other to form solid timber (monolith). The lift-off along cracks decreased the feature edge acuity of the pattern in this method. Thin films were formed on silanol group regions selectively and site-selective deposition was realized with our newly developed method. This resulted in high feature edge acuity of the patterns compared to our previous work.

Additionally, the micropattern of thin films was also fabricated by the site-selective immersion method. A solution containing a Ti precursor contacted the hydrophilic regions during the experiment and briefly came into contact with the hydrophobic regions. The solution on the hydrophilic surface was replaced with a fresh solution by continuous movement of bubbles. Thus TiO_2 was deposited and a thin film was grown

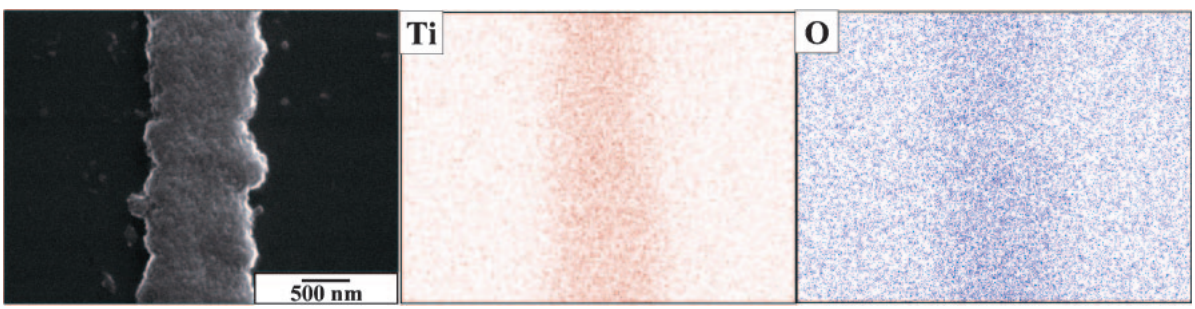

Figure 37. SEM micrograph of micropattern of anatase TiO_2 thin film and EDX images for Ti and O (The films were deposited for 4 h from the solution without the addition of HCl.).[104]

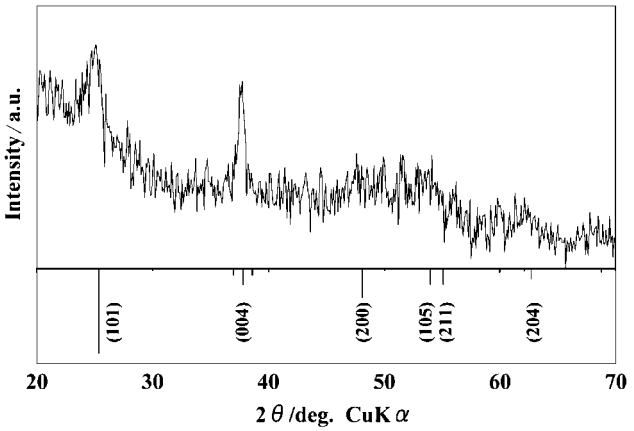

Figure 38. XRD pattern of deposited thin films on silanol group regions from an aqueous solution.[104]

on the hydrophilic regions selectively. This technique can be applied for the formation of many kinds of films from any solution and to fabricate micropatterns for many kinds of thin film because the technique creates the difference in contact time of the solution between hydrophilic regions and hydrophobic regions. However, it is difficult to form a solution layer on nano-scaled hydrophilic regions selectively and replace it with a fresh solution by continuous movement of bubbles while avoiding contact of the solution on hydrophobic regions. This prevents fabrication of nano-scaled pattern with this method. On the other hand, site-selective deposition was realized in solution with our newly developed method using the difference of adhesive strength of depositions to substrates. Heterogeneously nucleated deposition and homogeneously nucleated particles and/or clusters can be removed from octadecyl group regions even if these regions are designed in nanoscale order in which depositions are smaller. This allowed us to realize high feature edge acuity of the patterns compared to site-selective immersion.

The distribution of elements on the surface of the substrates was evaluated by energy dispersive X-ray analysis (EDX), which is built into SEM. Titanium was detected from thin films selectively and oxygen was detected mainly from silanol group regions by EDX (Figure 37). Other elements, except for silicon from the substrate, were not observed from the thin film and substrate by EDX. Oxygen was detected from not only the deposited thin film but also from the natural oxide layer (amorphous SiO_2 layer) formed on all surface areas of a silicon substrate. These observations showed predominant deposition of titanium oxide on silanol group regions.

Thin films deposited at pH 3.8 for 4 h showed an XRD pattern of anatase-type TiO_2 having orientation similar to that of films deposited in the solution at pH 1.5 or 2.8 (Figure 38). The diffraction from parallel to *c* plane such as (004) was observed as being strong compared to that of the randomly oriented powder diffraction pattern (Figure 38). Pizem et al. postulated that the commonly observed [00l] orientation of anatase films could be due to the slight polarity of the planes parallel to the [00l] axis, unlike other low-index planes of this structure such as {100}, (110), and (210). The orientation and crystal growth mechanism are further discussed in a separate article.

Thin films were further evaluated by X-ray photoelectron spectroscopy (XPS). The spectral peaks corresponding to Ti 2p (458.7 eV) were observed from thin films deposited on the silanol region. This binding energy is higher than that of Ti metal (454.0 eV), TiC (454.6 eV), TiO (455.0 eV), TiN (455.7 eV), and Ti_2O_3 (456.7 eV), and similar to that of TiO_2 (458.4–458.7 eV). This suggests that the titanium atoms in thin films are positively charged relative to that of titanium metal by formation of direct bonds with oxygen. On the other hand, this spectrum was not observed from octadecyl group regions. The O 1s spectrum was observed from the silanol regions and divided into O 1s (530.2 eV) and O 1s (532.3 eV). O 1s (532.3 eV) can be assigned to the silicon oxide layer on the surface of the silicon wafer (532.0 eV), whereas the binding energy of O 1s (530.2 eV) is similar to that of TiO_2 (529.9 and 530.1 eV) as observed by Shin et al.[42a] This shows that oxygen is negatively charged compared with neutral oxygen molecules (531.0 eV), possibly through the formation of chemical bonds with Ti. The ratio of titanium to oxygen was estimated from the Ti $2p_{3/2}$ (458.7 eV) spectrum and O 1s (530.2 eV) spectrum to be Ti:O = 1:2.0.

In summary, nano/micro-scaled patterns of anatase TiO_2 was fabricated in an aqueous solution at 50 °C. The difference in adhesive strength of thin films on substrates was employed for the site-selective elimination method. Heterogeneously nucleated TiO_2 and adhered homogeneously nucleated TiO_2 particles on OTS-SAM can be easily eliminated from the substrate by ultrasonication, whereas those on silanol groups maintained their adhesion during the immersion period. The essence of the site-selectivity of this method is a difference in adhesive strength. The site-selective elimination method can be applied to fabricate nano/micro-scaled patterns in the solution by the immersion of the substrate that has regions on which depositions adhere strongly and regions on which depositions adhere weakly enabling elimination by treatment such as ultrasonication.

4.4 Patterning by Catalyst-Induced Heterogeneous Nucleation. 4.4.1 An Example of ZnO: Saito et al. fabricated a ZnO micropattern on phenyl/hydroxy surfaces by a catalyst-induced local supersaturation.[177–179,212] A phenyltrichlorosilane (PTCS) SAM on a substrate was exposed to UV light through a photomask and Pd catalyst was pre-placed on the phenyl sites of the SAM template by selective attachment from a Pd/Sn colloid solution.[179] The substrate was immersed in an NaCl-based Pd/Sn colloid (Cataposit 44, SHIPLEY), which contained 1.8×10^{-3} M $PdCl_2$ and 4.2×10^{-2} M $SnCl_2$, and then accelerated with an acidic solution of HBF_4 (Accelerator 19, SHIPLEY). For deposition of ZnO, an electroless deposition process developed by Izaki and Omi[213] was attempted. The catalyzed SAM substrate was soaked in an aqueous solution of $Zn(NO_3)_2$ (0.05 M) and dimethylamineborane (DMAB) (0.01 M) at 55 °C for 30 min. The chemical reactions for the ZnO electroless deposition process can be written as follows;

$$(CH_3)_2NHBH_3 + OH^- \rightarrow (CH_3)_2NH + BH_3(OH)^- \quad (5)$$

$$BH_3(OH)^- \rightarrow \bullet BH_2(OH)^- + \bullet H \quad (6)$$

$$\bullet BH_2(OH)^- + OH^- \rightarrow BH_2(OH)_2{}^- + e^- \quad (7)$$

$$BH_2(OH)_2{}^- + OH^- \rightarrow BH(OH)_3{}^- + \bullet H + e^- \quad (8)$$

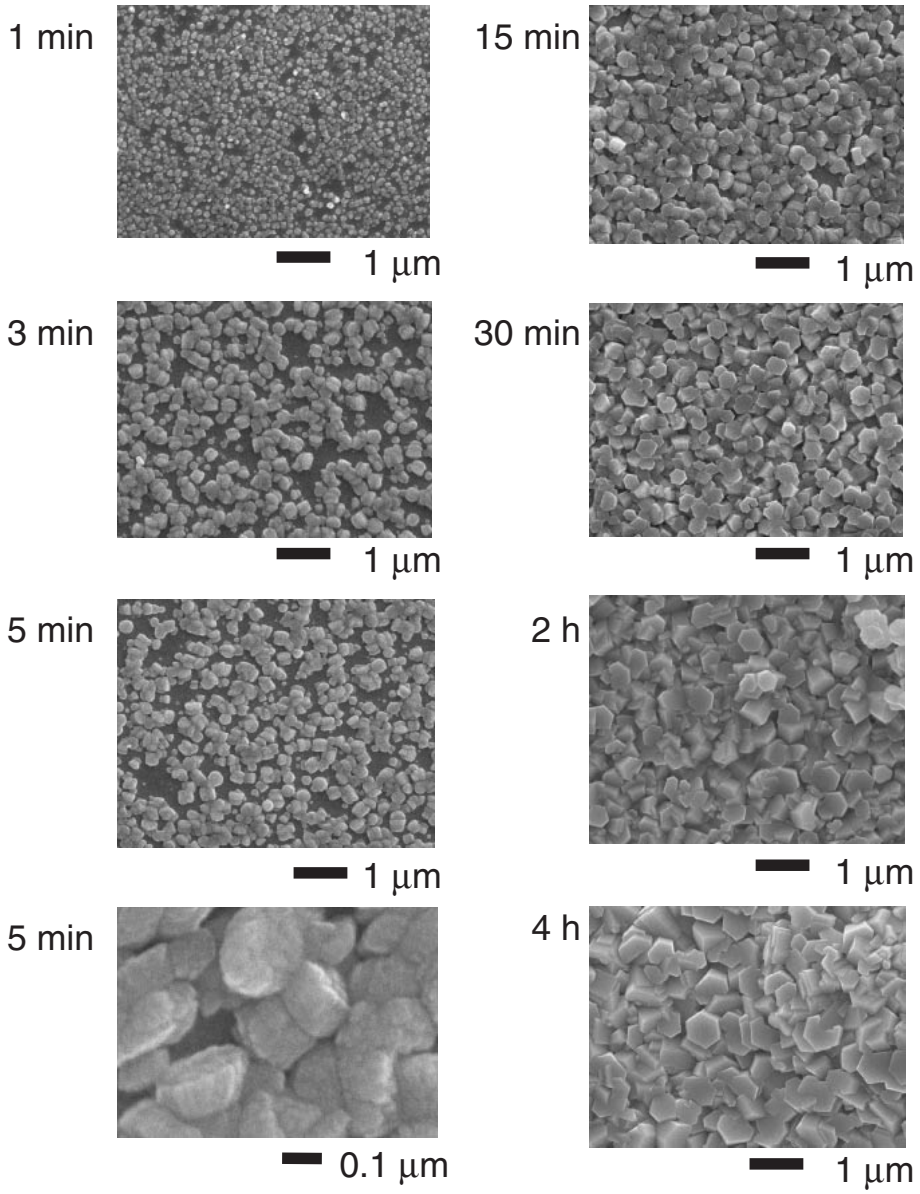

Figure 39. SEM photographs of the ZnO deposits prepared at 55 °C by soaking for 1–240 min. The concentrations of Zn and DMAB were 0.05 and 0.01 mol dm^{-3}, respectively.[216]

$$BH(OH)_3^- + OH^- \rightarrow B(OH)_4^- + \bullet H + e^- \quad (9)$$

$$\bullet H + \bullet H \rightarrow H_2 \quad (10)$$

$$\bullet H + OH^- \rightarrow H_2O + e^- \quad (11)$$

$$(CH_3)_2NH + H_2O \rightarrow (CH_3)_2NH_2^+ + OH^- \quad (12)$$

$$NO_3^- + H_2O + 2e^- \rightarrow NO_2^- + 2OH^- \quad (13)$$

$$Zn^{2+} + 2OH^- \rightarrow ZnO + H_2O \quad (14)$$

As Meerakker explained the oxidation process of reductants,[214] the first step is dehydrogenation, producing a borane radical, $\bullet BH_2(OH)^-$, and an atomic hydrogen, $\bullet H$ (eq 6). At the second step, an electron is produced from the oxidation of the $\bullet BH_2(OH)^-$ radical (eq 7). As shown in the equations 8 and 9, the dehydrogenation and oxidation process proceed, yielding $BH_{4-n}(OH)_n^-$ ($n = 1$–4). Pd catalyst works to promote the dehydrogenation processes.[215] The hydrogen atoms give H_2 gas by recombination (eq 10) or H_2O by oxidation (eq 11). $(CH_3)_2NH$ is ionized in water as eq 12. When the oxidation of DMAB proceeds, NO_3^- ions are reduced to NO_2^- with pH increase (eq 13). The pH of the solution in the vicinity of the catalyst increases and then ZnO becomes deposited (eq 14).

The solution of zinc nitrate and DMAB was transparent during the reaction, and hence deposition occurred via heterogeneous nucleation on the Pd-catalyzed substrate. No deposition was observed on the non-catalyzed substrate. The deposition began just after soaking in the solution. (Figure 39) Initially, the agglomerated particles of about 200 nm composed of small particles (10–30 nm) were deposited. According to the particle growth, the particles became hexagonal in shape. After the catalyst layer was covered by ZnO, the growth rate became slow, but the growth continued due to the thermal decomposition of DMAB.[216] On the catalyzed SAM template, a pattern of

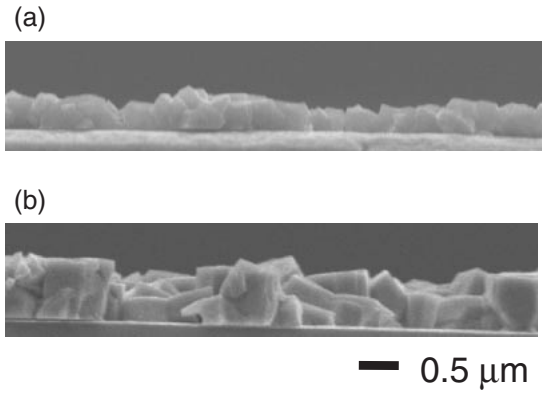

Figure 40. Cross-sectional SEM photographs of the ZnO films after (a) 30 min and (b) 120 min deposition at 55 °C. The concentrations of Zn and DMAB were 0.05 and 0.01 mol dm^{-3}, respectively.[216]

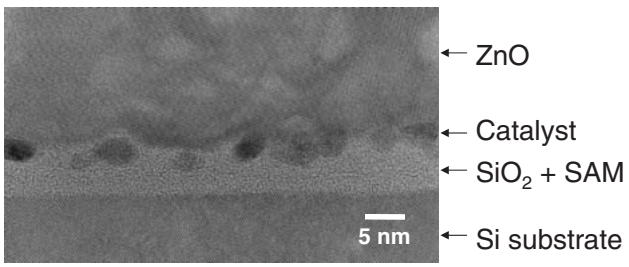

Figure 41. High-resolution transmission electron micrograph of ZnO deposited on the Pd-catalyzed SAM substrate.[179]

polycrystalline ZnO was grown on the phenyl surfaces. The finest line-pattern obtained by this method reached 1 μm in width. The feature edge roughness was estimated as several times of the particle size. Cross-sectional observation by both SEM (Figure 40) and TEM (Figure 41) suggested that the ZnO film was mono particulate layer with few particles being observed on them.

Time-of-flight secondary ion mass spectrometer (TOF-SIMS) is a useful tool to directly analyze a small amount of substances at the outermost surface layers with a spatial resolution of micrometer order. The molecules at the outermost surface are ejected and ionized by the primary ion beam, and the mass of the emitted secondary ions is analyzed by

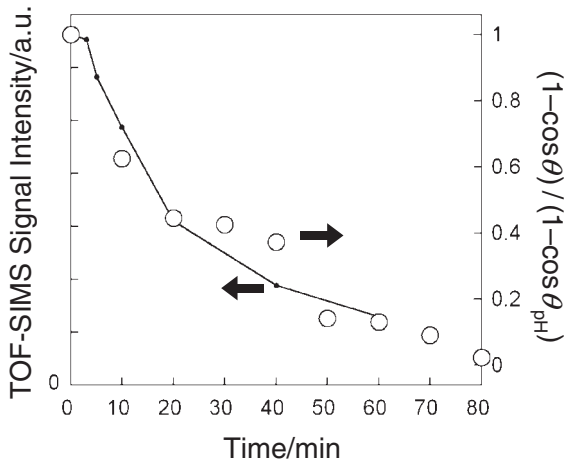

Figure 42. Dependence of TOF-SIMS signal intensity of $^{72}SiC_2H_4O^-$ and water drop contact angle θ on UV-irradiation time. θ_{pH} is contact angle on PTCS-SAM before UV-irradiation. $(1-\cos\theta)/(1-\cos\theta_{pH})$ is correspond to area fraction of phenyl-terminated regions.[212]

the time-of-flight system. It would enable us to analyze the chemical species on the patterned sample surfaces and to obtain their pattern-images. The PTCS-SAM template, the Pd/Sn-catalyzed surface, and ZnO patterns were characterized by using TOF-SIMS.[212] Organo-silane ions and silicon oxide ions were detected on the PTCS-SAM before and after UV-irradiation, respectively, and the dependence of the SIMS signal intensities on UV-irradiation time was studied. Successful mapping of the distribution of these ions on the micropatterned PTCS-SAM was demonstrated. The change in chemical bonds under UV irradiation was also measured using IR absorption spectroscopy with the attenuated total reflectance (ATR) technique. An IR absorption about 1100 cm^{-1}, assigned to planar ring vibration of the Si–C_6H_5 bond,[217] was detected in the PTCS-SAM before UV irradiation and it disappeared after UV-irradiation.[212] The TOF-SIMS and IR data were consistent to the wetting angle measurements data and they revealed that PTCS was modified by UV (Figure 42). By observing the catalyzed template, selective adhesion of Pd and Sn on the non-UV-irradiated PTCS-SAM areas was found (Figure 43). More Pd and Sn were detected in the phenyl-regions than in the OH-regions both before and after acceleration. Before acceleration, a significant amount of Sn was

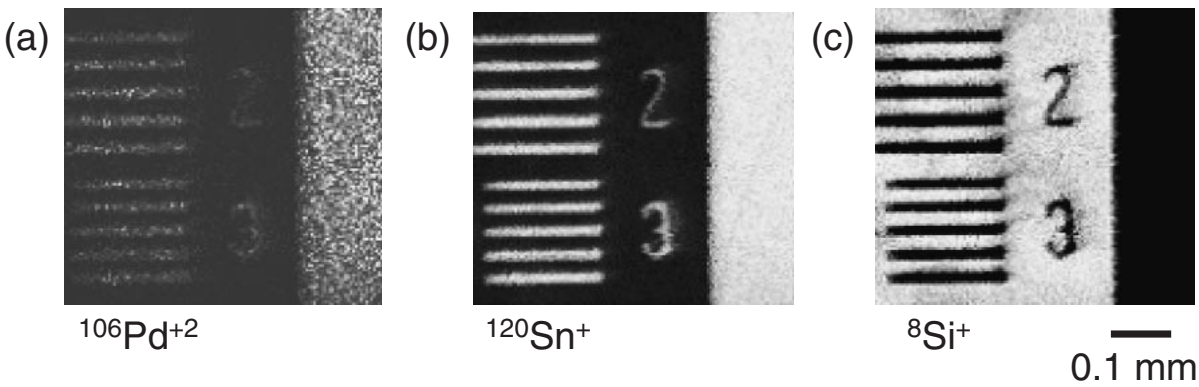

Figure 43. TOF-SIMS signal maps of (a) $^{106}Pd^+$, (b) $^{120}Sn^+$, and (c) $^{28}Si^+$ for catalyzed template before acceleration.[212]

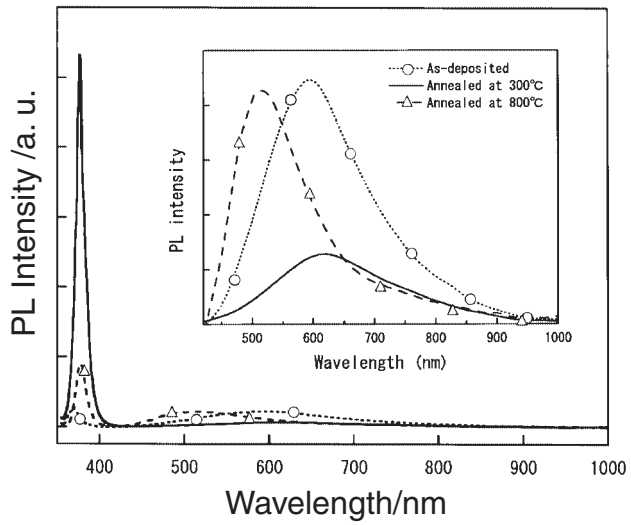

Figure 44. Photoluminescence spectra from the samples as-deposited and annealed at 300 and 800 °C. The inset shows the magnified spectra over 420 nm.[177]

detected on the OH-surface, while little Pd was detected on the OH-surfaces. The Pd/Sn catalyst colloid consists of an aqueous solution containing Sn ions and catalyst particles, where Pd–Sn alloy cores are surrounded by Sn^{II} layers, which play a role of stabilizing the colloid. The detection of Sn ions on OH-surfaces is probably due to the adsorption of Sn ions in the colloid solution. The signal intensity of Sn decreased to 1/6 and the signal intensity of Pd changed only a little after acceleration. This suggests that most Sn^{II} surrounding layer of the catalyst colloid was dissolved by acceleration, while Pd–Sn alloy particle cores remained. Analysis of the ZnO pattern revealed that zinc oxide, including boron, was deposited on the catalyzed phenyl regions.

The as-deposited ZnO micropattern showed broad visible-light (500–800 nm) luminescence[179] and the monochromatic cathodoluminescence (CL) imaging for 1 μm wide lines was demonstrated. Because the ZnO samples were produced under aqueous conditions at low temperatures, they contained hydroxide. As luminescence properties are sensitive to the quality of the crystal structure, the OH inclusion in ZnO can influence the luminescence colors and the efficiency. Post-deposition annealing influenced the luminescence properties of the ZnO patterns.[177] Thermal desorption spectroscopy (TDS) and infrared spectroscopy revealed the change of the amount of H_2O in ZnO. After annealing above 150 °C, UV exciton emission (377 nm) exhibited and the UV intensity peaked at 300 °C (Figure 44). A patterned monochromatic CL image of the UV emission was obtained for the annealed ZnO micro lines.

4.4.2 Examples of Iron Oxides: A similar consideration can be also extended to produce other metal oxides. For example, an iron oxide Fe_3O_4, and an iron hydroxide oxide (g-FeOOH) were also grown using DMAB and $Fe(NO_3)_3$ at 80 °C.[182] In this case, catalyst of Pd species was only adsorbed to amino-terminated SAMs, not to the photo-irradiated hydrophilic areas, which was confirmed experimentally by mapping using secondary ion mass spectroscopy (SIMS). The selectivity of catalyst adsorption was also confirmed by XPS, the results of which showed that the Pd element was only located on the NH_2-terminated regions, not on OH-terminated ones. XPS also revealed that the Pd element on the APTS-SAM mainly bonded to oxygen in the form of Pd–O or Pd–OH, but peaks for a Pd–N bond were not observed. The particle size for the Pd colloid was about 30 nm in diameter, which exceeds the thickness detection limit for XPS. Thus, the failure in detecting a Pd–N peak did not mean the nonexistence of it. However, the surface potentials at pH 5, typically, +27 mV for APTS-SAMs, −31 mV for Pd colloid particles, and −33 mV or UV-irradiated APTS-SAMs, strongly suggested that the selective adsorption of Pd might be driven by electrostatic force. When the substrate bearing of catalyst was soaked in a solution containing $Fe(NO_3)_3$ and DMAB, Pd–O and Pd–OH were reduced to metal Pd by a reduction reaction between adsorbed catalyst and DMAB. The reaction to magnetite might follow the formation of Pd. For yielding magnetite, Fe^{3+} should be reduced in part to Fe^{2+}, which requires regulating the solution conditions such as pH or solution temperature.

4.5 Pattern-Deposition on Polymer Substrates. Integration of functional ceramic films into flexible substrates such as plastics or papers has attracted increasing interest in the preparation of electronic or optical devices that may be low-weight, low-cost, transparent, and high performance. Patterning on such surfaces is fundamental for integration of structures and performance to meet these applications. Modification of surface properties using SAMs is a well-established method, which has been developed for substrates with surface hydroxy groups such as glass, Si, or other oxide surfaces. However, the polymer surface is usually hydrophobic and inactive to chemical reactions. Films are either difficult to grow or show weak adhesion to the surface. Typically, these problems are overcome by increasing the surface energy of the materials through introducing polar functionality by either physical (X-ray, laser, ion beam, plasma treatment, or flame treatment)[218–228] or chemical surface modification.[229–235] Plasma treatment using different gases produces different reactive radicals. Oxygen creates hydroxy, carbonyl, carboxyl, ester, ether, and hydroperoxyl functional groups, among others. Nitrogen and ammonia create amino groups. The plasma treatment using argon creates long-lived carbon radicals, which when exposed to air form mainly hydroperoxyl radicals. These can react with the silanes and form a SAM, which is basic for patterning using the method for ceramics. Recent progress in this area involves preparation of an intermediate active layer, a silica-like layer as thin as molecular scale on the surface of polymers, by either chemical grafting[229–235] or physical deposition.

We successfully developed a simple process for fabricating a silica-like layer on poly(ethylene terephthalate) (PET) under ambient conditions.[236] 3-Aminopropyltrimethoxysilane was employed to react with acetone to form dimethyliminopropyltrimethoxysilane (DIPTMS) after aging for 10 days at room temperature. After partial hydrolysis of alkoxy groups in DIPTMS, dimethylimine-modified silica clusters (oligomers) occurred resulting in the increase of the solution viscosity. Consequently, a dense and homogeneous thin layer was easily dip-coated onto a PET film. After thermal treatment at 150 °C, a smooth, flexible, and transparent silica-like film was formed via dehydration and condensation. TEM images and an elec-

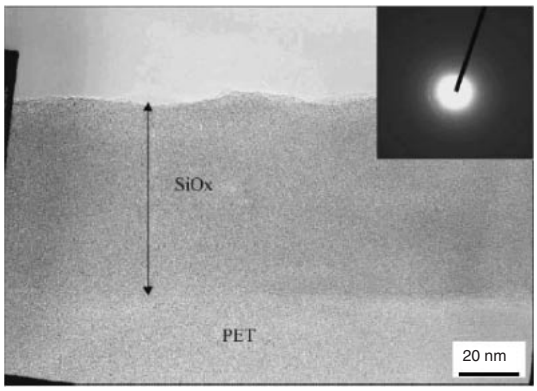

Figure 45. TEM photograph of silica-like coating on PET.[236]

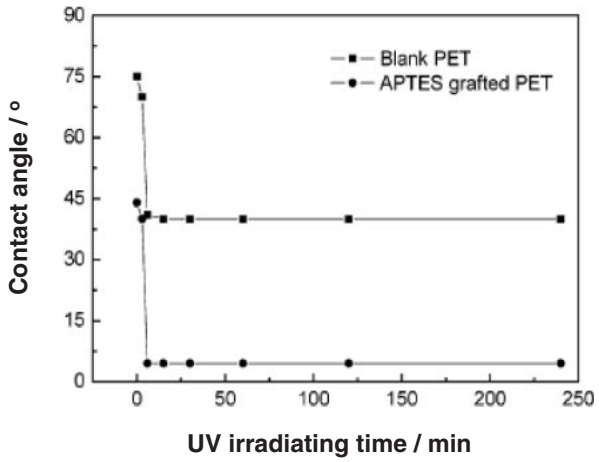

Figure 46. Changes of water contact angles of polymer surface as a function of UV irradiation time before and after buffer layer coating.[147]

tron diffraction pattern (Figure 45) showed that an amorphous coating formed on the PET with the thickness of about 70 nm. EDS revealed the presence of Si and O elements in the coating. The coating was a dense and flat film with such a high adhesion to the PET substrate that it could hardly be peeled off by the usual scotch tape peeling test. The chemical amide bond formation between the residual amine groups in the silica-like coatings and carboxyl groups on the PET should be responsible for the relatively high adhesion. No particulates could be observed even in TEM photographs. This is a major difference compared to the sol–gel coating of tetraethylorthosilicate.[237] The results of water contact angle (WCA) measurements revealed a significant decrease from 70 ± 2 to 45 ± 3^{o} after the modification with silica solution. Moreover, we achieved a hyper hydrophilic surface (WCA around 4 ± 1^{o}) on the modified PET after only 5 min UV irradiation while WCA remained constant at around 40 ± 2^{o} on pure PET even under UV irradiation for a very long time (Figure 46). As one practical application for silica-like layer coating, we attempted to prepare a gas barrier film, which was a thin film of lithium metasilicate on PET covered with a silica-like layer. The modified PET was directly dipped into 5 vol % lithium metasilicate solution and slowly lifted out. After 3 h of drying at room temperature, the films were heated at 120 °C for

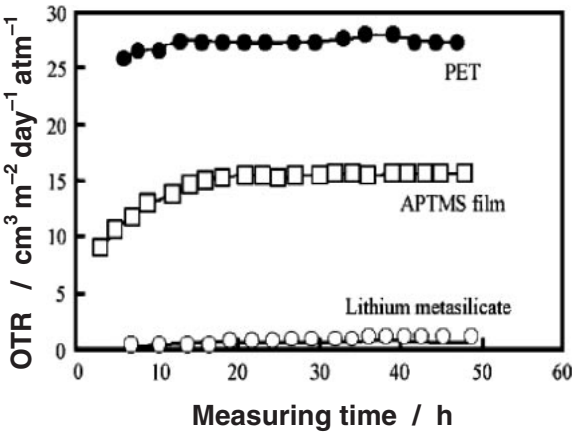

Figure 47. Oxygen permeability of pure PET, polymer silica-coated PET, and lithium-metasilicate-coated PET.[236]

10 min. Figure 47 shows the results of oxygen permeability of the PET before and after surface modification. Pure PET has the largest oxygen permeability of $\approx 30\,cm^3\,m^{-2}\,day^{-1}\,atm^{-1}$. The thick silica-like coating on the PET prepared by dip coating (about 600 nm) also showed better barrier property (about $15\,cm^3\,m^{-2}\,day^{-1}\,atm^{-1}$), and lithium metasilicate-coated PET (about 2.5 nm thick) exhibited the lowest oxygen permeability ($0.17\,cm^3\,m^{-2}\,day^{-1}\,atm^{-1}$).

Nanodevices, especially those integrated on flexible substrates, are expected to be applied in many fields since they offer many advantages, including suitability for any complex shape, minimum size, low power, and high performance. Despite of these advantages, nanodevices still await practical application due to the lack of an effective process for fabricating the functional materials coating on polymer substrates with high quality at a competitive cost. With the process of silica-like coating we also made the attempts in fabricating TiO_2 and metal copper micropattern on flexible substrates at room temperature.

By grafting (aminopropyl)triethoxysilane (APTES) as the buffer layer on a poly(ethylene terephthalate) (PET) surface, the SAMs of octadecyltrichlorosilane (OTS), phenyltrichlorosilane (PTCS), vinyltrichlorosilane (VTCS), and *p*-tolyltrichlorosilane (TTCS) were easily fabricated on the flexible polymer substrates. The contact angle is mainly affected by the terminal functional groups and the coverage of SAMs on substrates.[118a] The coverage of SAMs on substrates could be controlled by varying the immersing time in trichlorosilane solutions and the concentration of the solutions. To obtain the optimized immersing time, the substrates were immersed in toluene solution of PTCS and TTCS monomers for different times (Figure 48). The micropatterned SAMs through a photomask were submerged in the aqueous solution to form TiO_2 micro pattern by the liquid-phase deposition (LPD) process.[35a] TiO_2 was nucleated and combined with SiOH (OH-SAM) to form Ti–O–Si bonds and resulted in films. These films showed strong adhesion to the substrates and did not peel off when subjected to sonication. On the contrary, the hydrophobic (PTCS-SAM or TTCS-SAM) surface suppressed the nucleation of TiO_2. Accordingly, TiO_2 film was site-selectively deposited on the hydrophilic surface and a micropattern was obtained (Figure 49).

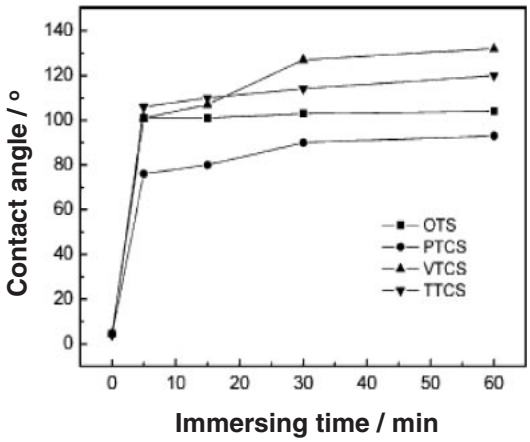

Figure 48. Changes of water contact angle on SAMs as a function of immersing time in alkoxysilane solutions.[147]

Moreover, we successfully prepared micropatterned metallic copper films on modified PET. Copper metal was found to selectively deposit onto PET substrate modified with thiol-group (SH) terminated SAM by the means of electroless (EL) deposition in a neutral solution without any catalysts (Figure 50)[238] Self-assembled monolayer terminated with SH groups by using 3-mercaptopropyltrimethoxysilane was formed on PET substrates covering with a silica-like layer and then irradiated by UV light through a photomask to prepare thiol-group regions and OH-group regions. XPS analysis was performed to detect the formation of MPTS-SAM on the modified PET. The S2p peak observed before UV irradiation (a) disappeared after UV irradiation (b) (Figure 51). Dimethylamineborane was employed as a reducing reagent in EL solutions. The selective deposition of copper metal was observed on thiol-SAM rather than on OH-SAM and subsequently micropatterning of Cu film was successfully achieved (Figure 52). The chemical affinity of

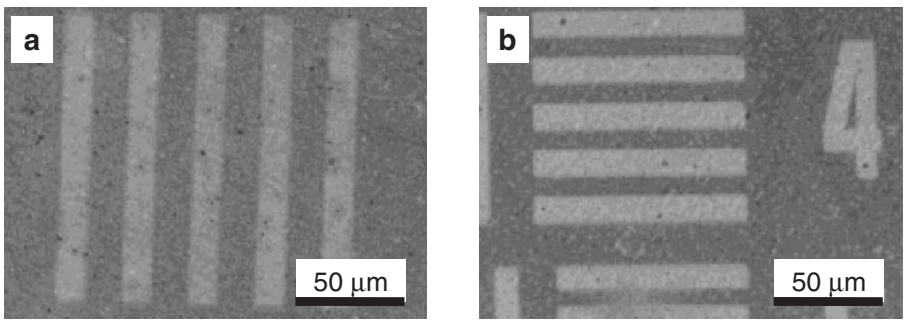

Figure 49. Optical micrographs of TiO_2 micropattern deposited on (a) PTCS-SAM and (b) TTCS-SAM.[147]

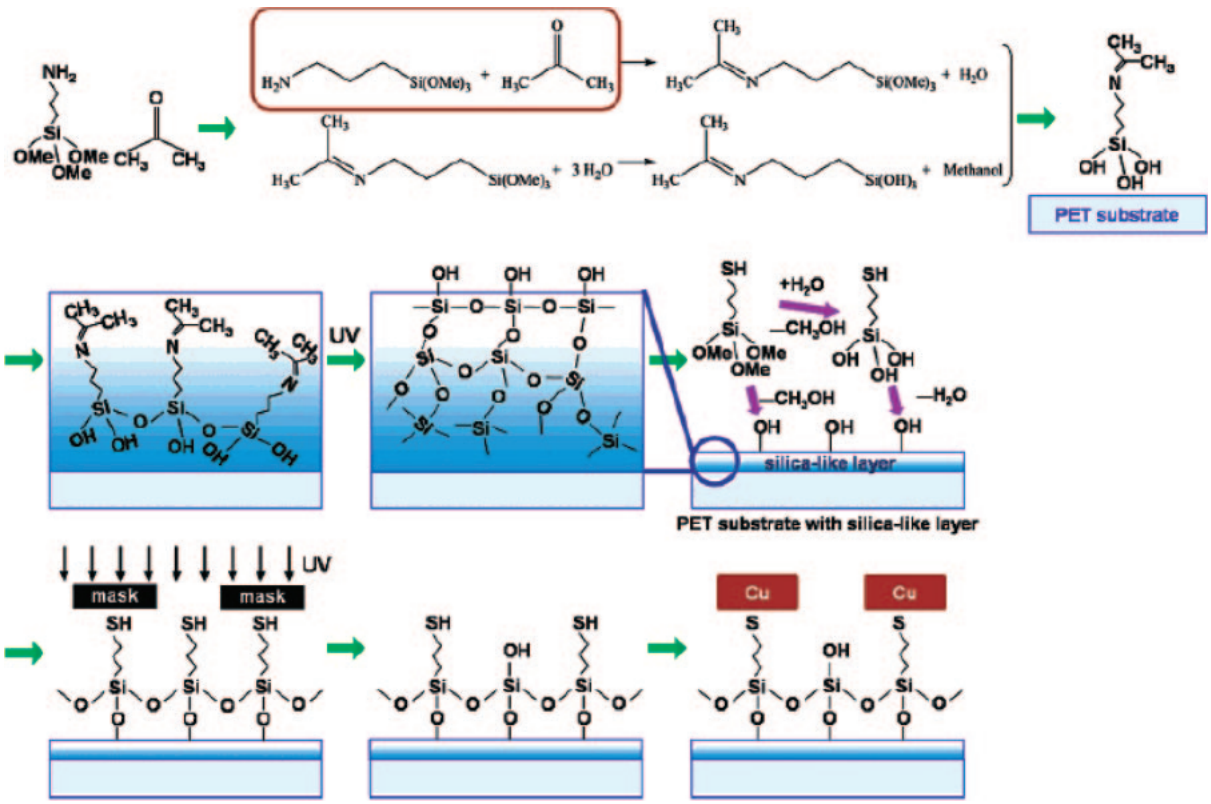

Figure 50. Conceptual process for fabricating a micropattern of metallic copper thin film.[201]

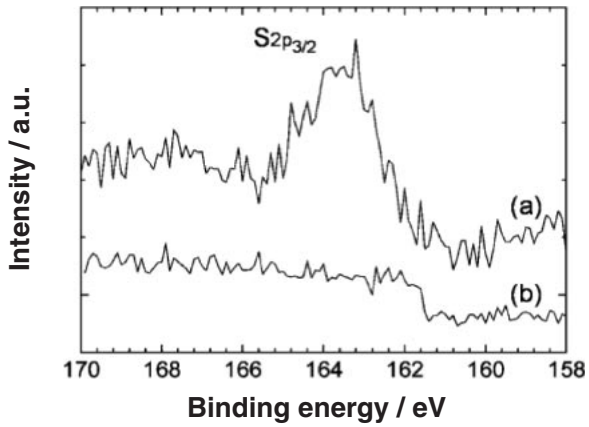

Figure 51. XPS spectra for PET films modified with an MPTS-SAM. (a) before and (b) after UV irradiation.[201]

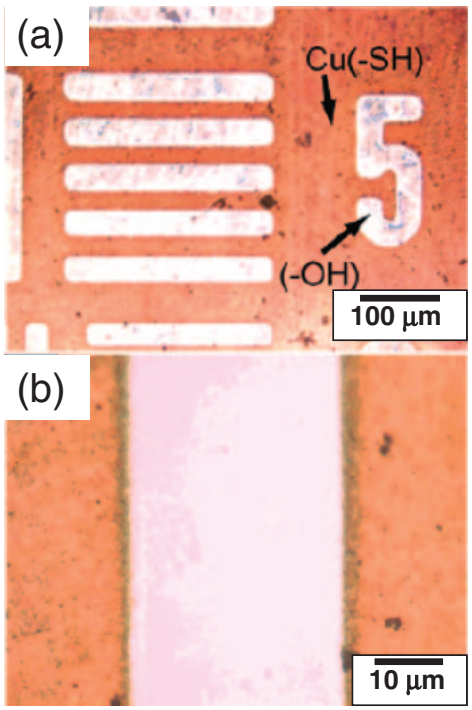

Figure 52. Optical microscope images of (a) the as-deposited film and (b) the magnified area. The white (–OH) and copper (–SH) regions show the films selective deposition of metal copper.[201]

Cu metal toward sulfur should be more effective and responsible for site-selective deposition. The mechanism was apparently different from the electrostatic adhesion of charged particles as described above so that the micro pattern resolution of copper films appeared to be comparatively very high. Although the electrical conductivity of the resulting Cu film was 7.9×10^4 ($S\,cm^{-1}$), which is relatively lower than that of standard Cu metal ($5.8 \times 10^5\,S\,cm^{-1}$),[239] this process sounds very attractive and is of potential application in many areas such as nano technology fields and very large scale integration (VLSI) systems if problems such as the rough condition at grain boundaries and low crystallization degree of metal films can be completely resolved.

In general, to improve the physical properties of solution-derived film so that they can be applied practically, all the problems such as interfacial reactions and diffusion, preparation of well-crystallized films, and optimization of their density, thickness, and roughness need to be addressed. All of these areas are interesting and attractive.

5. Summary

In the present article, two key points have been reviewed. First, the techniques are based on nucleation and growth onto functionalized interfaces; second, novel solution systems have been developed for the production of ceramic oxides through precipitation from aqueous solutions. The understanding of interface–surface interactions and solution chemistry has been partially achieved, and some basic and important results have been obtained.

(1) By the design of novel solution systems and the control of the supersaturation of solution, nanostructured ceramic oxides can be deposited on a substrate (plastic, ceramic, glass, metal, single crystal, etc.) with a large area and complex shape.

(2) SAMs can effectively modify the physical and chemical properties of the surface, which have effects on the improvement of adhesion, control of the morphology, and even the growth mechanism of the film.

(3) Selective UV-irradiation of a SAM surface can form a template with different functional groups, which results in different surface–interface interactions during the deposition process. Hence, patterned SAM templates can be employed for patterning of ceramic oxides directly in solutions.

(4) For the pattern-deposition by electrostatic interaction between the homogeneous nucleated particles and the substrate, patterned SAMs having negative/positive zeta potential were required. For the film formation via heterogeneous nucleation, SAM patterns with hydrophilic/hydrophobic surface functional groups or high/low surface energy were effective in site-selective deposition.

Bioinspired ceramic processing is a promising technique to replace conventional processes for the fabrication of ceramics in a cost-effective, environmentally friendly manner. Science and technologies developed in this study will hopefully make bioinspired ceramic processing more attractive and promising.

References

1 a) Y. Xia, G. M. Whitesides, *Angew. Chem., Int. Ed.* **1998**, *37*, 550. b) R. F. Service, *Science* **1996**, *273*, 1800. c) G. Moore, *Electrochem. Soc. Interface* **1997**, *6* 18. d) M. Geissler, Y. Xia, *Adv. Mater.* **2004**, *16*, 1249. e) Y. Xia, *Adv. Mater.* **2004**, *16*, 1245. f) G. Whitesides, *Angew. Chem., Int. Ed. Engl.* **1990**, *29*, 1209.

2 a) R. F. Pease, *Nature* **2002**, *417*, 802. b) S. M. Sze, *Semiconductor Devices: Physics and Technology*, John Wiley, New York, **1985**. c) T. Ito, S. Okazaki, *Nature* **2000**, *406*, 1027.

3 S. Hoeppener, R. Maoz, S. R. Cohen, L. F. Chi, H. Fuchs, J. Sagiv, *Adv. Mater.* **2002**, *14*, 1036.

4 C. B. Murray, C. R. Kagan, M. G. Bawendi, *Annu. Rev. Mater. Sci.* **2000**, *30*, 545.

5 A. C. Templeton, W. P. Wuelfing, R. W. Murray, *Acc. Chem. Res.* **2000**, *33*, 27.

6 K. C. Grabar, K. J. Allison, B. E. Baker, R. M. Bright,

K. R. Brown, R. G. Freeman, A. P. Fox, C. D. Keating, M. D. Musick, M. J. Natan, *Langmuir* **1996**, *12*, 2353.

7 M. T. Reetz, M. Winter, R. Breinbauer, T. Thurn-Albrecht, W. Vogel, *Chem.—Eur. J.* **2001**, *7*, 1084.

8 C. N. R. Rao, G. U. Kulkarni, P. J. Thomas, P. P. Edwards, *Chem.—Eur. J.* **2002**, *8*, 28.

9 X. Peng, L. Manna, W. Yang, J. Wickham, E. Scher, A. Kadavanich, A. P. Alivisatos, *Nature* **2000**, *404*, 59.

10 X. Peng, *Chem.—Eur. J.* **2002**, *8*, 334.

11 G. Schmid, L. F. Chi, *Adv. Mater.* **1998**, *10*, 515.

12 Y. Huang, X. Duan, Q. Wei, C. M. Lieber, *Science* **2001**, *291*, 630.

13 C. Durkan, M. E. Welland, *Phys. Rev. B* **2000**, *61*, 14215.

14 T. W. Ebbesen, H. J. Lezec, H. Hiura, J. W. Bennett, H. F. Ghaemi, T. Thio, *Nature* **1996**, *382*, 54.

15 W. Fudickar, J. Zimmermann, L. Ruhlmann, J. Schneider, B. Röder, U. Siggel, J.-H. Fuhrhop, *J. Am. Chem. Soc.* **1999**, *121*, 9539.

16 S. Hirano, T. Yogo, W. Sakamoto, S. Yamada, T. Nakamura, T. Yamamoto, H. Ukai, K. Banno, T. Nakafuku, Y. Ando, *J. Sol.-Gel Sci. Technol.* **2003**, *26*, 35.

17 C.-H. Chang, W.-C. Chen, *Chem. Mater.* **2002**, *14*, 4242.

18 For example: a) P. G. Clem, R. J. Ong, J. T. Dawley, *J. Mater. Res.* **2003**, *18*, 2310. b) H. Ohta, M. Orita, M. Hirano, H. Tanji, H. Kawazoe, H. Hosono, *Appl. Phys. Lett.* **2000**, *76*, 2740. c) G. Schottner, *Chem. Mater.* **2001**, *13*, 3422.

19 W.-G. Choi, E.-S. Choi, S.-G. Yoon, *Chem. Vap. Deposition* **2003**, *9*, 321.

20 C. W. Ong, D. G. Zong, M. Aravind, C. L. Choy, D. R. Lu, *J. Mater. Res.* **2003**, *18*, 2464.

21 R. Bhakta, F. Hipler, A. Devi, S. Regnery, P. Ehrhart, R. Waser, *Chem. Vap. Deposition* **2003**, *9*, 295.

22 R. L. Puurunen, *Chem. Vap. Deposition* **2003**, *9*, 327.

23 S. Fireman-Shoresh, D. Avnir, S. Marx, *Chem. Mater.* **2003**, *15*, 3607.

24 J. G. Lisoni, C. H. Lei, T. Hoffmann, V. M. Fuenzalida, *Surf. Sci.* **2002**, *515*, 431.

25 B. M. Trost, *Angew. Chem.* **1995**, *107*, 285.

26 Y. Masuda, Doctoral Thesis, Nagoya University, **2003**, p. 1.

27 T. P. Niesen, M. R. DeGuire, *J. Electroceram.* **2001**, *6*, 169.

28 C. D. Lokhande, *Mater. Chem. Phys.* **1991**, *27*, 1.

29 I. Grozdanov, *Semicond. Sci. Technol.* **1994**, *9*, 1234.

30 a) A. J. Varkey, A. F. Fort, *Thin Solid Films* **1993**, *235*, 47. b) B. Pejova, T. Kocareva, M. Najdoski, I. Grozdanov, *Appl. Surf. Sci.* **2000**, *165*, 271.

31 For example: a) V. P. Tolstoy, I. V. Murin, A. Reller, *Appl. Surf. Sci.* **1997**, *112*, 255. b) M. Ristov, G. J. Sinadinovski, I. Grozdanov, *Thin Solid Films* **1985**, *123*, 63.

32 a) S. Deki, Y. Aoi, Y. Asaoka, A. Kajinami, M. Mizuhata, *J. Mater. Chem.* **1997**, *7*, 733. b) S. Deki, Y. Aoi, *J. Mater. Res.* **1998**, *13*, 883, and refrences therein. c) T. Yao, Y. Uchimoto, T. Sugiyama, Y. Nagai, *Solid State Ionics* **2000**, *135*, 359.

33 a) F. Goto, M. Ichimura, E. Arai, *Jpn. J. Appl. Phys.* **1997**, *36*, L1146. b) M. Ichimura, F. Goto, E. Arai, *J. Electrochem. Soc.* **1999**, *146*, 1028.

34 See review article: M. Abe, *MRS Bull.* **2000**, *25*, 51.

35 a) K. Koumoto, S. Seo, T. Sugiyama, W. S. Seo, W. J. Dressick, *Chem. Mater.* **1999**, *11*, 2305. b) Y. Masuda, T. Sugiyama, K. Koumoto, *J. Mater. Chem.* **2002**, *12*, 2643.

36 a) Y. Masuda, T. Sugiyama, H. Lin, W. S. Seo, K. Koumoto, *Thin Solid Films* **2001**, *382*, 153. b) Y. Masuda, Y. Jinbo, T. Yonezawa, K. Koumoto, *Chem. Mater.* **2002**, *14*, 1236.

37 R. J. Collins, H. Shin, M. R. DeGuire, A. H. Heuer, C. N. Sukenik, *Appl. Phys. Lett.* **1996**, *69*, 860.

38 Y. Gao, Y. Masuda, T. Yonezawa, K. Koumoto, *J. Ceram. Soc. Jpn.* **2002**, *110*, 379.

39 a) M. Bartz, A. Terfort, W. Knoll, W. Tremel, *Chem.—Eur. J.* **2000**, *6*, 4149. b) T. P. Niesen, J. Bill, F. Aldinger, *Chem. Mater.* **2001**, *13*, 1552. c) H. Pizem, C. N. Sukenik, U. Sampathkumaran, A. K. McIlwain, M. R. DeGuire, *Chem. Mater.* **2002**, *14*, 2476.

40 a) Y. Gao, Y. Masuda, T. Yonezawa, K. Koumoto, *Chem. Mater.* **2002**, *14*, 5006. b) Y. Gao, Y. Masuda, K. Koumoto, *Chem. Mater.* **2003**, *15*, 2399.

41 P. X. Zhu, Y. Masuda, K. Koumoto, *J. Colloid Interface Sci.* **2001**, *243*, 31.

42 a) H. Shin, R. J. Collins, M. R. DeGuire, A. H. Heuer, C. N. Sukenik, *J. Mater. Res.* **1995**, *10*, 692. b) S. Supothina, M. R. DeGuire, *Thin Solid Films* **2000**, *371*, 1.

43 a) H. Shin, M. Agarwal, M. R. DeGuire, A. H. Heuer, *Acta Mater.* **1998**, *46*, 801. b) J. Aizenberg, P. V. Braun, P. Wiltzius, *Phys. Rev. Lett.* **2000**, *84*, 2997.

44 D. Huang, Z. D. Xiao, J. H. Gu, N. P. Huang, C. W. Yuan, *Thin Solids Films* **1997**, *305*, 110.

45 S. Baskaran, L. Song, J. Liu, Y. L. Chen, G. L. Graff, *J. Am. Ceram. Soc.* **1998**, *81*, 401.

46 a) S. Y. Chou, C. Keimel, J. Gu, *Nature* **2002**, *417*, 835. b) S. Y. Chou, P. R. Krauss, P. J. Renstrom, *Science* **1996**, *272*, 85.

47 a) G. M. Whitesides, B. Grzybowski, *Science* **2002**, *295*, 2418. b) H. Yan, S. H. Park, G. Finkelstein, J. H. Reif, T. H. LaBean, *Science* **2003**, *301*, 1882. c) J. Aizenberg, D. A. Muller, J. L. Grazul, D. R. Hamann, *Science* **2003**, *299*, 1205. d) T. Douglas, *Science* **2003**, *299*, 1192. e) Y. Lin, H. Skaff, T. Emrick, A. D. Dinsmore, T. P. Russell, *Science* **2003**, *299*, 226. f) B. C. Bunker, P. C. Rieke, B. J. Tarasevich, A. A. Campbell, G. E. Fryxell, G. L. Graff, L. Song, J. Liu, J. W. Virden, G. L. McVay, *Science* **1994**, *264*, 48.

48 a) X.-M. Zhao, Y. Xia, G. M. Whitesides, *J. Mater. Chem.* **1997**, *7*, 1069. b) P. M. Moran, F. F. Lange, *Appl. Phys. Lett.* **1999**, *74*, 1332. c) J. H. Kim, F. F. Lange, C. I. Cheon, *J. Mater. Res.* **1999**, *14*, 1194.

49 a) E. Kim, Y. Xia, G. M. Whitesides, *J. Am. Chem. Soc.* **1996**, *118*, 5722. b) C. R. Martin, I. A. Aksay, *J. Phys. Chem. B* **2003**, *107*, 4261. c) M. Yu, J. Lin, Z. Wang, J. Fu, S. Wang, H. J. Zhang, Y. C. Han, *Chem. Mater.* **2002**, *14*, 2224.

50 A. Matsuda, Y. Matsuno, M. Tatsumisago, T. Minami, *J. Am. Ceram. Soc.* **1998**, *81*, 2849.

51 a) T. Yogo, Y. Takeichi, K. Kikuta, S. Hirano, *J. Am. Ceram. Soc.* **1995**, *78*, 1649. b) K. Kikuta, K. Suzumori, K. Takagi, S. Hirano, *J. Am. Ceram. Soc.* **1999**, *82*, 1569.

52 a) C. S. Ganpule, A. Stanishevsky, Q. Su, S. Aggarwal, J. Melngaillis, E. Wiliams, R. Ramesh, *Appl. Phys. Lett.* **1999**, *75*, 409. b) C. S. Ganpule, A. Stanishevsky, S. Aggarwal, J. Melngaillis, E. Wiliams, R. Ramesh, V. Joshi, C. P. de Araujo, *Appl. Phys. Lett.* **1999**, *75*, 3874.

53 S. Okamura, K. Mori, T. Tsukamoto, T. Shiosaki, *Integr. Ferroelectr.* **1997**, *18*, 311.

54 S. Y. Chou, P. R. Krauss, P. J. Renstrom, *Science* **1996**, *272*, 85.

55 R. J. Jackman, J. L. Wilbur, G. M. Whitesides, *Science* **1995**, *269*, 664.

56 D. Eaglesham, M. Cerullo, *Phys. Rev. Lett.* **1990**, *64*, 1943.

57 Y. Lin, H. Skaff, T. Emrik, A. D. Dinsmore, T. P. Russell,

Science **2003**, *299*, 226.
58 C. R. Martin, I. A. Aksay, *J. Electroceram.* **2004**, *12*, 53.
59 M. Alexe, C. Harnagea, D. Hesse, *J. Electroceram.* **2004**, *12*, 69.
60 a) E. Bäuerlein, *Angew. Chem., Int. Ed.* **2003**, *42*, 614. b) S. Mann, *Biomimetic Materials Chemistry*, VCH, New York, **1996**, p. 1. c) I. A. Aksay, M. Trau, S. Manne, I. Honma, N. Yao, L. Zhou, P. Fenter, P. M. Eisenberger, S. M. Gruner, *Science* **1996**, *273*, 892. d) W. M. Tolles, *MRS Bull.* **2000**, *25*, 36.
61 J. H. Fendler, F. C. Meldrum, *Adv. Mater.* **1995**, *7*, 607.
62 a) M. Zharnikov, M. Grunze, *J. Vac. Sci. Technol., B* **2002**, *20*, 1793. b) A. J. Wagner, S. R. Carlo, C. Vecitis, D. H. Fairbrother, *Langmuir* **2002**, *18*, 1542. c) A. J. Wagner, K. Han, A. L. Vaught, D. H. Fairbrother, *J. Phys. Chem. B* **2000**, *104*, 3291. d) S. R. Carlo, A. J. Wagner, D. H. Fairbrother, *J. Phys. Chem. B* **2000**, *104*, 6633. e) Y.-H. La, Y. J. Jung, H. J. Kim, T.-H. Kang, K. Ihm, K.-J. Kim, B. Kim, J. W. Park, *Langmuir* **2003**, *19*, 4390. f) R. R. Rye, *J. Polym. Sci. B* **1988**, *26*, 2133. g) W. K. Fisher, J. C. Corelli, *J. Polym. Sci., Part A: Polym. Chem.* **1981**, *19*, 2465.
63 a) N. Mino, S. Ozaki, K. Ogawa, M. Hatada, *Thin Solid Films* **1994**, *243*, 374. b) R. Krupke, S. Malik, H. B. Weber, O. Hampe, M. M. Kappes, H. v. Lohneysen, *Nano Lett.* **2002**, *2*, 1161.
64 a) C. Evans, N. Wade, F. Pepi, G. Strossman, T. Schuerlein, R. G. Cooks, *Anal. Chem.* **2002**, *74*, 317. b) J. Shen, V. Grill, C. Evans, R. G. Cooks, *J. Mass Spectrom.* **1999**, *34*, 354. c) P. Cyganik, Z. Postawa, C. A. Meserole, E. Vandeweert, N. Winograd, *Nucl. Instrum. Methods Phys. Res., Sect. B* **1999**, *148*, 137.
65 a) N. Saito, K. Hayashi, H. Sugimura, O. Takai, *J. Mater. Chem.* **2002**, *12*, 2684. b) Z. Yang, W. Frey, T. Oliver, A. Chilkoti, *Langmuir* **2000**, *16*, 1751. c) D. A. Hutt, E. Cooper, G. J. Leggett, *J. Phys. Chem. B* **1998**, *102*, 174. d) W. J. Dressick, C. S. Dulcey, J. H. Georger, J. M. Calvert, *Chem. Mater.* **1993**, *5*, 148. e) J. Jennane, T. Boutros, R. Giasson, *Can. J. Chem.* **1996**, *74*, 2509. f) K. Lee, F. Pan, G. T. Carroll, N. J. Turro, J. T. Koberstein, *Langmuir* **2004**, *20*, 1812. g) J. P. Lee, H. K. Kim, C. R. Park, G. Park, H. T. Kwak, S. M. Koo, M. M. Sung, *J. Phys. Chem. B* **2003**, *107*, 8997.
66 a) W. J. Dressick, J. M. Calvert, *Jpn. J. Appl. Phys.* **1993**, *32*, 5829. b) W. J. Dressick, C. S. Dulcey, M.-S. Chen, J. M. Calvert, *Thin Solid Films* **1996**, *284–285*, 568. c) W. J. Dressick, M.-S. Chen, S. L. Brandow, *J. Am. Chem. Soc.* **2000**, *122*, 982.
67 a) B. J. Tarasevich, P. C. Rieke, J. Liu, *Chem. Mater.* **1996**, *8*, 292. b) P. C. Rieke, R. Wiecek, B. D. Marsh, L. L. Wood, J. Liu, L. Song, G. E. Fryxell, B. J. Tarasevich, *Langmuir* **1996**, *12*, 4266.
68 a) J. Aizenberg, A. J. Black, G. M. Whitesides, *Nature* **1998**, *394*, 868. b) J. Aizenberg, A. J. Black, G. M. Whitesides, *J. Am. Chem. Soc.* **1999**, *121*, 4500.
69 a) J. P. Jolivet, M. Henry, J. Livage, *Metal Oxide Chemistry and Synthesis*, John Wiley & Sons, Chichester, **2000**, p. 37. b) T. Sugimoto, *Adv. Colloid Interface Sci.* **1987**, *28*, 65.
70 a) H. J. Butt, K. Graf, M. Kappl, *Physics and Chemistry of Interfaces*, Wiley-VCH, Weinheim, **2003**. b) E. J. W. Verwey, J. Th. G. Overbeek, *Theory of Stability of Hydrophobic Colloids*, Elsevier, Amsterdam, **1948**.
71 a) J.-J. Shyue, M. R. DeGuire, T. Nakanishi, Y. Masuda, K. Koumoto, C. N. Sukenik, *Langmuir* **2004**, *20*, 8693. b) Y. Tang, M. R. DeGuire, *J. Mater. Chem.* **2004**, *14*, 1173.
72 J. N. Israelachvili, G. E. Adams, *J. Chem. Soc., Faraday Trans.* **1978**, *74*, 975.
73 a) W. A. Ducker, T. J. Senden, R. M. Pashley, *Langmuir* **1992**, *8*, 1831. b) A. L. Weisenhorn, P. K. Hansma, T. R. Albrechet, C. F. Quate, *Appl. Phys. Lett.* **1989**, *54*, 2651. c) A. L. Weisenhorn, P. Maivald, H.-J. Butt, P. K. Hansma, *Phys. Rev. B* **1992**, *45*, 11226. d) N. A. Burnham, D. D. Dominguez, R. L. Mowery, R. Colton, *Phys. Rev. Lett.* **1990**, *64*, 1931. e) G. S. Blackman, C. M. Mate, M. R. Philpott, *Phys. Rev. Lett.* **1990**, *65*, 2270. f) H. A. Mizes, K.-G. Loh, R. J. D. Miller, S. K. Ahuja, E. F. Grabowski, *Appl. Phys. Lett.* **1991**, *59*, 2901. g) T. P. Weihs, Z. Nawaz, S. P. Jarvis, J. B. Pethica, *Appl. Phys. Lett.* **1991**, *59*, 3536. h) J. H. Hoh, J. P. Revel, P. K. Hansma, *Nanotechnology* **1991**, *2*, 119. i) K. Feldman, T. Tervoort, P. Smith, N. D. Spencer, *Langmuir* **1998**, *14*, 372. j) R. M. Ralich, Y. Wu, R. D. Ramsier, P. N. Henriksen, *J. Vac. Sci. Technol., A* **2000**, *18*, 1345. k) R. W. Carpick, N. Agrait, D. F. Ogletree, M. Salmeron, *Langmuir* **1996**, *12*, 3334. l) T. Thundat, X. Y. Zheng, G. Y. Chen, R. J. Warmack, *Surf. Sci. Lett.* **1993**, *294*, L939. m) T. Aoki, Y. Sowa, H. Yokota, M. Hiroshima, M. Tokunaga, Y. Ishii, T. Yanagida, *Single Mol.* **2001**, *2*, 183.
74 J. N. Israelachvili, *Intermolecular and Surface Forces*, Academic Press, California, **1992**, p. 139.
75 K. Sawada, in *Crystallization Process*, ed. by H. Ohtaki, John Wiley & Sons, Chichester, **1998**.
76 D. Horn, J. Rieger, *Angew. Chem., Int. Ed.* **2001**, *40*, 4330.
77 a) G. H. Peters, J. Eggebrecht, *J. Phys. Chem.* **1991**, *95*, 909. b) H. Arstila, *J. Chem. Phys.* **1997**, *107*, 3196.
78 a) J. F. Banfield, S. A. Welch, H. Zhang, T. T. Ebert, R. L. Penn, *Science* **2000**, *289*, 751. b) H. Colfen, S. Mann, *Angew. Chem., Int. Ed.* **2003**, *42*, 2350. c) O. Grassmann, R. B. Neder, A. Putnis, P. Lobmann, *Am. Mineral.* **2003**, *88*, 647. d) R. L. Penn, J. F. Banfield, *Science* **1998**, *281*, 969. e) A. Chemseddine, T. E. Moritz, *Eur. J. Inorg. Chem.* **1999**, 235. f) J. K. Bailey, C. J. Brinker, M. L. Mecartney, *J. Colloid Interface Sci.* **1993**, *157*, 1. g) C. Pacholski, A. Kornowski, H. Weller, *Angew. Chem., Int. Ed.* **2002**, *41*, 1188.
79 M. Vanni, *J. Colloid Interface Sci.* **2000**, *221*, 143.
80 R. C. Hoffmann, S. Jia, J. C. Bartolomé, T. M. Fuchs, J. Bill, P. C. J. Graat, F. Aldinger, *J. Eur. Ceram. Soc.* **2003**, *23*, 2119.
81 a) S. H. Yu, H. Cölfen, M. Antonietti, *Chem.—Eur. J.* **2002**, *8*, 2937. b) J. H. Adair, E. Suvaci, *Curr. Opin. Colloid Interface Sci.* **2000**, *5*, 160. c) E. Matijevic, *Acc. Chem. Res.* **1981**, *14*, 22. d) E. Matijevic, *Langmuir* **1986**, *2*, 12. e) E. Matijevic, *Chem. Mater.* **1993**, *5*, 412. f) E. Matijevic, *Curr. Opin. Colloid Interface Sci.* **1996**, *1*, 176. g) H. Colfen, *Macromol. Rapid Commun.* **2001**, *22*, 219. h) L. Qi, H. Colfen, M. Antonietti, M. Li, J. D. Hopwood, A. J. Ashley, S. Mann, *Chem.—Eur. J.* **2001**, *7*, 3526. i) J. D. Hartgerink, E. Beniash, S. I. Stupp, *Science* **2001**, *294*, 1684. j) A. Taubert, G. Glasser, D. Palms, *Langmuir* **2002**, *18*, 4488. k) M. Oner, J. Norwig, W. H. Meyer, G. Wegner, *Chem. Mater.* **1998**, *10*, 460.
82 R. Turgeman, S. Tirosh, A. Gedanken, *Chem.—Eur. J.* **2004**, *10*, 1845.
83 Z. R. Tian, J. A. Voigt, J. Liu, B. Mckenzie, M. J. Mcdermott, M. A. Rodriguez, H. Konishi, H. Xu, *Nat. Mater.* **2003**, *2*, 821.
84 L. Vayssieres, K. Keis, S.-E. Lingdquist, A. Hagfeldt, *J. Phys. Chem. B* **2001**, *105*, 3350.
85 Y. Gao, M. Nagai, *Langmuir* **2006**, *22*, 3936.
86 M. H. Huang, S. Mao, H. Feick, H. Yan, Y. Wu, H. Kind, E. Weber, R. Russo, P. Yang, *Science* **2001**, *292*, 1897.

87 L. Vayssieres, K. Keis, A. Hagfeldt, S.-E. Lingdquist, *Chem. Mater.* **2001**, *13*, 4395.
88 J. Zhang, L. Sun, J. Yin, H. Su, C. Liao, C. Yan, *Chem. Mater.* **2002**, *14*, 4172.
89 Z. R. Tian, J. A. Voigt, J. Liu, B. Mckenzie, M. J. Mcdermott, *J. Am. Chem. Soc.* **2002**, *124*, 12954.
90 S. Mann, in *Biomineralization: Chemical and Biochemical Perspectives*, ed. by S. Mann, J. Webb, R. J. P. Williams, VCH, Weinheim, **1989**, p. 35.
91 D. T. Richens, M. R. S. C. Chem, *The Chemistry of Aqua Ions*, John Wiley & Sons, Chichester, **1997**, p. 1.
92 M. Agarwal, M. R. DeGuire, A. H. Heuer, *J. Am. Ceram. Soc.* **1997**, *80*, 2967.
93 Y. Gao, Y. Masuda, H. Ohta, K. Koumoto, *Chem. Mater.* **2004**, *16*, 2615.
94 B. Aiken, W. P. Hsu, E. Matijevic, *J. Mater. Sci.* **1990**, *25*, 1886.
95 a) T. Yao, T. Inui, A. Ariyoshi, *J. Am. Ceram. Soc.* **1996**, *79*, 3329. b) T. Yao, *J. Mater. Res.* **1998**, *13*, 1091. c) N. Ozawa, T. Yao, *Trans. Mater. Res. Soc. Jpn.* **2003**, *28*, 321.
96 Y. F. Gao, M. Nagai, Y. Masuda, F. Sato, K. Koumoto, *J. Cryst. Growth* **2006**, *286*, 445.
97 L. Vayssieres, *Adv. Mater.* **2003**, *15*, 464.
98 L. Vayssieres, N. Beermann, S. E. Lindquist, A. Hagfeldt, *Chem. Mater.* **2001**, *13*, 233.
99 L. Vayssieres, *Int. J. Nanotechnol.* **2005**, *2*, 411.
100 J. Zhang, L. Sun, C. Liao, C. Yan, *Chem. Commun.* **2002**, 262.
101 J. Zhang, L. Sun, X. Jiang, C. Liao, C. Yan, *Cryst. Growth Des.* **2004**, *4*, 309.
102 B. Liu, H. C. Zeng, *Langmuir* **2004**, *20*, 4196.
103 B. Liu, S.-H. Yu, F. Zhang, L. Li, Q. Zhang, L. Ren, K. Jiang, *J. Phys. Chem. B* **2004**, *108*, 4338.
104 Y. Masuda, N. Kinoshita, F. Sato, K. Koumoto, *Cryst. Growth Des.* **2006**, *6*, 75.
105 S. Yin, T. Sato, *J. Mater. Chem.* **2005**, *15*, 4584.
106 M. Law, L. E. Greene, J. C. Johnson, R. Saykally, P. Yang, *Nat. Mater.* **2005**, *4*, 455.
107 A. Taubert, D. Palms, O. Weiss, M.-T. Piccini, D. N. Batchelder, *Chem. Mater.* **2002**, *14*, 2594.
108 A. Taubert, C. Kubel, D. C. Martin, *J. Phys. Chem. B* **2003**, *107*, 2660.
109 Y. Peng, A.-W. Xu, B. Deng, M. Antonietti, H. Colfen, *J. Phys. Chem.* **2006**, *110*, 2988.
110 F. Li, Y. Ding, P. Gao, X. Xin, Z. L. Wang, *Angew. Chem., Int. Ed.* **2004**, *43*, 5238.
111 H. Imai, Y. Oaki, A. Kotachi, *Bull. Chem. Soc. Jpn.* **2006**, *79*, 1834.
112 L. P. Bauermann, A. D. Campo, J. Bill, F. Aldinger, *Chem. Mater.* **2006**, *18*, 2016.
113 R. C. Hoffmann, S. Jia, J. Bill, M. R. De Guire, F. Aldinger, *J. Ceram. Soc. Jpn.* **2004**, *112*, S1089.
114 A.-W. Xu, Y. Ma, H. Colfen, *J. Mater. Chem.* **2007**, *17*, 415.
115 Y. F. Gao, unpublished data.
116 H. Colfen, M. Antonietti, *Angew. Chem., Int. Ed.* **2005**, *44*, 5576.
117 *Metal Oxide Chemistry and Synthesis: From Solution to Solid State*, ed. by J. P. Jolivet, M. Henry, J. Livage, John Wiley & Sons, Chichester, **2000**, p. 169.
118 J. Sun, J. Bian, H. Liang, J. Zhao, L. Hu, Z. Zhao, W. Liu, G. Du, *Appl. Surf. Sci.* **2007**, *253*, 5161.
119 X. Liu, Z. Jin, Z. Liu, K. Yu, S. Bu, *Appl. Surf. Sci.* **2006**, *252*, 8668.
120 Y. Gao, M. Nagai, T.-C. Chang, J.-J. Shyue, *Cryst. Growth Des.* **2007**, *7*, 2467.
121 Y. F. Gao, H. Y. Miao, H. J. Luo, M. Nagai, J. J. Shyue, *J. Phys. Chem. C* **2008**, in press.
122 a) Y. Gao, M. Nagai, W.-S. Seo, K. Koumoto, *J. Am. Ceram. Soc.* **2007**, *90*, 831. b) Y. Gao, Y. Masuda, K. Koumoto, *Chem. Mater.* **2004**, *16*, 1062. c) Y. Gao, Y. Masuda, Z. Peng, T. Yonezawa, K. Koumoto, *J. Mater. Chem.* **2003**, *13*, 608.
123 Y.-F. Gao, M. Nagai, W. S. Seo, K. Koumoto, *Langmuir* **2007**, *23*, 4712.
124 a) A. Ulman, *Chem. Rev.* **1996**, *96*, 1533. b) A. Ulman, *An Introduction to Ultrathin Organic Films: From Langmuir–Blodgett to Self-Assembly*, Academic Press, San Diego, **1991**.
125 a) Y. Wang, M. Lieberman, *Langmuir* **2003**, *19*, 1159. b) N. Rozlosnik, M. C. Gerstenberg, N. B. Larsen, *Langmuir* **2003**, *19*, 1182. c) S. Tosatti, R. Michel, M. Textor, N. D. Spencer, *Langmuir* **2002**, *18*, 3537. d) M. K. Ferguson, E. R. Low, J. R. Morris, *Langmuir* **2004**, *20*, 3319. e) H. Sugimura, A. Hozumi, T. Kameyama, O. Takai, *Surf. Interface Anal.* **2002**, *34*, 550. f) U. Jonsson, G. Olofsson, M. Malmqvist, I. Ronnberg, *Thin Solid Films* **1985**, *124*, 117. g) H. Tada, H. Nagayama, *Langmuir* **1995**, *11*, 136. h) H. Tada, *J. Electrochem. Soc.* **1995**, *142*, L11. i) H. Sugimura, N. Nakagiri, *Langmuir* **1995**, *11*, 3623. j) H. Tada, K. Shimoda, K. Goto, *J. Electrochem. Soc.* **1995**, *142*, L230. k) P. W. Hoffmann, M. Stelzle, J. F. Rabolt, *Langmuir* **1997**, *13*, 1877. l) H. Sugimura, N. Nakagiri, *J. Photopolym. Sci. Technol.* **1997**, *10*, 661. m) A. Y. Fadeev, T. J. McCarthy, *Langmuir* **1999**, *15*, 3759. n) A. Hozumi, K. Ushiyama, H. Sugimura, O. Takai, *Langmuir* **1999**, *15*, 7600.
126 a) C. S. Dulcey, J. H. Georger, Jr., V. Krauthamer, D. A. Stenger, T. L. Fare, J. M. Calvert, *Science* **1991**, *252*, 551. b) S. Sun, K. S. L. Chong, G. J. Leggett, *J. Am. Chem. Soc.* **2002**, *124*, 2414. c) S. Xu, S. Miller, P. E. Laibinis, G. Liu, *Langmuir* **1999**, *15*, 7244. d) J. R. Kenseth, J. A. Harnisch, V. W. Jones, M. D. Porter, *Langmuir* **2001**, *17*, 4105. e) J.-F. Liu, S. Cruchon-Dupeyrat, J. C. Garno, J. Frommer, G.-Y. Liu, *Nano Lett.* **2002**, *2*, 937. f) G.-Y. Liu, N. A. Amro, *Proc. Natl. Acad. Sci. U.S.A.* **2002**, *99*, 5165. g) J. C. Garno, Y. Yang, N. A. Amro, S. Cruchon-Dupeyrat, S. Chen, G.-Y. Liu, *Nano Lett.* **2003**, *3*, 389. h) M. Kaholek, W.-K. Lee, B. LaMattina, K. C. Caster, S. Zauscher, *Nano Lett.* **2004**, *4*, 373. i) M. J. Lercel, R. C. Tiberio, P. F. Chapman, H. G. Craighead, C. W. Sheen, A. N. Parikh, D. L. Allara, *J. Vac. Sci. Technol., B* **1993**, *11*, 2823. j) J. A. M. Sondag-Huethorst, H. R. J. van Helleputte, L. G. Fokkink, *Appl. Phys. Lett.* **1994**, *64*, 285. k) G. Gillen, S. Wight, J. Bennett, M. J. Tarlov, *Appl. Phys. Lett.* **1994**, *65*, 534. l) M. J. Lercel, H. G. Craighead, A. N. Parikh, K. Seshadri, D. L. Allara, *Appl. Phys. Lett.* **1996**, *68*, 1504. m) R. Maoz, E. Frydman, S. R. Cohen, J. Sagiv, *Adv. Mater.* **2000**, *12*, 424. n) R. Maoz, E. Frydman, S. R. Cohen, J. Sagiv, *Adv. Mater.* **2000**, *12*, 725. o) S. Hoeppener, R. Maoz, S. R. Cohen, L. Chi, H. Fuchs, J. Sagiv, *Adv. Mater.* **2002**, *14*, 1036. p) S. Liu, R. Maoz, G. Schmid, J. Sagiv, *Nano Lett.* **2002**, *2*, 1055. q) C. B. Gorman, R. L. Carroll, R. R. Fuierer, *Langmuir* **2001**, *17*, 6923. r) R. R. Fuierer, R. L. Carroll, D. L. Feldheim, C. B. Gorman, *Adv. Mater.* **2002**, *14*, 154. s) G. M. Credo, A. K. Boal, K. Das, T. H. Galow, V. M. Rotello, D. L. Feldheim, C. B. Gorman, *J. Am. Chem. Soc.* **2002**, *124*, 9036. t) J. Gun, J. Sagiv, *J. Colloid Interf. Sci.* **1986**, *112*, 457.
127 M. J. Williamson, R. M. Tromp, P. M. Vereecken, R. Hull, F. M. Ross, *Nat. Mater.* **2003**, *2*, 532.

128 a) N. Shirahata, T. Yonezawa, W.-S. Seo, K. Koumoto, *Langmuir* **2004**, *20*, 1517. b) Y. Wang, S. Supothina, M. R. DeGuire, A. H. Heuer, R. Collins, C. N. Sukenik, *Chem. Mater.* **1998**, *10*, 2135.
129 N. Saito, Y. Wu, K. Hayashi, H. Sugimura, O. Takai, *J. Phys. Chem. B* **2003**, *107*, 664.
130 a) L. Wang, J. Jiang, Y. Song, B. Zhang, E. Wang, *Langmuir* **2003**, *19*, 4953. b) D. Liu, G. J. Szulczewski, L. D. Kispert, A. Primak, T. A. Moore, A. L. Moore, D. Gust, *J. Phys. Chem. B* **2002**, *106*, 2933. c) O. Gershevitz, C. N. Sukenik, *J. Am. Chem. Soc.* **2004**, *126*, 482. d) S. C. B. Mannsfeld, T. W. Canzler, T. Fritz, H. Proehl, K. Leo, S. Stumpf, G. Goretzki, K. Gloe, *J. Phys. Chem. B* **2002**, *106*, 2255. e) R. G. Nuzzo, L. H. Dubois, D. L. Allara, *J. Am. Chem. Soc.* **1990**, *112*, 558. f) E. L. Smith, C. A. Alves, J. W. Anderegg, M. D. Porter, L. M. Siperko, *Langmuir* **1992**, *8*, 2707. g) S. S. Cheng, D. A. Scherson, C. N. Sukenik, *Langmuir* **1995**, *11*, 1190.
131 a) K. V. Wolf, D. A. Cole, S. L. Bernasek, *Anal. Chem.* **2002**, *74*, 5009. b) L. Sun, J. A. Gardella, Jr., *Langmuir* **2002**, *18*, 9289. c) D. J. Graham, B. D. Ratner, *Langmuir* **2002**, *18*, 5861. d) D. J. Graham, D. D. Price, B. D. Ratner, *Langmuir* **2002**, *18*, 1518.
132 a) R. Sfez, L. De-Zhong, I. Turyan, D. Mandler, S. Yitzchaik, *Langmuir* **2001**, *17*, 2556. b) G. Kalyuzhny, A. Vaskevich, G. Ashkenasy, A. Shanzer, I. Rubinstein, *J. Phys. Chem. B* **2000**, *104*, 8238.
133 a) J. Noh, E. Ito, K. Nakajima, J. Kim, H. Lee, M. Hara, *J. Phys. Chem. B* **2002**, *106*, 7139. b) K. Shabtai, I. Rubinstein, S. R. Cohen, H. Cohen, *J. Am. Chem. Soc.* **2000**, *122*, 4959. c) W. Zhou, T. Baunach, V. Ivanova, D. M. Kolb, *Langmuir* **2004**, *20*, 4590. d) S.-Y. Lin, T.-K. Tsai, C.-M. Lin, C.-h. Chen, Y.-C. Chan, H.-W. Chen, *Langmuir* **2002**, *18*, 5473.
134 a) J. L. Shepherd, A. Kell, E. Chung, C. W. Sinclar, M. S. Workentin, D. Bizzotto, *J. Am. Chem. Soc.* **2004**, *126*, 8329. b) E. A. McArthur, T. Ye, J. P. Cross, S. Petoud, E. Borguet, *J. Am. Chem. Soc.* **2004**, *126*, 2260. c) J. Sagiv, *J. Am. Chem. Soc.* **1980**, *102*, 92. d) M. A. Fox, W. Li, M. Wooten, A. McKerrow, J. K. Whitesell, *Thin Solid Films* **1998**, *327–329*, 477. e) M. Montalti, L. Prodi, N. Zaccheroni, R. Baxter, G. Teobaldi, F. Zerbetto, *Langmuir* **2003**, *19*, 5172. f) S. Flink, F. C. J. M. van Veggel, D. N. Reinhoudt, *J. Phys. Org. Chem.* **2001**, *14*, 407.
135 a) Y. Liu, L. K. Wolf, M. C. Messmer, *Langmuir* **2001**, *17*, 4329. b) S. C. Clear, P. F. Nealey, *Langmuir* **2001**, *17*, 720. c) S. Sun, G. J. Leggett, *Nano Lett.* **2002**, *2*, 1223.
136 a) K. Hayashi, N. Saito, H. Sugimura, O. Takai, N. Nakagiri, *Langmuir* **2002**, *18*, 7469. b) S. D. Evans, A. Ulman, *Chem. Phys. Lett.* **1990**, *170*, 462. c) Y. Miura, S. Kimura, S. Kobayashi, M. Iwamoto, Y. Imanishi, J. Umemura, *Chem. Phys. Lett.* **1999**, *315*, 1. d) R. W. Zehner, B. F. Parsons, R. P. Hsung, L. R. Sita, *Langmuir* **1999**, *15*, 1121. e) J. Lu, E. Delamarche, L. Eng, R. Bennewitz, E. Meyer, H.-J. Guntherodt, *Langmuir* **1999**, *15*, 8184. f) H. Sugimura, K. Hayashi, N. Saito, O. Takai, N. Nakagiri, *Jpn. J. Appl. Phys.* **2001**, *40*, 4373.
137 a) D. Shen, M. Huang, L.-M. Chow, M. Yang, *Sens. Actuators, B* **2001**, *77*, 664. b) M. Satjapipat, R. Sanedrin, F. Zhou, *Langmuir* **2001**, *17*, 7637. c) A. Tsuchida, K. Matsuura, K. Kobayshi, *Macromol. Chem. Phys.* **2000**, *201*, 2245. d) L. L. Nordyke, D. A. Buttry, *Langmuir* **1991**, *7*, 380.
138 a) K. Sugihara, K. Shimazu, K. Uosaki, *Langmuir* **2000**, *16*, 7101. b) S. Howell, D. Kuila, B. Kasibhatla, C. P. Kubiak, D. Janes, R. Reifenberger, *Langmuir* **2002**, *18*, 5120. c) X.-M. Li, J. Huskens, D. N. Reinhoudt, *J. Mater. Chem.* **2004**, *14*, 2954.
139 a) C. D. Bain, G. M. Whitesides, *Langmuir* **1989**, *5*, 1370. b) S. E. Creager, J. Clarke, *Langmuir* **1994**, *10*, 3675. c) T. R. Lee, R. I. Carey, H. A. Biebuyck, G. M. Whitesides, *Langmuir* **1994**, *10*, 741. d) G. S. Ferguson, M. K. Chaudhury, H. A. Biebuyck, G. M. Whitesides, *Macromolecules* **1993**, *26*, 5870. e) S. R. Wasserman, Y. T. Tao, G. M. Whitesides, *Langmuir* **1989**, *5*, 1074.
140 a) E. Menard, L. Bilhaut, J. Zaumseil, J. A. Rogers, *Langmuir* **2004**, *20*, 6871. b) Y.-L. Loo, R. L. Willett, K. W. Baldwin, J. A. Rogers, *J. Am. Chem. Soc.* **2002**, *124*, 7654.
141 a) R. D. Piner, J. Zhu, F. Xu, S. Hong, C. A. Mirkin, *Science* **1999**, *283*, 661. b) S. Hong, J. Zhu, C. A. Mirkin, *Science* **1999**, *286*, 523. c) D. A. Weinberger, S. Hong, C. A. Mirkin, B. W. Wessels, T. B. Higgins, *Adv. Mater.* **2000**, *12*, 1600. d) H. Zhang, S.-W. Chung, C. A. Mirkin, *Nano Lett.* **2003**, *3*, 43.
142 T. P. Sullivan, W. T. S. Huck, *Eur. J. Org. Chem.* **2003**, 17.
143 H. Shin, M. R. DeGuire, A. H. Heuer, *J. Appl. Phys.* **1998**, *83*, 3311.
144 a) Z. Xiao, J. Gu, D. Huang, Z. Lu, Y. We, *Appl. Surf. Sci.* **1998**, *125*, 85. b) S. Baskaran, L. Song, J. Liu, Y. L. Chen, G. L. Graff, *J. Am. Ceram. Soc.* **1998**, *81*, 401. c) Z. Xiao, L. Su, N. Gu, Z. Lu, Y. Wei, *Thin Solid Films* **1998**, *333*, 25.
145 Z. Xiao, M. Xu, J. Gu, D. Huang, Z. Lu, *Mater. Chem. Phys.* **1998**, *52*, 170.
146 T. M. Fuchs, R. C. Hoffmann, T. P. Niesen, H. Tew, J. Bill, F. Aldinger, *J. Mater. Chem.* **2002**, *12*, 1597.
147 J. H. Xiang, P. X. Zhu, Y. Masuda, K. Koumoto, *Langmuir* **2004**, *20*, 3278.
148 Y. Masuda, S. Ieda, K. Koumoto, *Langmuir* **2003**, *19*, 4415.
149 Y. Masuda, T. Sugiyama, W. S. Seo, K. Koumoto, *Chem. Mater.* **2003**, *15*, 2469.
150 H. Tokuhisa, P. T. Hammond, *Langmuir* **2004**, *20*, 1436.
151 J. P. Lee, Y. J. Jang, M. M. Sung, *Adv. Funct. Mater.* **2003**, *13*, 873.
152 B.-C. Kang, J.-H. Lee, H.-Y. Chae, D.-Y. Jung, S.-B. Lee, J.-H. Boo, *J. Vac. Sci. Technol., B* **2003**, *21*, 1773.
153 Y. Masuda, W. S. Seo, K. Koumoto, *Langmuir* **2001**, *17*, 4876.
154 M. H. Park, Y. J. Jang, H. M. Sung-Suh, M. M. Sung, *Langmuir* **2004**, *20*, 2257.
155 E. K. Seo, J. W. Lee, H. M. Sung-Suh, M. M. Sung, *Chem. Mater.* **2004**, *16*, 1878.
156 J. P. Lee, M. M. Sung, *J. Am. Chem. Soc.* **2004**, *126*, 28.
157 H.-Z. Yu, A. W. Rowe, D. M. Waugh, *Anal. Chem.* **2002**, *74*, 5742.
158 V. V. Roddatis, D. S. Su, E. Beckmann, F. C. Jentoft, U. Braun, J. Krohnert, R. Schlogl, *Surf. Coat. Technol.* **2002**, *151–152*, 63.
159 K. A. Ritley, K.-P. Just, F. Schreiber, H. Dosch, T. P. Niesen, F. Aldinger, *J. Mater. Res.* **2000**, *15*, 2706.
160 J. Wang, S. Yang, X. Liu, S. Ren, F. Guan, M. Chen, *Appl. Surf. Sci.* **2004**, *221*, 272.
161 A. D. Polli, T. Wagner, A. Fischer, G. Weinberg, F. C. Jentoft, R. Schlogl, M. Ruhle, *Thin Solid Films* **2000**, *379*, 122.
162 M. Aslam, S. Pethkar, K. Bandyopadhyay, I. S. Mulla, S. R. Sainkar, A. B. Mandale, K. Vijayamohanan, *J. Mater. Chem.* **2000**, *10*, 1737.
163 N. Shirahata, Y. Masuda, T. Yonezawa, K. Koumoto, *Langmuir* **2002**, *18*, 10379.
164 S. Supothina, M. R. DeGuire, A. H. Heuer, *J. Am. Ceram. Soc.* **2003**, *86*, 2074.

165 M. Heule, U. P. Schonholzer, L. J. Gauckler, *J. Eur. Ceram. Soc.* **2004**, *24*, 2733.
166 Y. Tang, Y. Liu, U. Sampathkumaran, M. Z. Hu, R. Wang, M. R. DeGuire, *Solid State Ionics* **2002**, *151*, 69.
167 N. Shirahata, Y. Masuda, T. Yonezawa, K. Koumoto, *J. Eur. Ceram. Soc.* **2004**, *24*, 427.
168 N. Shirahata, Y. Yokogawa, T. Kameyama, A. Hozumi, *J. Vac. Sci. Technol.* **2004**, *22*, 1734.
169 N. Shirahata, W. Shin, N. Murayama, A. Hozumi, Y. Yokogawa, T. Kameyama, Y. Masuda, K. Koumoto, *Adv. Funct. Mater.* **2004**, *14*, 580.
170 M. Agarwal, M. R. DeGuire, A. H. Heuer, *Appl. Phys. Lett.* **1997**, *71*, 891.
171 Y. Masuda, M. Yamagishi, K. Koumoto, *Chem. Mater.* **2007**, *19*, 1002.
172 R. Turgeman, O. Gershevitz, O. Palchik, M. Deutsch, B. M. Ocko, A. Gedanken, C. N. Sukenik, *Cryst. Growth Des.* **2004**, *4*, 169.
173 N. I. Kovtyukhova, E. V. Buzaneva, C. C. Waraksa, B. R. Martin, T. E. Mallouk, *Chem. Mater.* **2000**, *12*, 383.
174 N. Saito, H. Haneda, W.-S. Seo, K. Koumoto, *Langmuir* **2001**, *17*, 1461.
175 M. Yan, Y. Koide, J. R. Babcock, P. R. Markworth, J. A. Belot, T. J. Marks, R. P. H. Chang, *Appl. Phys. Lett.* **2001**, *79*, 1709.
176 R. C. Hoffmann, J. C. Bartolome, T. M. Fuchs, J. Bill, P. C. J. Graat, F. Aldinger, *Surf. Interface Anal.* **2002**, *34*, 708.
177 N. Saito, H. Haneda, T. Sekiguchi, T. Ishigaki, K. Koumoto, *J. Electrochem. Soc.* **2004**, *151*, H169.
178 N. Saito, H. Haneda, D. Li, K. Koumoto, *J. Ceram. Soc. Jpn.* **2002**, *110*, 386.
179 N. Saito, H. Haneda, T. Sekiguchi, N. Ohashi, I. Sakaguchi, K. Koumoto, *Adv. Mater.* **2002**, *14*, 418.
180 Y. Gao, Y. Masuda, K. Koumoto, *J. Colloid Interface Sci.* **2004**, *274*, 392.
181 Y. Masuda, S. Wakamatsu, K. Koumoto, *J. Eur. Ceram. Soc.* **2004**, *24*, 301.
182 a) T. Nakanishi, Y. Masuda, K. Koumoto, *Chem. Mater.* **2004**, *16*, 3484. b) T. Nakanishi, Y. Masuda, K. Koumoto, *J. Cryst. Growth* **2005**, *284*, 176.
183 a) H. Shin, H. Im, J. U. Jeon, E. S. Kim, Y. E. Pak, *Mol. Cryst. Liq. Cryst.* **2001**, *371*, 473. b) H. Shin, J. U. Jeon, Y. E. Pak, H. Im, E. S. Kim, *J. Mater. Res.* **2001**, *16*, 564.
184 M. Nagtegaal, P. Stroeve, W. Tremel, *Thin Solid Films* **1998**, *327–329*, 571.
185 M. Nagtegaal, P. Stroeve, J. Ensling, P. Gutlich, M. Schurrer, H. Voit, J. Flath, J. Kashammer, W. Knoll, W. Tremel, *Chem.—Eur. J.* **1999**, *5*, 1331.
186 A. K. Dutta, G. Jarero, L. Zhang, P. Stroeve, *Chem. Mater.* **2000**, *12*, 176.
187 M. Nagtegaal, J. Kuther, J. Ensling, P. Gutlich, W. Tremel, *J. Mater. Chem.* **1999**, *9*, 1115.
188 a) J. Aizenberg, A. J. Black, G. M. Whitesides, *Nature* **1999**, *398*, 495. b) Y.-J. Han, J. Aizenberg, *Angew. Chem., Int. Ed.* **2003**, *42*, 3668. c) A. M. Travaille, L. Kaptijn, P. Verwer, B. Hulsken, J. A. A. W. Elemans, R. J. M. Nolte, H. van Kempen, *J. Am. Chem. Soc.* **2003**, *125*, 11571.
189 a) J. Aizenberg, *Adv. Mater.* **2004**, *16*, 1295, and references therein. b) G. Xu, N. Yao, I. A. Aksay, J. T. Groves, *J. Am. Chem. Soc.* **1998**, *120*, 11977.
190 a) P. X. Zhu, Y. Masuda, T. Yonezawa, K. Koumoto, *J. Am. Ceram. Soc.* **2003**, *86*, 782. b) K. Onuma, A. Oyane, T. Kokubo, G. Treboux, N. Kanzaki, A. Ito, *J. Phys. Chem. B* **2000**, *104*, 11950. c) B. J. Tarasevich, C. C. Chusuei, D. L. Allara, *J. Phys. Chem. B* **2003**, *107*, 10367. d) Y. Xu, C. B. Musgrave, *Chem. Mater.* **2004**, *16*, 646. e) S. Asakura, M. Hirota, A. Fuwa, *J. Vac. Sci. Technol.* **2003**, *21*, 1152. f) C. K. Luscombe, H.-W. Li, W. T. S. Huck, A. B. Holmes, *Langmuir* **2003**, *19*, 5273. g) M. Aslam, G. Gopakumar, T. L. Shoba, I. S. Mulla, K. Vijayamohanan, S. K. Kulkarni, J. Urban, W. Vogel, *J. Colloid Interface Sci.* **2002**, *255*, 79. h) J. Kuther, M. Bartz, R. Seshadri, G. B. M. Vaughan, W. Tremel, *J. Mater. Chem.* **2001**, *11*, 503.
191 Y. Masuda, Y. F. Gao, P. X. Zhu, N. Shirahata, N. Saito, K. Koumoto, *J. Ceram. Soc. Jpn. Suppl.* **2004**, *112*, 1495.
192 Y. Masuda, D. J. Wang, T. Yonezawa, K. Koumoto, *Key Eng. Mater.* **2002**, *228–229*, 125.
193 D. J. Wang, Y. Masuda, W. S. Seo, K. Koumoto, *Key Eng. Mater.* **2002**, *214*, 163.
194 Y. Masuda, D. J. Wang, W. S. Seo, K. Koumoto, *Key Eng. Mater.* **2002**, *214*, 157.
195 N. Shirahata, W. Shin, N. Murayama, Y. Masuda, K. Koumoto, *J. Ceram. Soc. Jpn.* **2004**, *112*, 562.
196 Y. F. Gao, Y. Masuda, K. Koumoto, *J. Korean Ceram. Soc.* **2003**, *40*, 213.
197 Y. Gao, Y. Masuda, T. Yonezawa, K. Koumoto, *Mater. Sci. Eng., B* **2003**, *99*, 290.
198 Y. F. Gao, Y. Masuda, K. Koumoto, *Key Eng. Mater.* **2003**, *248*, 73.
199 P. X. Zhu, Y. Masuda, K. Koumoto, *J. Ceram. Soc. Jpn.* **2001**, *109*, 676.
200 Y. Masuda, T. Koumura, T. Okawa, K. Koumoto, *J. Colloid Interface Sci.* **2003**, *263*, 190.
201 S. Sawada, Y. Masuda, P. Zhu, K. Koumoto, *Langmuir* **2006**, *22*, 332.
202 Y. Masuda, N. Saito, R. Hoffmann, M. R. De Guire, K. Koumoto, *Sci. Technol. Adv. Mater.* **2003**, *4*, 461.
203 P. Zhu, Y. Masuda, K. Koumoto, *Biomaterials* **2004**, *25*, 3915.
204 T. Kokubo, *Thermochim. Acta* **1996**, *280–281*, 479.
205 J. C. Elliot, *Structure, Chemistry of the Apatites and Other Calcium Orthophosphates*, Amsterdam, Elsevier, **1994**. p. 157.
206 a) P. Calvert, S. Mann, *Nature* **1997**, *386*, 127. b) S. Hayakawa, K. Tsuru, C. Ohtsuki, A. Osaka, *J. Am. Ceram. Soc.* **1999**, *82*, 2155.
207 A. J. S. Peaker, J. T. Czernuszka, *Thin Solid Films* **1996**, *287*, 174.
208 K. Yamashita, N. Oiawa, T. Umegaki, *Chem. Mater.* **1996**, *8*, 2697.
209 a) K. Sato, Y. Kumagai, J. Tanaka, *J. Biomed. Mater. Res., Part A* **2000**, *50*, 16. b) H. Lin, W. S. Seo, K. Kuwabara, K. Koumoto, *J. Ceram. Soc. Jpn.* **1996**, *104*, 291. c) M. Tanahashi, T. Matsuda, *J. Biomed. Mater. Res., Part A* **1997**, *34*, 305.
210 G. H. Nancollas, B. Tomazic, *J. Phys. Chem.* **1974**, *78*, 2218.
211 P. Zhu, Y. Masuda, K. Koumoto, *J. Mater. Chem.* **2004**, *14*, 976.
212 N. Saito, H. Haneda, M. Komatsu, K. Koumoto, *J. Electrochem. Soc.* **2006**, *153*, C170.
213 M. Izaki, T. Omi, *J. Electrochem. Soc.* **1997**, *144*, L3.
214 J. E. A. M. van den Meerakker, *J. Appl. Electrochem.* **1981**, *11*, 395.
215 T. Homma, H. Nakai, M. Onishi, T. Osaka, *J. Phys. Chem. B* **1999**, *103*, 1774.
216 N. Saito, H. Haneda, K. Koumoto, *J. Ceram. Soc. Jpn.*

2007, *115*, 850.
217 N. B. Colthup, L. H. Daly, S. E. Wiberley, *Introduction to Infrared and Raman Spectroscopy*, 3rd ed., Academic Press, New York, **1990**.
218 N. Inagaki, S. Tasaka, T. Baba, *J. Adhes. Sci. Technol.* **2001**, *15*, 749.
219 L. Supriya, R. O. Claus, *Langmuir* **2004**, *20*, 8870.
220 M. Kuzuya, J. Niwa, H. Ito, *Macromolecules* **1993**, *26*, 1990.
221 L. J. Gerenser, *J. Adhes. Sci. Technol.* **1987**, *1*, 303.
222 R. M. France, R. D. Short, *Langmuir* **1998**, *14*, 4827.
223 H. Lim, Y. Lee, S. Han, J. Cho, K.-J. Kim, *J. Vac. Sci. Technol., A* **2001**, *19*, 1490.
224 E. C. Onyiriuka, L. S. Hersh, W. Hertl, *J. Colloid Interface Sci.* **1991**, *144*, 98.
225 J. Y. Zhang, H. Esrom, U. Kogelschatz, G. Emig, *Appl. Surf. Sci.* **1993**, *69*, 299.
226 A. Holländer, J. E. Klemberg-Sapieha, M. R. Wertheimer, *Macromolecules* **1994**, *27*, 2893.
227 H. Dong, T. Bell, *Surf. Coat. Technol.* **1999**, *111*, 29.
228 a) E. C. Onyiriuka, L. S. Hersh, W. Hertl, *Appl. Spectrosc.* **1990**, *44*, 808. b) E. C. Onyiriuka, *J. Appl. Polym. Sci.* **1993**, *47*, 2187.
229 K. W. Lee, S. P. Kowalczyk, J. M. Shaw, *Macromolecules* **1990**, *23*, 2097.
230 K. W. Lee, S. P. Kowalczyk, J. M. Shaw, *Langmuir* **1991**, *7*, 2450.
231 E. Ranucci, Å. Sandgren, N. Andronova, A.-C. Albertsson, *J. Appl. Polym. Sci.* **2001**, *82*, 1971.
232 A. Y. Fadeev, T. J. McCarthy, *Langmuir* **1998**, *14*, 5586.
233 A. Dutschke, C. Diegelmann, P. Lobmann, *Chem. Mater.* **2003**, *15*, 3501.
234 A. Dutschke, C. Diegelmann, P. Lobmann, *J. Mater. Chem.* **2003**, *13*, 1058.
235 A. Hozumi, T. Masuda, H. Sugimura, T. Kameyama, *Langmuir* **2003**, *19*, 7573.
236 P. Zhu, M. Teranishi, J. Xiang, Y. Masuda, W.-S. Seo, K. Koumoto, *Thin Solid Films* **2005**, *473*, 351.
237 S. Satsuka, *Application of Sol–Gel Process*, Agune Shofusha Press, Tokyo, Japan, **1997**, p. 15.
238 S. Sawada, Y. Masuda, P. Zhu, K. Koumoto, *Langmuir* **2006**, *22*, 332.
239 Electrical conductivity of the International Annealed Copper Standard (IACS) at 20 °C (1.7241 μΩ cm, $5.8 \times 105\ \mathrm{S\,cm^{-1}}$).

Kunihito Koumoto is a professor in the Graduate School of Engineering at Nagoya University. He received his B.S., M.S., and Ph.D. degrees in applied chemistry from the University of Tokyo in 1974, 1976, and 1979, respectively. He served as a research associate, assistant professor, and associate professor at the University of Tokyo before joining Nagoya University as a full professor in 1992. His research focuses on bio-inspired processing of inorganic materials and thermoelectric materials. He received the R. M. Fulrath Award in 1993 and the Academic Achievement Award of the Ceramic Society of Japan in 2000. He became a fellow of the American Ceramic Society and received the Chinese Ceramic Society Award in 2005. He serves as a board member of the CSJ.

Noriko Saito is a senior researcher in National Institute for Materials Science (NIMS) from 1994. She graduated from Tohoku University in 1992, and received her Master of Science from Tohoku University in 1994. Ph.D. degree in Applied Chemistry from Nagoya University in the group of Prof. K. Koumoto in 2004. She was a visiting researcher at Nagoya Univ. in 1999–2000 and Massachusetts Institute of Technology in 2005–2006. Her research area is synthesis of thin films and powders from aqueous solutions.

Yanfeng Gao got his Bachelor and Master degrees in ceramics engineering from Shaanxi University of Science and Technology. From 1999, he studied for over 7 years in Japan. He obtained Ph.D. from Nagoya University in 2004, studying with Professor K. Koumoto on bio-inspired materials chemistry to ceramics. After one-year training as a postdoctoral fellow at Nagoya University, he moved to Tokyo and experienced for over 2 years as an Assistant Professor in the Musashi Institute of Technology. He was selected as a Scholar of the one-hundred-talent program of Chinese Academy of Sciences, and went back to China in 2007. He is now serving as a Principal Investigator in the SICCAS, studying on energy-saving oxide films and functionalizing ceramic powders by surface modification. Dr. Gao also got several awards in the earlier career stage including a Chinese Government Award for Outstanding Self-financed Students Abroad in 2003 from The China Scholarship Council, an International Exchange Award for the Commemoration of 21st Century in 2005, and an award for Japan–China Exchange on Ceramics Science and Technology in 2007, both from the Ceramics Society of Japan.

Yoshitake Masuda is a researcher at the National Institute of Advanced Industrial Science and Technology (AIST). He graduated from Tsukuba University in 1994, and received his Master of Engineering degree from Tsukuba University in 1996. He was an engineer at NGK Spark Plug Co., Ltd., from 1996 to 1998. Dr. Masuda was an assistant professor at Nagoya University from 2000 to 2006. He received his Doctor of Engineering degree from Nagoya University in 2004. His Ph.D. thesis was on the Patterning of TiO_2 Thin Films and Particles using Self-assembled Monolayers.

Peixin Zhu is a senior researcher at Kawamura Institute of Chemical Research. He obtained his Ph.D. degree in Graduate School of Engineering, Nagoya University in Japan in 2002. His current researches involve inorganic–organic hybrids, nano metal & metal oxides, as well as photocatalyst, gas-barrier films, etc.